Signal Processing Techniques for Modern Radar Systems

by

Mostafa Kamal Kamel Elhoshy
B.Sc., Alexandria University
M.Sc., Alexandria University

A Dissertation Submitted in Partial Fulfillment of the
Requirements for the Degree of

DOCTOR OF PHILOSOPHY

in the Department of Electrical and Computer Engineering

Signal Processing Techniques for Modern Radar Systems

by

Mostafa Kamal Kamel Elhoshy
B.Sc., Alexandria University
M.Sc., Alexandria University

Supervisory Committee

Dr. T. Aaron Gulliver, Supervisor
(Department of Electrical and Computer Engineering)

Dr. Fayez Gebali, Supervisor
(Department of Electrical and Computer Engineering)

Dr. Phalguni Mukhopadhyaya, Outside Member
(Department of Civil Engineering)

ABSTRACT

This dissertation considers radar detection and tracking of weak fluctuating targets using dynamic programming (DP) based track-before-detect (TBD). TBD combines target detection and tracking by integrating data over consecutive scans before making a decision on the presence of a target. A novel algorithm is proposed which employs order statistics in dynamic programming based TBD (OS-DP-TBD) to detect weak fluctuating targets. The well-known Swerling type 0, 1 and 3 targets are considered with non-Gaussian distributed clutter and complex Gaussian noise. The clutter is modeled using the Weibull, K and $G0$ distributions. The proposed algorithm is shown to provide better performance than well-known techniques in the literature. In addition, a novel expanding window multiframe (EW-TBD) technique is presented to improve the detection performance with reasonable computational complexity compared to batch processing. It is shown that EW-TBD has lower complexity than existing multiframe processing techniques. Simulation results are presented which confirm the superiority of the proposed expanding window technique in detecting targets even when they are not present in every scan in the window. Further, the throughput of the proposed technique is higher than with batch processing. Depending on the range and azimuth resolution of the radar system, the target may appear as a point in some radar systems and there will be target energy spillover in other systems. This dissertation consider both extended targets with different energy spillover levels and point targets. Simulation results are presented which confirm the superiority of the proposed algorithm in both cases.

Contents

List of Tables

List of Figures

List of Algorithms

List of Acronyms

ATC	Air Traffic Control
CFAR	Constant False Alarm Rate
DP	Dynamic Programming
DBT	Detection Before Tracking
EW-TBD	Expanding Window Track Before Detect
LLR	Logarithm Likelihood Ratio
HT	Hough Transform
H-PMHT	Histogram probabilistic Multiple Hypothesis Tracking
$h^{r,b}$	Point Spread Function which accounts for the Spillover of Target Energy
LELR	Logarithm of the Envelope Likelihood Ratio
LCLR	Logarithm of the Complex Likelihood Ratio
L	Target Energy Spillover
ML-PDA	Maximum Likelihood Probabilistic Data Association
OS	Order Statistics
OS-DP-TBD	Order Statistics Dynamic Programming based Track Before Detect
PC	Pulse Compression
P_D	Probability of Detection
P_{fa}	Probability of False Alarm
P_{MD}	Probability of Missed Detection

PDF	Probability Density Function
PF	Particle Filter
radar	Radio detection and ranging
RCS	Radar Cross Section
SA	Squared Amplitude
SNR	Signal to Noise Ratio
SCR	Signal to Clutter Ratio
SCNR	Signal to Clutter and Noise Ratio
TBD	Track Before Detect
Th	Throughput
SW-TBD	Sliding Window Track Before Detect
UAV	Unmanned Aerial Vehicle
U	Workload per output
V	Workload per frame

Chapter 1

Background and Motivation

Radar is an electromagnetic system used for the detection, location and tracking of reflecting objects. The principle of radar (radio detection and ranging) is based on radiating electromagnetic waves into space and detecting the echo signal reflected from targets. By comparing the received echo signal with the signal that was transmitted, radar can determine the presence of targets as well as their locations. Radar can perform in different weather conditions such as darkness, haze, fog, wind, rain and snow. A portion of the transmitted energy is reflected by the target and radiated in many directions. This reflected signal is received by the radar antenna. In the receiver, the reflected signal is processed to detect the presence of a target and its location [1].

Radar has for a long time played a very important role in areas such as air traffic control (ATC), surveillance, target tracking and ship navigation. The range (or distance), to a target is found by measuring the time it takes for the radar signal to travel to the target and return to the radar. Although modern radars can extract more information from the target echo signal than the target range, range measurement is the most important function.

Choosing a particular waveform type and a signal processing technique in a radar

system depends on the radar specific mission and role. Radar systems can use Continuous Waveforms (CW) or pulsed waveforms with or without modulation. Pulsed radars use a train of pulsed waveforms (mainly with modulation). In this category, radar systems can be classified on the basis of the Pulse Repetition Frequency (PRF) as low PRF, medium PRF, and high PRF radars. CW radars continuously emit electromagnetic energy and use separate transmit and receive antennas. Unmodulated CW radars can accurately measure target radial velocity (Doppler shift) and angular position [2]. Frequency Modulation Continuous Waveform (FMCW) radars have been used in various areas of radar research and industry. Measuring the height of aircraft, detecting the speed of vehicles, and checking product dimensions in automated systems are some military and commercial applications of FMCW. The main limitations of this type of radar reside in the low range detection due to low peak transmission power.

The achievements of radar were limited in the early 20th century by the power limitations of the transmitters used to send the radar waves in the form of short pulses. Even if higher power were supplied, the range resolution was worse due to the wider pulse width. Pulse compression (PC) was proposed to solve this dilemma. The idea is to transmit a long pulse of constant amplitude. At the receiver, the signal is processed through a filter with an impulse response equal to the conjugated time-reverse of the transmitted signal. The received signal is therefore compressed to a short pulse which accumulates the energy in the long pulse [3]. This provides a long detection range and high range resolution.

The range R is the distance between the radar and target. The elevation angle is the angle between the horizontal plane and the direction in which the radar antenna points. The azimuth angle ω is the angle between true north and a line pointed directly at the target on the horizontal plane. The transformation from radar angle and range to Cartesian

coordinates introduces nonlinearities into the system.

This dissertation considers a pulsed radar. The radar transmits a pulse of width τ, and this pulse is reflected by the target and is measured by the radar after t seconds. The range to the target is then given by

$$R = \frac{ct}{2}, \tag{1.1}$$

where c is the speed of light and the factor 2 is due to the fact that the pulse has to travel to and from the target. When the target is in motion relative to the radar R will change. The corresponding Doppler effect changes the frequency of the signal that propagates from the radar to a moving target and back. The rate of change of the range with time is the radial velocity $v_r = \frac{dR}{dt}$. The rate of change of the phase with time is the angular frequency $\omega_d = 2\pi f_d$, and the Doppler frequency shift is

$$f_d = \frac{2v_r}{\lambda} = \frac{2f_t v_r}{c}, \tag{1.2}$$

where f_t is the radar carrier frequency and λ is the wavelength. The Doppler shift gives information about the target speed. A practical system checks for a return pulse by matching the received pulse against a set of discrete delayed versions of the transmitted pulse. These discrete ranges are referred to as bins. A target not centered in a given range bin will have its energy spread across adjacent bins [4]. Computing the discrete Fourier transform of the received signal separates the return energy into a discrete number of Doppler bins.

The reflected energy is dependent on the characteristics of the target such as shape, material, size, and area exposed to the radar. The Radar Cross Section (RCS) is a parameter used to characterize the scattering properties of the radar target. It is defined as the ratio of

the power reflected back to the radar to the power density incident on the target

$$\sigma = \frac{P_r}{P_{td}}, \tag{1.3}$$

where P_r is the power reflected from the target and P_{td} is the power density (power per unit area) at a point in space away from the radar

$$P_{td} = \frac{P_t}{4\pi R^2}, \tag{1.4}$$

where P_t is the peak transmitted power and $4\pi R^2$ is the surface area of a sphere of radius R. The RCS is a function of the electrical properties of the target and the radar frequency. Therefore two targets with the same physical size and shape can have different RCSs [5].

1.1 Detection and Tracking

Target detection and tracking is essential for surveillance systems. Sensor data is collected which consists of reflections from the target, clutter and noise. Many methods have been developed to decide if there is a target present in the surveillance region. Most methods are based on thresholding the radar data and making a hard decision on target existence. The thresholds are determined considering the reflected target power and receiver noise. Methods based on constant thresholds and adaptive thresholding techniques such as Constant False Alarm Rate (CFAR) have been introduced in the literature. Tracking techniques can be classified as Detect Before Track (DBT) and Track Before Detect (TBD). As the name implies, DBT is based on detection using a threshold on the received data. Data association and filtering are done after detection to obtain the final track output. However, in TBD

techniques the decision is made at the end of the processing chain after all information from the radar data has been used and integrated over time [3]. Figure 1.1 presents the steps involved in the detection and tracking process.

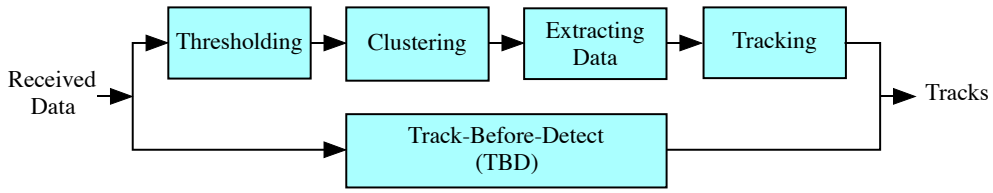

Figure 1.1: Detection and tracking processing chain. The conventional technique is represented by the top boxes and Track-Before-Detect (TBD) by the bottom box.

1.1.1 Conventional Radar

In a classical radar, detection decisions are based on comparing the magnitude of the complex radar echo to a predetermined threshold. If the signal amplitude exceeds this threshold, a detection is made. In this way the space of all measurements is divided into two regions, detection and no detection. When using a threshold to determine whether a target is present or not, two different errors can occur. The first, called false alarm, occurs when the threshold is exceeded even though there is no target present. The false alarm probability is denoted by P_{fa}. For example, high measurement noise can be detected as a target. The other error is called missed detection and occurs when the threshold is not exceeded even though a target is present. The probability of missed detection is denoted by $P_{MD} = 1 - P_D$, where P_D is the probability of detection. Depending on the signal to noise ratio (SNR) of the target and background clutter the detection made can be a target or clutter, i.e clouds, waves, trees or birds.

Conventional DBT has the processing chain thresholding and clustering, data association, and filtering to yield final track output as shown in Fig 1.1. In this approach, the

detection decision is the first step in the tracking process. The detection process normally has two stages, thresholding and clustering. A practical radar design will check for a return pulse at a number of discrete ranges by matched filtering the return pulse against a set of discrete delayed versions of the transmitted pulse. These discrete ranges are referred to as bins. The energy in the range-Doppler bins is compared to a threshold. Those bins with energy exceeding the threshold are called hits. Only the bins with hits are considered in this process. Clustering is applied to hits close to each other as they probably originate from the same target. The output of these two stages is the measurements in the cells in which a target is located. These measurements are called plots and consist of range, elevation, azimuth, and Doppler [2].

After a detection is made based on the threshold, the next step is to extract data and construct tracks from the measurements as shown in Fig 1.1. Because of noise and clutter, not all of the measurements are from actual targets. Data association is used to decide which of the measurements correspond to tracks. A common association method is nearest neighbor which uses only the closest observation to a given state to perform the measurement update [6]. Other more advanced algorithms exist that for example use the statistical properties of the clutter to reduce the false alarm rate. The most general technique is multiple hypothesis tracking [7].

1.1.2 Track Before Detect

The decision as to whether a target is present or not is typically based on information from a single scan. Stealth aircraft and other small targets such as missiles and Unmanned Aerial Vehicles (UAVs) increase the need to detect low SNR and low observable targets called dim targets. The conventional approach to detecting these targets is to lower the threshold

which results in a high false alarm rate.

Track Before Detect (TBD) is an alternative way to track dim targets. TBD is a combination of signal processing and tracking so that target state estimation and detection are done simultaneously as shown in Fig. 1.1. In TBD, a very low or no threshold is used. In this way, most or all available information is used and integrated over time by the tracking filter. This advantage of TBD leads to better detection and tracking performance especially for dim targets [8]. In TBD, detection is done using the track output over multiple scans. The detection decision is made when all information has been used and integrated over time. Although it is called track before detect, the tracking and detection processes are done simultaneously [9]. In this way, the energy of a (dim) target is integrated and correlated over time and position. This leads to better performance in detecting and tracking targets.

Various algorithms are applicable to TBD. Histogram based Probabilistic Multiple Hypothesis Tracking (H-PMHT) was introduced as a multi-signal tracking algorithm based on quantized raw data in a histogram [10]. Each cell is assumed to be associated with a target or noise in a similar way as DBT associates plots. The Hough Transform (HT) has been used to detect and track simultaneously from multiple scans. The aim of this transform is to locate lines in a noisy frame [11]. This allows the use of multiple scans to improve the performance which in turn increases the amount of data to be stored. A maximum likelihood approach was proposed in [12] to detect and track low SNR targets using raw data. A particle filter (PF) was used in the implementation of TBD algorithms in [13]. In this dissertation, Dynamic Programming (DP) based TBD (DP-TBD) is considered.

1.2 Problem Statement and Motivation

DP-TBD is a strong competitor among the algorithms to implement the integration of consecutive scans [9]. DP-TBD employs non-coherent integration of multiple frames of data with no or a very low threshold to preserve weak target information. This data is integrated to improve the Signal-to-Clutter Ratio (SCR). The presence of targets and their tracks are determined jointly after multiframe integration. DP-TBD employs integration in the absence of any prior information to estimate the possible target trajectories using a merit function which is a multiframe test statistic. Figure 1.2 shows merit function integration for N consecutive frames.

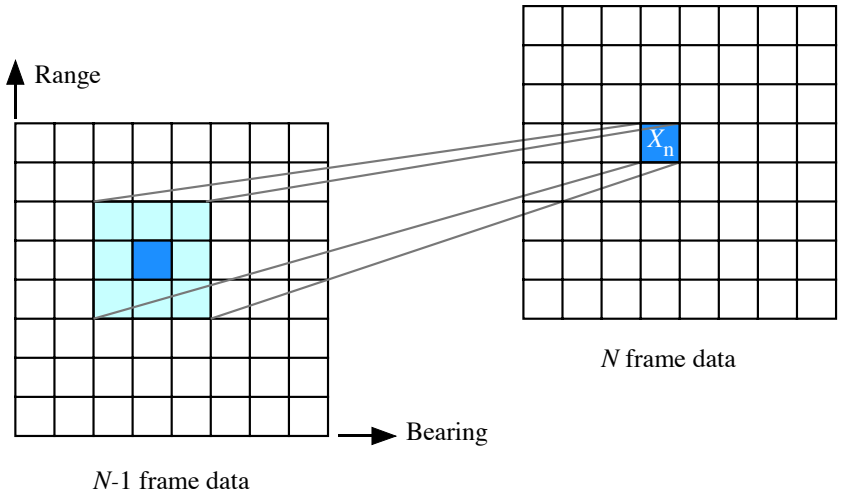

Figure 1.2: Illustration of the merit function integration.

The selection of the scoring function has a significant influence on the performance of DP-TBD. Three scoring functions commonly used in the literature with DP-TBD are the amplitude, Squared Amplitude (SA) and the Logarithm of the Envelope Likelihood Ratio (LELR). The amplitude and SA scoring functions lead to identical detection performance in Gaussian distributed background noise. The LELR scoring function usually provides better performance due to the utilization of both noise-only and noise-plus-target distributions.

The amplitude scoring function is easy to calculate, but the performance is poor in the presence of non-Gaussian clutter. DP-TBD usually employs either the SA or LELR scoring functions [14].

Generally, the choice of a scoring function is a tradeoff between performance and computational complexity, and the measurement model is an important consideration in choosing a scoring function. In this dissertation, the LELR scoring function is used as in DP-TBD.

1.3 Research Objectives

The goal of this research is to improve the detection performance of fluctuating targets with low SCR in radar systems using DP-TBD. In addition, the computational complexity of multiframe TBD is reduced. The effect of non-Gaussian distributed background clutter is also considered. The research objectives for this work are as follows.

1. Develop a new algorithm based on order statistics dynamic programming track-before-detect (OS-DP-TBD) to improve the target detection and tracking performance.

2. Develop a new multiframe expanding window (EW)-TBD technique with reasonable computational complexity compared to the existing sliding and batch window multiframe techniques.

3. Investigate several finite duration target scenarios which assume the target is not present in all scans to assess the effectiveness of the proposed technique in detecting a target.

4. Study the effect of different types of non-Gaussian clutter such as Weibull, K and $G0$

distributions on the proposed techniques.

5. Investigate the detection performance of the proposed algorithm with extended targets having different energy spillover levels and point targets.

1.4 Organization of the Dissertation

The remainder of this dissertation is organized as follows. Chapter 2 presents the proposed order statistics dynamic programming track-before-detect OS-DP-TBD technique for Weibull distributed clutter. A new expanding window multiframe technique is given which uses order statistics dynamic programming in each processing window. Simulation results are provided to verify the performance of the proposed techniques. Chapter 3 discusses the performance of the proposed OS-DP-TBD algorithm with non-Gaussian distributed clutter and complex Gaussian noise. Swerling type 1 and 3 targets in K distributed clutter and Swerlin type 0 and 1 targets in $G0$ distributed clutter are evaluated in this chapter. Extended targets with different target energy spillover and complex Gaussian noise are considered in Chapter 4. Swerling type 0, 1 and 3 extended targets with different target energy spillover in Weibull distribution background clutter are also discussed in this chapter. Chapter 5 summarizes the dissertation and presents suggestions for future work.

Chapter 2

Expanding Window Multiframe Order Statistics Dynamic Programming Track-Before-Detect in Weibull Distributed Clutter

2.1 Introduction

Target detection is an important task in radar signal processing and is typically the first step. This determines whether a target is present in a resolution cell by comparing the decision statistic with a threshold. The results are then processed by traditional tracking algorithms [15], [16]. Conventional algorithms [7] make a detection decision each frame and then use the results for tracking. These techniques suffer from performance degradation especially when the target signal to noise ratio (SNR) is low. In this case, the target signal is often discarded since the detection technique only maintains measurements above

an intensity threshold which results in low detection performance. Track-before-detect (TBD) techniques employ joint target detection and tracking and are effective in low SNR environments. A decision on the presence of a target is made using several consecutive frames of data [17], [9]. TBD uses no threshold or a very low threshold in order to capture low SNR radar measurements and then detection and tracking is conducted [18].

Various methods have been used to implement TBD such as the Hough transform [11], particle filtering [13], and maximum likelihood probabilistic data association (ML-PDA) [12]. Dynamic programming (DP) is commonly employed for the integration of consecutive frames in TBD. DP-TBD was introduced in [19] and applied to radar systems in [20] and [16]. Multi-target TBD problem was considered in [21]. The target is detected and tracked as the maximum of the energy which is integrated recursively over N frames [22]. The integration is done over consecutive scans using scoring functions along physically admissible trajectories and produces the possible tracks with the highest function values [23]. DP-TBD has been shown to be effective with slow maneuvering targets [24].

The scoring function for the radar scan data is the main focus of DP-TBD research because it plays an essential role in the solution. The amplitude of the radar data was employed in [8]. In [25], the logarithm of likelihood ratio (LLR) of both the target-present and null-target hypotheses was used. DP-TBD using the LLR as the scoring function results in better detection and tracking performance than using the amplitude of the radar measurements [14]. Both of these functions consider only the magnitude of the radar data in each resolution cell. The phase information was considered in [26] to improve DP-TBD detection performance. In particular, the logarithm of the complex data based likelihood ratio (LCLR) was used as the scoring function. Depending on the range and azimuth resolution, the target may appear as a point in some radar systems and there will be target

energy spillover in other systems. This chapter assumes there is sufficient resolution so only point targets are considered.

The Weibull distribution was first validated with land clutter returns observed by high-resolution radars. The Weibull distribution is used in many applications, such as weather forecasting and data fitting of all kinds, while it is widely applied in radar systems to model the dispersion of the received signals level produced by some types of clutters [27] The skewness of this distribution was shown to increase as the radar depression angle decreased [28]. Recently, this distribution used to characterize weather clutter and sea clutter. These results motivate the use of the Weibull clutter model [28].

Order statistics (OS) is a well known technique which is widely employed in wireless communication systems which are affected by fading [29]. It has shown to be effective with different types of fading distributions with unknown parameters. This chapter considers the detection of Swerling type 0, 1 and 3 targets in heterogeneous background clutter which is Weibull distributed. The logarithm of the envelope likelihood ratio (LELR) is used as the scoring function in a DP-TBD technique. The contributions of this chapter are as follows.

1. Order statistic DP-TBD (OS-DP-TBD) is proposed which selects the best candidate targets in each scan. The proposed algorithm provides a significant improvement in detection performance compared to basic DP-TBD in [26].

2. Expanding window TBD (EW-TBD) is proposed to improve the detection performance while keeping the computational complexity low compared to the batch window and sliding window techniques in [30].

3. Several finite duration target scenarios which assume the target is not present in all scans are considered to assess the effectiveness of the proposed EW-TBD technique

in detecting a target.

The rest of the chapter is organized as follows. The system model and notation are given in Section 2.2. Section 2.3 provides the problem formulation and the OS-DP-TBD technique is introduced in Section 2.4. Section 2.5 presents the proposed expanding window TBD (EW-TBD) method. The performance of the OS-DP-TBD and EW-TBW techniques are evaluated in Section 2.6 for Swerling type 0, 1 and 3 targets. Finally, some concluding remarks are given in Section 2.7.

2.2 System Model and Notation

In this section, the dynamic target model and measurement model are introduced.

2.2.1 Dynamic Target Model

We assume a two-dimensional surveillance radar in the range-azimuth plane. The surveillance region consists of $N_r \times N_b$ cells where $N_r = R/\Delta_r$ and $N_b = \omega/\Delta_b$ are the number of range and azimuth cells, respectively. R is the maximum range while ω is the azimuth extension of the surveillance region. The range resolution Δ_r is determined by the waveform bandwidth B, i.e. $\Delta_r = c/(2B)$ where c is the speed of light. The azimuth resolution Δ_b is given by the 3-dB beamwidth.

Let N be the number of consecutive frames processed with DP-TBD. The target is assumed to move in the surveillance region with target state in the nth frame given by

$$\boldsymbol{x}_n = [x_{n,r}, v_{n,r}, x_{n,b}, v_{n,b}]', \qquad 1 \leq n \leq N, \tag{2.1}$$

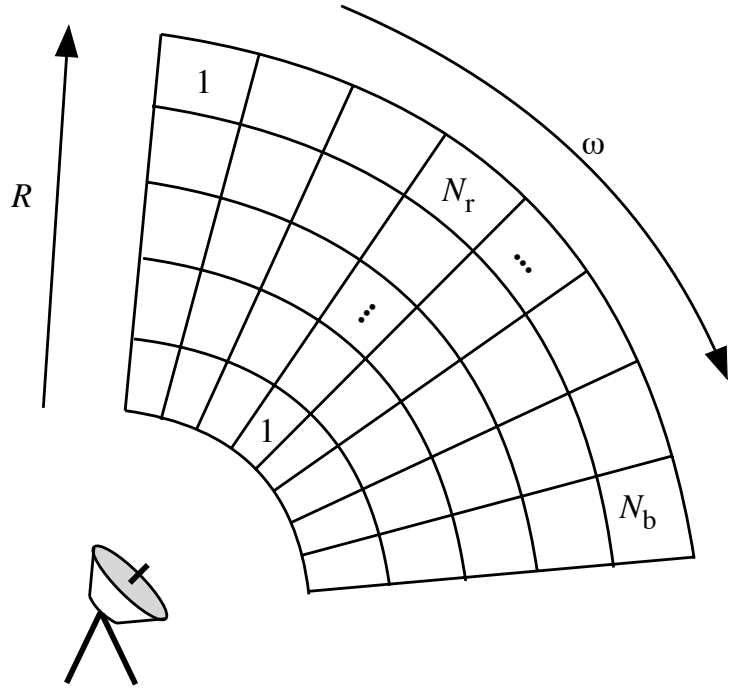

Figure 2.1: The radar surveillance region in the range and azimuth dimensions.

where $'$ denotes transpose, $x_{n,r}$ and $x_{n,b}$ are the range and azimuth target positions, respectively, and $v_{n,r}$ and $v_{n,b}$ are the range and azimuth target velocities, respectively. The target state evolution can be described by the Markov process

$$\boldsymbol{x}_{n+1} = F\boldsymbol{x}_n + \nu_n, \tag{2.2}$$

where ν_n is independent and identically distributed (i.i.d.) Gaussian noise and F is the transition matrix given by

$$F = I_2 \otimes \begin{bmatrix} 1 & T \\ 0 & 1 \end{bmatrix}, \tag{2.3}$$

where $\otimes$ is the Kronecker product, I_2 is the two-dimensional identity matrix, and T is the time between consecutive scans. This model is suitable for slow moving targets. Although a single target is considered in this chapter, the proposed technique can easily be extended

to multiple targets.

2.2.2 Measurement Model

The observation region is divided into $N_r \times N_b$ resolution cells, and it is assumed that a target can only occupy and affect one cell at a given time as shown in Fig. 4.1. When a target is present in resolution cell (r, b), $1 \leq r \leq N_r$, $1 \leq b \leq N_b$, the radar measurement is given by

$$z_n^{r,b} = A_n \exp(j\phi_n) + C_n^{r,b}, \tag{2.4}$$

where A_n is the amplitude of the complex measurement of the target in the nth scan, ϕ_n is the corresponding target phase which is assumed to be uniformly distributed over $[0, 2\pi)$, and $C_n^{r,b}$ denotes i.i.d. clutter which is assumed to be Weibull distributed. If there is no target, the measurement in cell (r, b) in the nth frame is given by

$$z_n^{r,b} = C_n^{r,b}, \tag{2.5}$$

with amplitude

$$a_n^{r,b} = |z_n^{r,b}|,$$

where $1 \leq r \leq N_r,\ 1 \leq b \leq N_b,\ 1 \leq n \leq N$.

The measurements for frame n can be expressed as

$$\boldsymbol{z}_n = [z_n^{1,1}, \cdots, z_n^{1,N_b}, \cdots, z_n^{N_r,N_b}]'. \tag{2.6}$$

The measurements for the N frames can be expressed as an $N_r N_b \times N$ matrix

$$\mathbf{Z}_{1:N} = [z_1, z_2, \ldots, z_N], \tag{2.7}$$

where $\mathbf{Z}_{1:N}$ denotes columns 1 to N.

The Swerling models were introduced in [15] to describe the statistical properties of the radar cross-sections of targets. The scattering of the electromagnetic energy from a target depends on many factors such as target geometry, size, shape, viewing aspect and polarization. The models for Swerling type 0, 1 and 3 targets are given below.

Swerling Type 0 Target

The Swerling type 0 model describes an idealized target without any fluctuations (constant radar cross-section) and constant amplitude A_n given by

$$A_n = \sqrt{\sigma_t}, \tag{2.8}$$

where σ_t is the mean squared target amplitude.

Swerling Type 1 Target

For the Swerling type 1 model, the radar cross-section is constant from pulse to pulse, but varies independently from scan to scan. The target amplitude A_n is Rayleigh distributed with probability density function (PDF)

$$P(A_n) = \frac{2A_n}{\sigma_t} \exp\left(-\frac{A_n^2}{\sigma_t}\right). \tag{2.9}$$

Swerling Type 3 Target

For the Swerling type 3 model, the radar cross-section is constant during the radar antenna dwell time, but varies from scan to scan. The target amplitude A_n is chi-square distributed with four degrees of freedom and PDF

$$P(A_n) = \frac{8\ A_n^3}{\sigma_t^2} \exp\left(-\frac{2\ A_n^2}{\sigma_t}\right). \tag{2.10}$$

2.2.3 Weibull Distributed Clutter

Clutter is a term used to describe any object that generates unwanted radar return backscatter. In many cases, the clutter signal level is much higher than the receiver noise level. The ability of a radar to detect targets embedded in clutter depends on the Signal-to-Clutter Ratio (SCR) [2]. Clutter includes earth surface echoes (terrain and sea), weather echoes (rain and clouds), and man-made clutter such as chaff clouds which consist of strips of reflective material. Clutter echoes differ from both target echoes and noise, and can appear as either a target or noise [3]. The mean and variance of the Weibull distributed clutter are

$$\mu = A\Gamma\left(1 + \frac{1}{B}\right), \tag{2.11}$$

$$Var = A^2\left(\Gamma\left(1 + \frac{2}{B}\right) - \left(\Gamma\left(1 + \frac{1}{B}\right)\right)^2\right), \tag{2.12}$$

respectively [2], $\Gamma(.)$ denotes the Gamma function and A and B are the Weibull scale and shape parameters, respectively. The Weibull distribution has been used to model clutter at low grazing angles (less than five degrees) for frequencies between 1 GHZ and 10 GHZ [2]. Further, shadowing at low grazing angles can hide large scatterers so that the

clutter distribution has long tails. The PDF of the Weibull distribution is

$$f(x|A,B) = \frac{B}{A}(x/A)^{(B-1)}e^{-(x/A)^B}. \tag{2.13}$$

Figure 4.2 shows the effect of changing B on the PDF with scale parameter $A = 1$. For

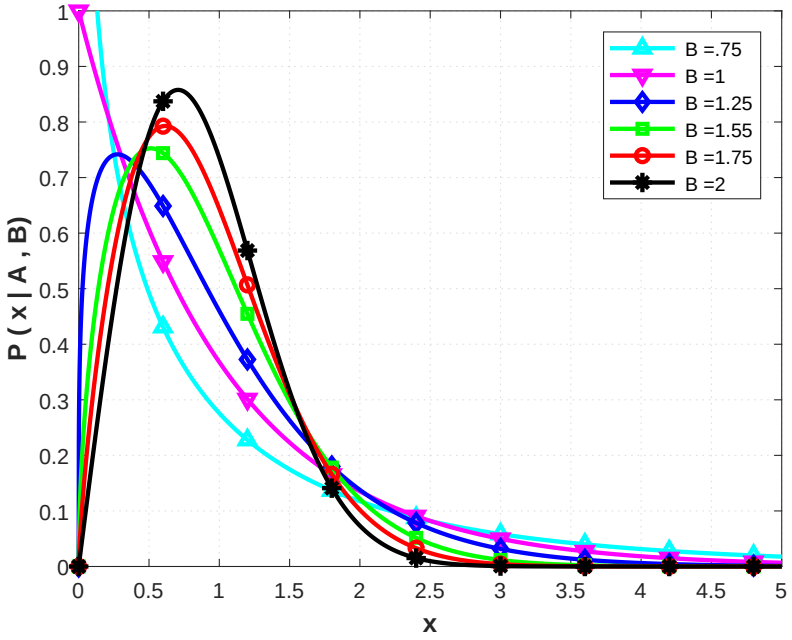

Figure 2.2: The PDF of the Weibull distribution for values of the shape parameter B.

$B = 2$, the Weibull distribution becomes a Rayleigh distribution, and for small values of B the tail is long. For $B \leq 1$, the Weibull distribution becomes an exponential distribution. In this chapter, the SCR is defined as

$$SCR = 10\log_{10}\left(\frac{\sigma_t}{\sigma_c}\right), \tag{2.14}$$

where σ_c denotes the mean of the Weibull distributed clutter power.

2.3 Problem Formulation

At the nth scan, a list of candidate targets is obtained through the receiver processing chain consisting of matched filtering, moving target detection, CFAR (constant false alarm rate), detection, clustering and data extraction. In this chapter a low pre-processing threshold is employed with the radar measurements (4.5) to provide a good tradeoff between performance and computational complexity. The sequence of candidate targets acquired at scan n is $m_n = 1, 2, \ldots, M_n$. This may include false targets due to the background clutter.

The DP-TBD algorithm has two steps. First a decision is made concerning whether a target is present or not. Then the trajectories which are most likely to correspond to actual targets are extracted. For the N consecutive scans $\boldsymbol{Z}_{1:N}$, the integration process is given by [31]

$$I(\boldsymbol{x}_n|\boldsymbol{Z}_{1:n}) = \max_{x_{n-1}\in\Omega(x_n)} I(\boldsymbol{x}_{n-1}|\boldsymbol{Z}_{1:n-1}) + S(\boldsymbol{z}_n|\boldsymbol{x}_n), \tag{2.15}$$

where $I(\boldsymbol{x}_n|\boldsymbol{Z}_{1:n})$ is the merit function for state x_n, $S(z_n|x_n)$ is the scoring function [14], [26], and $\Omega(x_n)$ is the set of states at scan $(n-1)$ for which a transition to x_n is possible and is given by

$$\Omega(\boldsymbol{x}_n) = \arg \max_{\boldsymbol{x}_{n-1}\in\Omega(\boldsymbol{x}_{n-1})} I(\boldsymbol{x}_{n-1}). \tag{2.16}$$

The following commonly employed DP-TBD scoring functions are considered.

1. Amplitude scoring function [31], [8]

$$S(\boldsymbol{z}_n|\boldsymbol{x}_n) = a_n^{x_{rn},x_{bn}}. \tag{2.17}$$

2. Squared amplitude (SA) scoring function [22]

$$S(\boldsymbol{z}_n|\boldsymbol{x}_n) = (a_n^{x_{rn},x_{bn}})^2. \tag{2.18}$$

3. Logarithm of envelope likelihood ratio (LELR) scoring function [16], [32]

$$S(\boldsymbol{z}_n|\boldsymbol{x}_n) = \ln\left(\frac{P(\boldsymbol{a}_n|\boldsymbol{x}_n)}{P(\boldsymbol{a}_n)}\right), \tag{2.19}$$

where $\boldsymbol{a}_n = [a_n^{1,1}, \ldots, a_n^{1,N_r}, \ldots, a_n^{N_r,N_b}]$ is the amplitude vector for the nth scan.

It was shown in [33] that DP-TBD with the LELR scoring function (4.20) provides better performance than with (4.18) or (4.19). This is due to the use of both clutter-only and clutter-plus-target distributions. The LELR for the three Swerling types are given below [26].

1. Swerling 0 model

$$L_E(\boldsymbol{a}_n|\boldsymbol{x}_n) = -\frac{2A_n^2}{\sigma_c}\sum_{r=1}^{N_r}\sum_{b=1}^{N_b}\ln\left(I_0\left(\frac{2A_n a_n^{r,b}}{\sigma_c}\right)\right), \tag{2.20}$$

where $I_0(.)$ is the modified first order Bessel function.

2. Swerling 1 model

$$\begin{aligned} L_E(\boldsymbol{a}_n|\boldsymbol{x}_n) &= -\frac{1}{\sigma_c}\sum_{r=1}^{N_r}\sum_{b=1}^{N_b}\frac{\sigma_t}{\sigma_t+\sigma_c}\left(a_n^{r,b}\right)^2 \\ &+ \sum_{r=1}^{N_r}\sum_{b=1}^{N_b}\ln\left(\frac{\sigma_c}{\sigma_c+\sigma_t}\right). \end{aligned} \tag{2.21}$$

3. Swerling 3 model

$$
\begin{aligned}
L_E(\boldsymbol{a}_n|\boldsymbol{x}_n) &= \sum_{r=1}^{N_r}\sum_{b=1}^{N_b} \ln\left(\frac{4\sigma_c^2}{(2\sigma_c+\sigma_t)^2}\right) \\
&+ \sum_{r=1}^{N_r}\sum_{b=1}^{N_b} \ln\left(1+\frac{\sigma_t (a_n^{r,b})^2}{\sigma_c(\,2\sigma_c+\sigma_t)}\right) \\
&+ \frac{1}{\sigma_c}\sum_{r=1}^{N_r}\sum_{b=1}^{N_b} \frac{\sigma_t}{2\sigma_c+\sigma_t}\left(a_n^{r,b}\right)^2 . \qquad (2.22)
\end{aligned}
$$

2.4 Order Statistics Dynamic Programming TBD (OS-DP-TBD) with Complex Gaussian Noise

Order statistics (OS) is used to determine the best candidate targets in a radar scan. This controls the number of targets to be processed based on the merit function values. Prior work uses thresholding to extract the targets to be processed. However, thresholding offers little control over the number of targets and so the workload per batch can vary greatly. Order statistics fixes the number of candidate targets and thus provides a known processing workload. Back-tracking is then used to estimate the trajectories of these targets. Pseudo code for the order statistics dynamic programming track-before-detect (OS-DP-TBD) algorithm is given in Algorithm 4.1.

The algorithm requires the following input parameters: number of integration frames N, dimensions of the range and azimuth cells N_r and N_b, respectively, the scan frames to be processed F_n and the number of ordered candidate targets to be processed D. D is a design parameter that is a compromise between detection performance and computational complexity. If the value of D is high the detection performance will be improved, but the processing time will be increased. In this chapter, $D = N_r \times N_b/100$ is employed which

Algorithm 2.1 The OS-DP-TBD Algorithm with Complex Gaussian Noise and Weibull Distributed Clutter

Input: N, N_r, N_b, F, D, d_r, d_b

1: **for** $n = 1$ to N **do**
2: $[\boldsymbol{X}_n, M_n]$ = point_threshold(F, n);
3: **end for**
4: **for** $n = 1$ to N **do**
5: **if** $n = 1$ **then**
6: **for** $m = 1, 2, \ldots, M_n$ **do**
7: $I(\boldsymbol{x}_{n,m}) = S(\boldsymbol{z}_n|\boldsymbol{x}_{n,m})$;
8: $\Omega(\boldsymbol{x}_{n,m}) = Null$;
9: **end for**
10: **else**
11: **for** $m = 1, 2, \ldots, M_n$ **do**
12: $I(\boldsymbol{x}_{n,m}) = \max_{x_{n-1} \in \Omega(x_{n,m})} I(\boldsymbol{x}_{n-1,m}) + S(\boldsymbol{z}_n|\boldsymbol{x}_{n,m})$;
13: $\Omega(\boldsymbol{x}_{n,m}) = \arg \max_{\boldsymbol{x}_{n-1} \in \Omega(\boldsymbol{x}_{n-1})} I(\boldsymbol{x}_{n-1,m})$;
14: **end for**
15: **end if**
16: **end for**
17: Ordered_targets_list = SORT $(I(\boldsymbol{x}_{N,M_N}))$;
18: Best_targets = SELECT (Ordered_targets_list, D);
19: Search_zone = CONE(d_r, d_b);
20: Trajectory = BACKTRACK (Best_targets, Search_zone);

was determined to provide good performance with reasonable complexity. As discussed in Section 2.2, N_r and N_b depend upon the range and azimuth resolution of the radar system, respectively. d_r and d_b are the number of cells that the target can move to in the next scan in the range and azimuth directions, respectively, according to the motion model.

Line 2 applies the *point_threshold* function to the nth frame to extract the number of potential targets M_n and their associated states

$$\boldsymbol{X}_n = [\boldsymbol{x}_{n,1},\ \boldsymbol{x}_{n,2},\ \cdots,\ \boldsymbol{x}_{n,M_n}],$$

where $\boldsymbol{x}_{n,m}$ is the state vector for candidate target m, $1 \leq m \leq M_n$. The pre-processing

threshold on the the received measurements $\boldsymbol{z}_n$ at each scan is a key factor in the computational complexity of the proposed algorithm. An adaptive pre-processing threshold is used here which is $0.1 \times \text{mean}(\boldsymbol{z}_n)$.

Lines 4 to 16 evaluate the merit function $I(\boldsymbol{x}_{n,m})$ and $\Omega(\boldsymbol{x}_{n,m})$ for each scan. $\Omega(\boldsymbol{x}_{n,m})$ in lines 8 and 13 is the set of target states in the $(n-1)$th scan from which a transition to $\boldsymbol{x}_n$ is possible and is used to identify potential target trajectories.

The scoring function $S(\boldsymbol{z}_n|\boldsymbol{x}_{n,m})$ in lines 7 and 12 is evaluated using (4.21), (4.23) and (4.25) for Swerling type 0, 1 and 3 targets, respectively.

Lines 4 to 9 initialize the merit function $I(\boldsymbol{x}_{1,m})$ and $\Omega(\boldsymbol{x}_{1,m})$ for states $\boldsymbol{x}_{1,m}$.

Lines 11 to 14 integrate the merit function values $I(\boldsymbol{x}_{n,m})$ and $\Omega(\boldsymbol{x}_{n,m})$ for all candidate target states $\boldsymbol{x}_{n,m}$ in the nth scan obtained using the scoring function, $2 \leq n \leq N$.

Line 17 applies the OS-DP-TBD algorithm to the candidate targets in the last scan N to sort the merit function values $I(\boldsymbol{x}_{N,M_N})$ in the last scan.

Line 18 selects the D best targets that have the highest merit scores.

Line 19 uses the parameters d_r and d_b to define the search zone in the previous scan relative to the position of the selected target in the current scan.

Line 20 constructs the target trajectories using backtracking. The D best targets in the last scan were selected. The trajectory for each target is built using the corresponding search zones. Moving targets with a constant velocity are considered in this chapter.

2.5 Proposed Expanding Window Technique

Before discussing the proposed expanding window TBD technique, we review the batch and sliding window techniques proposed in [30]. We also define several performance measures

for the batch, sliding window and expanding window TBD processing techniques. These measures are related to the processing workload required to produce a detection decision and the ability of a technique to detect a finite duration target.

Most of the research on multiframe processing assumes that a target exists in the surveillance region starting at the first scan [34]. However, in practical situations a target may exist only after several scans and can disappear after a limited number of scans. Thus, expanding window TBD (EW-TBD) is proposed to detect and track a finite duration target which may appear at any scan and not necessarily the first. A moving target is the most difficult to detect and track but is also the most realistic model.

2.5.1 Batch Window Processing

Batch window processing considers several consecutive frames as one processing window. Dynamic programming is used to integrate the target energy by exploiting the space-time correlation among consecutive frames to improve detection performance. DP-TBD jointly processes the entire window of N frames and outputs the final merit values. Figure 2.3 illustrates the batch processing mechanism where $N = 4$ frames are jointly processed to make a target detection decision after 4 frames. The red boxes in the figure indicate when a target detection decision is made.

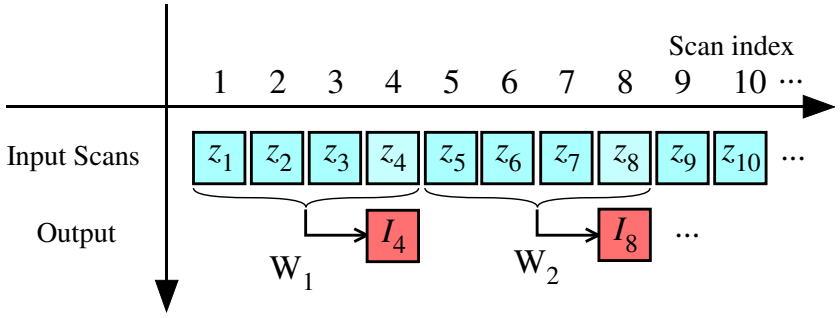

Figure 2.3: Batch window processing for window size $N = 4$.

The choice of the window size N is a compromise. Small values of N reduce the computational complexity with reduced target detection probability. Conversely, large values of N increase the computational complexity but reduce the probability of target detection. However, the detection performance suffers if the target trajectory covers only part of the batch window. For example, if a target trajectory or track has length $N = 4$ but starts in frame 3 and ends in frame 6 in Fig. 2.3, then batches W_1 and W_2 will each have only two frames that contain a target. This degrades the detection probability compared to other starting points even though the target trajectory is equal to the window size N. In fact, the maximum number of windows that can contain a target of length N is only 1.

Throughput is defined as the number of detection decisions per scan. Thus, the throughput of batch window processing is

$$Th_B = \frac{1}{N}. \tag{2.23}$$

The workload per output is defined as the number of scans that must be processed to obtain a detection decision. Thus, the batch window processing workload per output is

$$U_B = N. \tag{2.24}$$

The workload per frame is defined as the number of frames that are processed at a given frame. The batch window processing workload per frame is

$$V_B = 1. \tag{2.25}$$

2.5.2 Sliding Window Processing

Sliding window TBD (SW-TBD) processing considers N consecutive frames and moves forward by one scan each step to include the N latest frame measurements. Figure 2.4 shows the sliding window technique where each window processes $N = 4$ scans. Two consecutive windows share $N - 1$ frames, so each frame is processed in N consecutive windows.

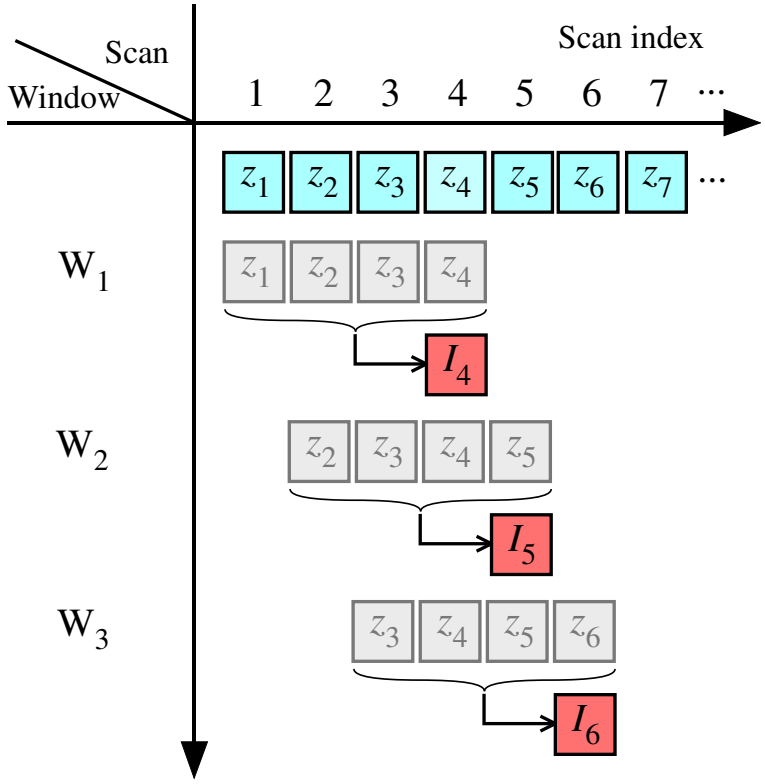

Figure 2.4: Sliding window processing for window size $N = 4$.

Similar to batch window processing, the choice of a window size N is a compromise. The main advantage of the sliding window technique is that a target trajectory of length N will be covered completely by one of the sliding windows. If as in the previous example a target trajectory of length $N = 4$ starts in frame 3 and covers frames $3 - 6$, then window W_3 in Fig. 2.4 will completely cover the target trajectory. Therefore, the probability of detection is high regardless of the location of the target trajectory in the frame sequence.

Ignoring the initial latency, the sliding window processing throughput is

$$Th_S = 1, \tag{2.26}$$

the workload per output is

$$U_S = N, \tag{2.27}$$

and the workload per frame is

$$V_S = N. \tag{2.28}$$

2.5.3 Expanding Window Processing

The proposed expanding window (EW-TBD) technique for multiframe processing has been developed to have low computational complexity and high detection probability. This technique uses a variable window size between a minimum window size N_1 and a maximum window size $N_2 = 2N_1 - 1$. The choice of the window size limits is a compromise between computational complexity and detection performance. Figure 2.5 illustrates this technique with $N_1 = 4$ and $N_2 = 7$. Window W_1 has size $N_1 = 4$ while window W_2 has size 5. The input for W_2 is obtained from the output of W_1 and the scoring function for z_5. This is indicated by the arrow connecting z_4 and z_5. The windows keep expanding to provide outputs until window W_4 which has maximum size $N_2 = 2N_1 - 1 = 7$. Then the window size returns to N_1.

Similar to the sliding window technique, a target trajectory of any length N will be covered completely by at least one of the expanding windows. For example, if a target trajectory has length $N = 4$ but starts in frame 3 and covers frames $3 - 6$, then windows W_3 and W_4 in Fig. 2.5 will completely cover the target trajectory. Therefore the target

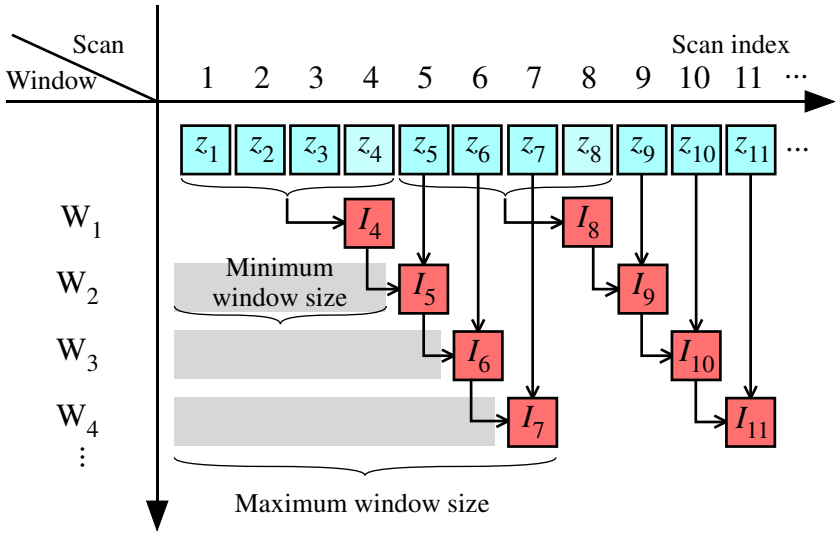

Figure 2.5: Expanding window processing with $N_1 = 4$ and $N_2 = 7$.

probability of detection is improved compared to the batch window technique regardless of the location of the target trajectory in the frame sequence. The number of windows that contain a target of length N varies between 1 and N.

Ignoring the initial latency, the expanding window processing throughput is

$$Th_E = 1. \tag{2.29}$$

For one period in Fig. 2.5, the processing required to produce N outputs is $2N - 1$. The expanding window workload per output is then

$$U_E = \frac{2N-1}{N} = 2 - \frac{1}{N}, \tag{2.30}$$

and the workload per scan is

$$V_E = 2. \tag{2.31}$$

Table 2.1 gives the throughput and workload of the three TBD window techniques.

Table 2.1: Throughout and Workload of Three TBD Window Techniques

Technique	**Throughput**	**Workload per Output**	**Workload per Frame**
	(Th)	(U)	(V)
Batch Window	$1/N$	N	1
Sliding Window	1	N	N
Expanding Window	1	$2-1/N$	2

This shows that batch window processing has the lowest throughput and the sliding and expanding windows have a throughput that is N times higher. However, this increased throughput results in more target tracking information which should prove useful for target detection and classification [35]. Furthermore, the throughput of batch window processing decreases with increasing window size while the throughput of SW-TBD and EW-TBD is independent of the window size. The workload per output for the batch and SW-TBD techniques is N, while for the proposed EW-TBD approaches a fixed value of 2 as N increases. This is much less than with the other two techniques even for moderate values of N. The workload per frame for batch window processing and EW-TBD is constant whereas for SW-TBD it increases with increasing window size. Thus, the proposed EW-TBD technique provides a good tradeoff between throughout and workload.

2.6 Performance Results

The performance of the proposed techniques is examined in this section. First, the performance of OS-DP-TBD is presented for Swerling type 0, 1 and 3 targets. These results are compared with those with DP-TBD to demonstrate the improvement with the proposed

algorithm. Then the performance of EW-TBD is evaluated. We define the probability of detection P_D as the probability of determining the target trajectory within 2 cells of the actual target cell throughout the entire trajectory. The probability of false alarm P_{fa} defined as the probability of detecting a false track in absence of target. The P_D vs SNR curves of the proposed algorithm are set based on the desired P_{fa} which assumed to be 10^{-4} in this chapter. Moreover, SNR is defined as

$$\text{SNR} = 10\log_{10}\left(\frac{\sigma_t}{\sigma_n}\right), \tag{2.32}$$

where σ_n is the complex Gaussian noise power.

The position root-mean-squared error (RMSE), which is a valid metric as long as the track stays on the target, is defined as

$$RMSE = \frac{1}{MN}\sum_{m=1}^{M}\sum_{n=1}^{N}\sqrt{(\hat{x}_{r,n}^{m} - x_{r,n}^{m})^2 + (\hat{x}_{b,n}^{m} - x_{b,n}^{m})^2}, \tag{2.33}$$

where $(\hat{x}_{r,n}^{m}, \hat{x}_{b,n}^{m})$ and $(x_{r,n}^{m}, x_{b,n}^{m})$ are the estimated and true target positions at the nth scan during the mth simulation, respectively. The simulation parameters are $N_r = 50$, $N_b = 50$, and number of integration frames $N = 5$ and 10. The scale and shape parameters for the Weibull distribution are $A = 1$ and $B = 1.7$, respectively. The number of simulation trials was $100,000$ for each probability of detection result. Simulation results were obtained from MATLAB. Long running simulations were performed on WestGrid using the MATLAB.

2.6.1 OS-DP-TBD Performance

The detection performance of OS-DP-TBD using the LELR score function for Swerling type 0, 1 and 3 targets is shown in Figs. 2.6, 2.7 and 2.8, respectively, for $N = 5$. Basic-

DP-TBD in these figures denotes LELR-DP-TBD [26] with no spillover of target energy in adjacent cells. OS-DP-TBD performs better than basic DP-TBD because of the noncoherent intraframe integration with the order statistics algorithm. Fig. 2.6 shows that the gain with OS-DP-TBD over basic DP-TBD for $P_D = 0.5$ and a Swerling type 0 target is 1.81 dB.

Figure 2.7 for Swerling type 1 shows that the performance gain is 1.21 dB. Figure 2.8 for Swerling type 1 shows that the performance gain is 1.13 dB.

Table 2.2: Performance Gain of OS-DP-TBD Compared with Basic DP-TBD for $N = 5$ and $P_D = 0.5$.

Swerling Type	**Performance Gain (dB)**
0	1.81 $\longrightarrow$ from Fig. 2.6
1	1.21 $\longrightarrow$ from Fig. 2.7
3	1.13 $\longrightarrow$ from Fig. 2.8

Table 2.2 gives the performance gain of OS-DP-TBD over basic DP-TBD for Swerling type 0, 1 and 3 targets, $N = 5$ and $P_D = 0.5$. This shows that the improvement with the proposed technique is between 1 and 2 dB. Further, the processing gain of the proposed algorithm increases with the number of integration frames, but the workload also increases.

The detection performance of OS-DP-TBD for Weibull distributed background clutter and $N = 5$ and 10 is shown in Figs. 2.9, 2.10 and 2.11 for Swerling type 0, 1, and 3 targets, respectively. These results indicate that as the number of integration frames N increased from 5 to 10, the detection performance improves. The detection performance with different scale and shape parameters for the Weibull distributed clutter and $N = 10$ for Swerling type 0, 1, and 3 targets is given in Figs. 2.12, 2.13 and 2.14, respectively. These results indicate that as the shape parameter increases towards 2, the detection performance improves. The

corresponding RMSE values are shown in Fig.2.15 for different types of Swerling targets 0, 1 and 3 to evaluate the estimated trajectory compared with the actual trajectory in each case. Figure 2.15 shows that as the SNR increased the difference between the estimated trajectory and the actual trajectory in each case of Swerling target type 0, 1 and 3 decreased.

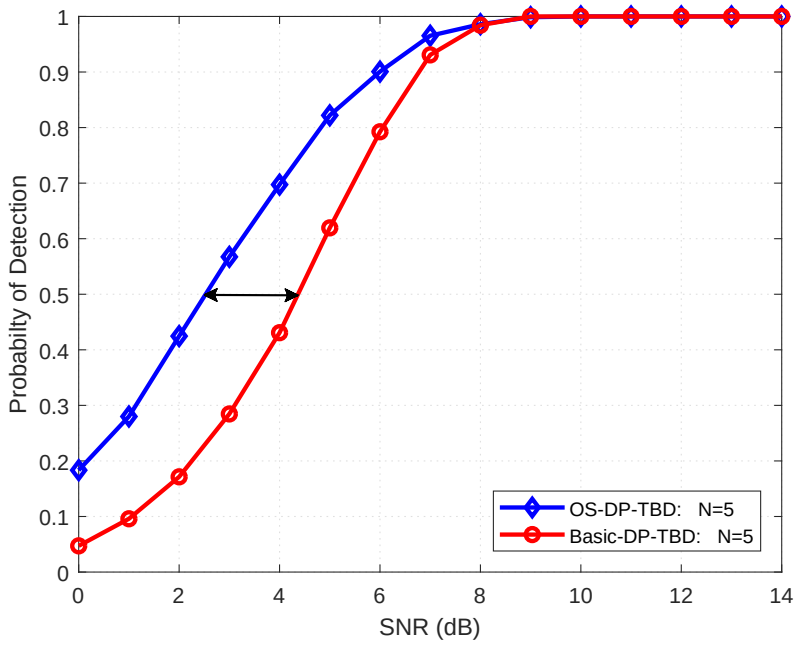

Figure 2.6: Probability of detection of a Swerling 0 target using OS-DP-TBD and Basic DP-TBD with complex Gaussian distributed noise and $N = 5$.

2.6.2 EW-TBD Performance

In this section, the effect of the target duration (start scan to end scan) on the performance of DP-TBD is investigated. Two multiframe DP-TBD techniques are investigated. The first is the proposed OS-DP-TBD algorithm and the second is the proposed EW-TBD technique. Three target scenarios are considered as discussed below.

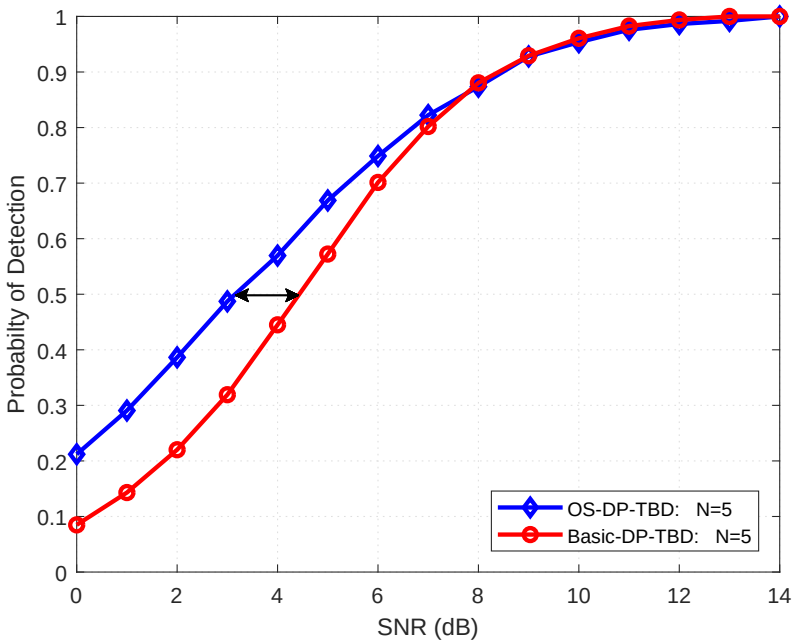

Figure 2.7: Probability of detection of a Swerling 1 target using OS-DP-TBD and Basic DP-TBD with complex Gaussian distributed noise and $N = 5$.

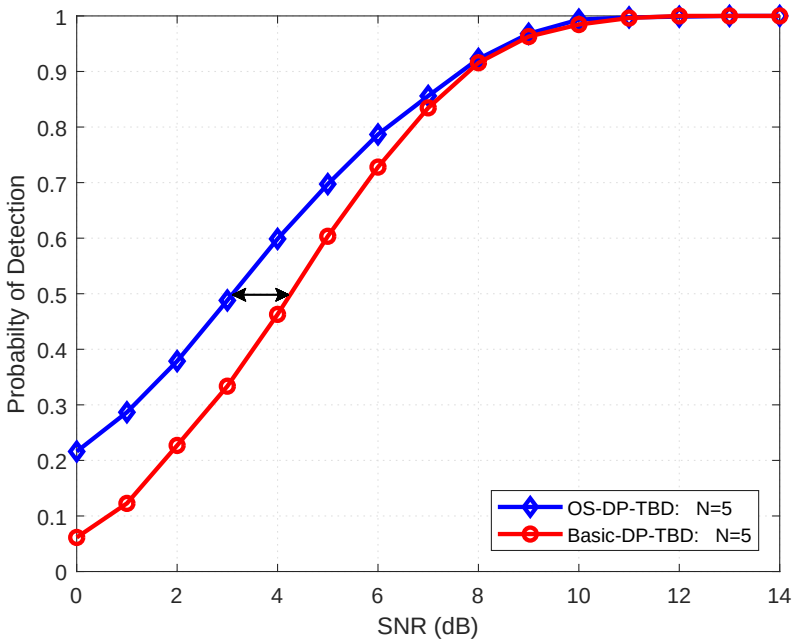

Figure 2.8: Probability of detection of a Swerling 3 target using OS-DP-TBD and Basic DP-TBD with complex Gaussian distributed noise and $N = 5$.

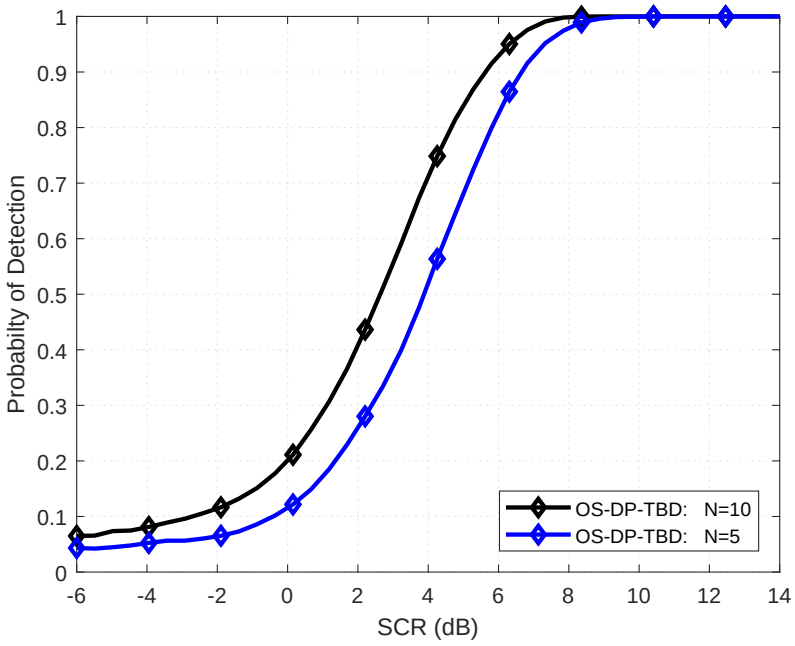

Figure 2.9: Probability of detection of a Swerling 0 target with Weibull distributed clutter and $N = 5$ and 10.

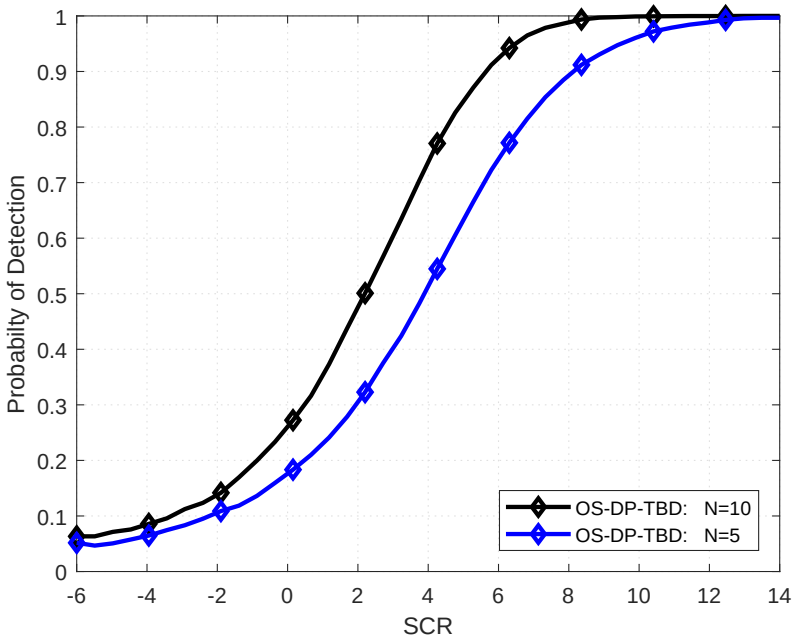

Figure 2.10: Probability of Detection of a Swerling 1 target with Weibull distributed clutter and $N = 5$ and 10.

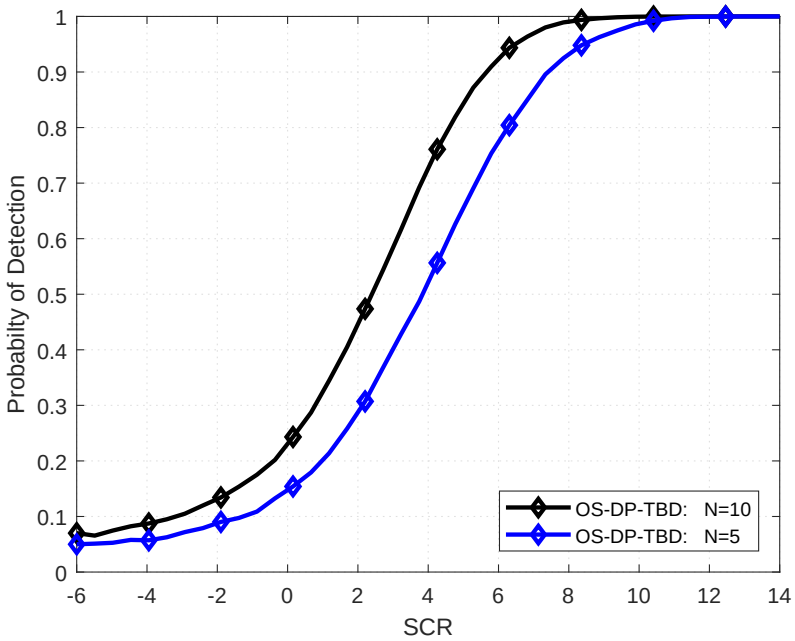

Figure 2.11: Probability of detection of a Swerling 3 target with Weibull distributed clutter and $N = 5$ and 10.

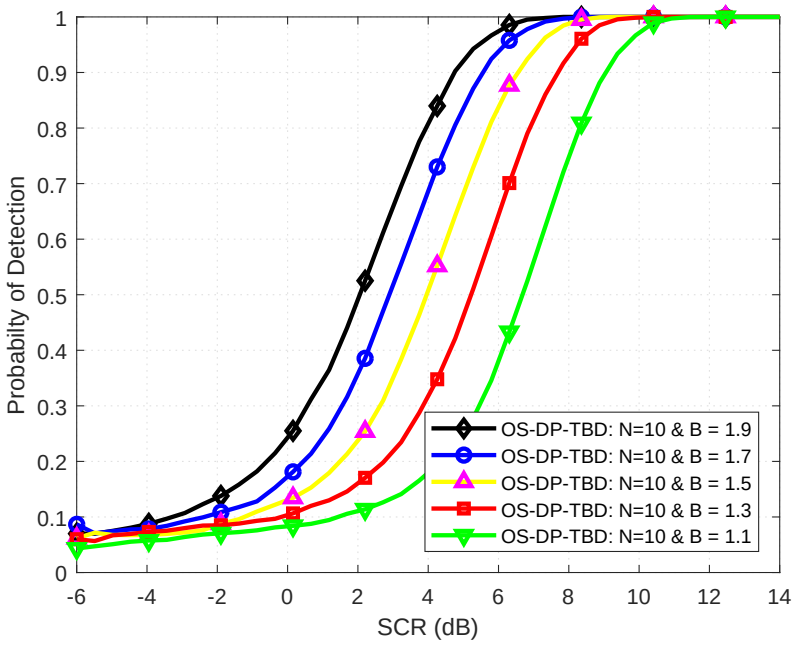

Figure 2.12: OS-DP-TBD probability of detection of a Swerling 0 target with Weibull distributed clutter for different shape parameters B, and scale parameter $A = 1$ and $N = 10$.

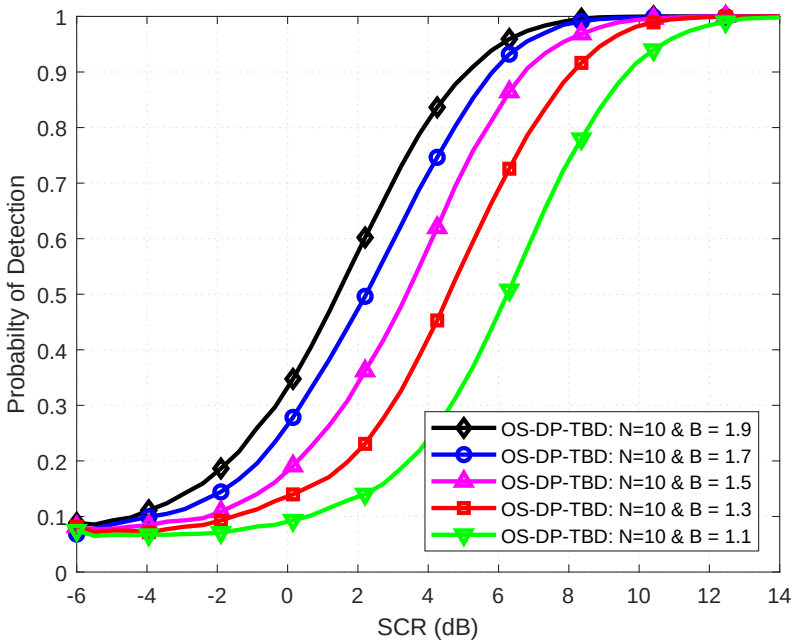

Figure 2.13: OS-DP-TBD probability of detection of a Swerling 1 target with Weibull distributed clutter for different shape parameters B, and scale parameter $A = 1$ and $N = 10$.

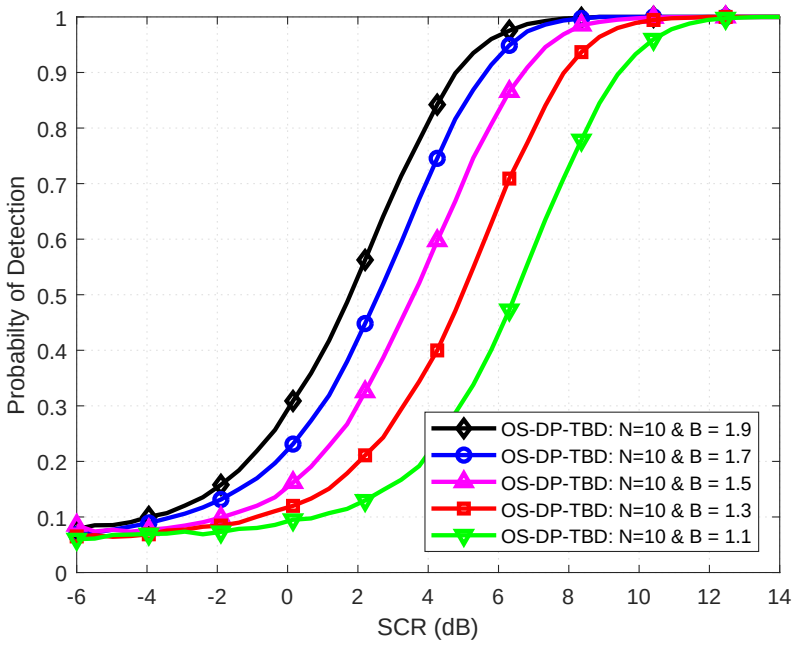

Figure 2.14: OS-DP-TBD probability of detection of a Swerling 3 target with Weibull distributed clutter for different shape parameters B, and scale parameter $A = 1$ and $N = 10$.

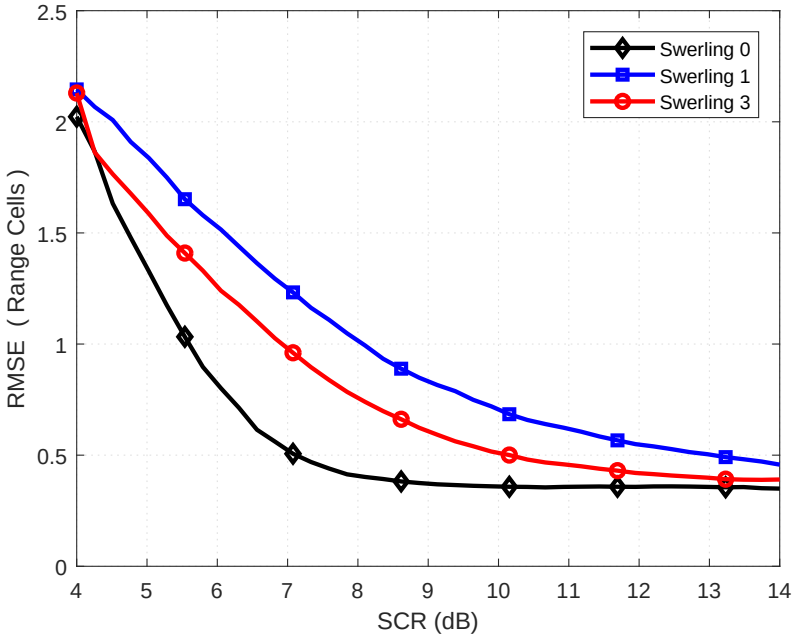

Figure 2.15: RMSE of different Swerling target of types 0, 1 and 3 with Weibull distributed clutter for $N = 5$.

Case 1

In this case the target is present in all scans. Figure 2.16 shows the received signal amplitude for four scans in Weibull distributed clutter with SCR = 10 dB. An asterisk $*$ indicates that the target is present in the scan and a white circle indicates the target location.

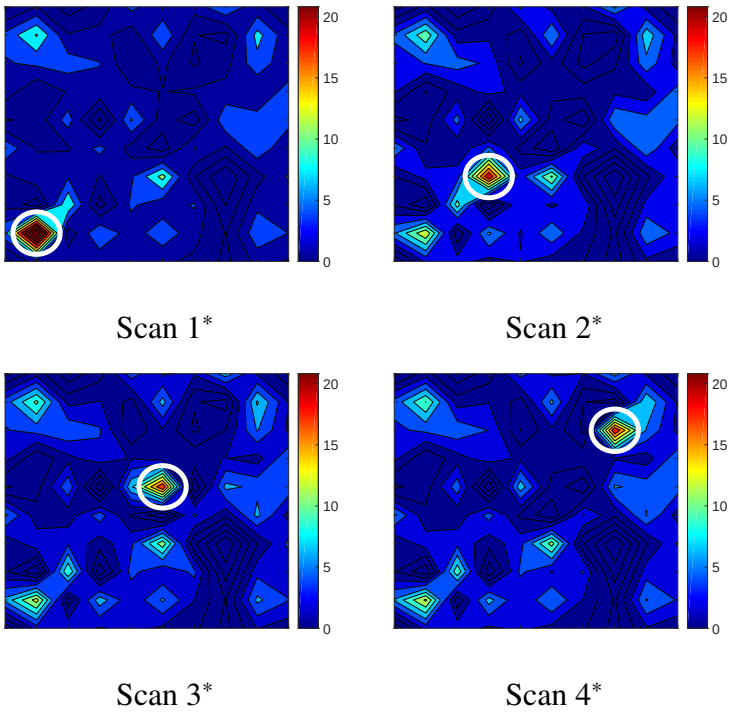

Figure 2.16: Received signal amplitude for four scans in Weibull distributed clutter with SCR = 10 dB. An asterisk $*$ indicates that the target is present in the scan and a white circle indicates the target location.

Figure 2.17 presents the detection performance of batch window processing using order statistics with $N = 4$ and EW-TBD for $N_2 = 5, 6$ and 7. Batch window processing has the worst performance because the batch window covers only 4 frames while the target duration is 5 frames. EW-TBD provides better performance as shown by the red line which corresponds to a window that covers the entire target duration. Moreover, the blue and black lines are similar because the expanded windows W_3 and W_4 in Fig. 2.5 cover the target

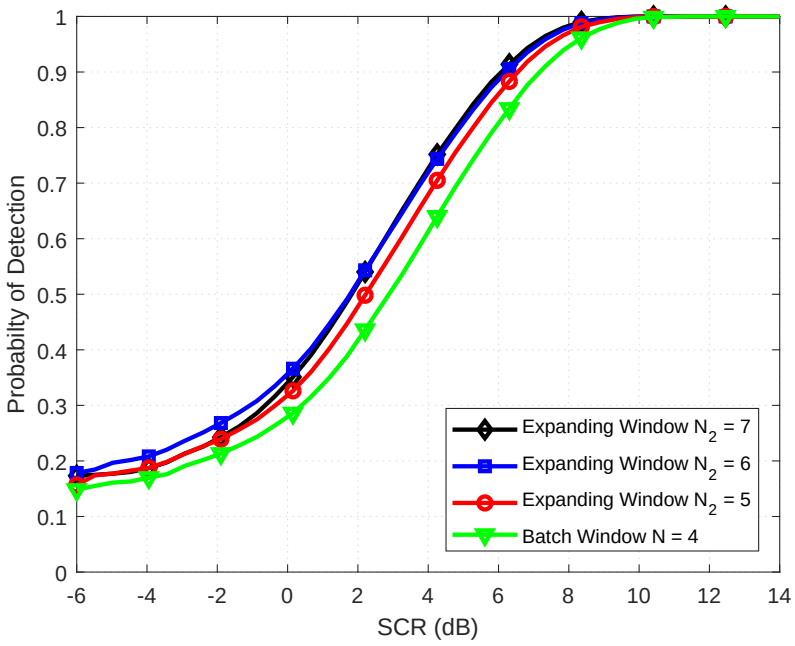

Figure 2.17: Probability of detection with expanding window processing for Case 1.

duration and any new frames which contain only clutter. The expanded windows W_3 and W_4 decrease the effect of the background clutter while maintaining the detection performance. In addition, the difference in performance between batch and expanding window processing is not significant because both techniques cover all the target duration.

Case 2

In this case the target is present for a finite duration as it appears in only scans 4 to 7. Figure 2.18 shows the received signal amplitude for eight scans in Weibull distributed clutter with SCR = 10 dB. An asterisk $*$ indicates that the target is present in the scan and a white circle indicates the target location. Figure 2.19 shows the detection performance of batch processing using order statistics with $N = 4$ and EW-TBD with $N_2 = 5$, 6 and 7. The performance with batch window processing is poor because the target only appears in the last scan of the first window. Further, this technique requires waiting N frames to process

another batch to detect this target. On the other hand, EW-TBD can detect the target at $N_2 = 5$, and the detection performance improves as the number of integration frames N_2 increases. Moreover, there is no latency in detection with EW-TBD and the workload is reasonable. This case is more practical than Case 1 because there is no restriction on when the target appears in the scans.

Case 3

In this case the target is present for a finite duration as it appears in only scans 3 to 6. Figure 2.21 shows the received signal amplitude for eight scans in Weibull distributed clutter with SCR = 10 dB. An asterisk $*$ indicates that the target is present in the scan and a white circle indicates the target location.

Figure 2.20 shows the detection performance for batch processing using order statistics and EW-TBD. The green line represents the batch window technique using order statistics for $N = 4$, and the blue, red and black lines represent EW-TBD for $N_2 = 5$, 6 and 7, respectively. Batch processing provides the worst performance because the batch window covers only 2 of the 4 frames which have a target. EW-TBD provides better performance as shown by the blue line when the expanded window W_2 covers 3 of the frames with a target. The red line is the best because the target duration is completely covered by W_3 in Fig. 2.5. The detection performance improves as N_2 increases from $N_1 \leq N_2 \leq 2N_1 - 1$. EW-TBD with $N_2 = 7$ gives the best performance with reasonable workload. However, batch window processing must wait until the second output with W_2 in Fig. 2.3.

2.7 Conclusion

This chapter considered the detection of fluctuating targets in Weibull distribution clutter. An OS-DP-TBD algorithm was proposed and evaluated for Swerling type 0, 1 and 3 targets. In addition, an expanding window technique EW-TBD for multiframe integration was proposed. It was shown that EW-TBD outperforms conventional batch window processing in terms of both detection performance and computational complexity. Simulation results were presented which show that the proposed OS-DP-TBD performs better than basic DP-

TBD with a gain of 1 to 2 dB. Furthermore, the effect of Weibull distributed clutter was examined. It was shown that the performance with EW-TBD is better than batch window processing with reasonable computational complexity and no latency.

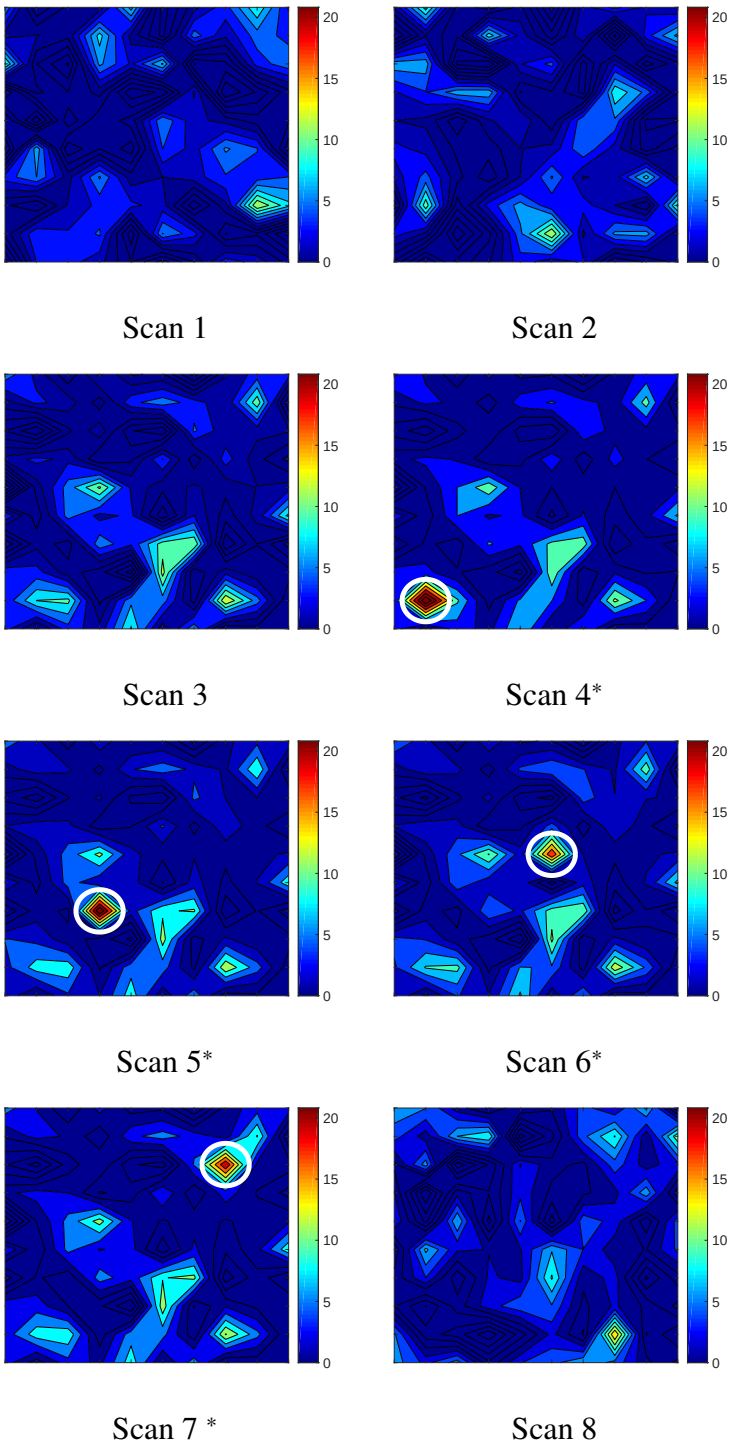

Figure 2.18: Received signal amplitude for eight scans in Weibull distributed clutter with SCR = 10 dB. An asterisk $*$ indicates that the target is present in the scan and a white circle indicates the target location.

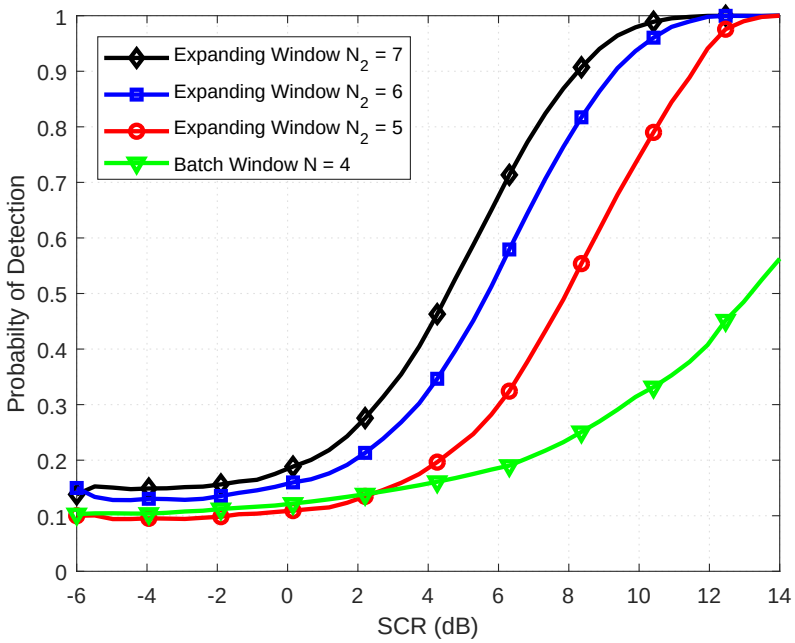

Figure 2.19: Probability of detection with expanding window processing for Case 2.

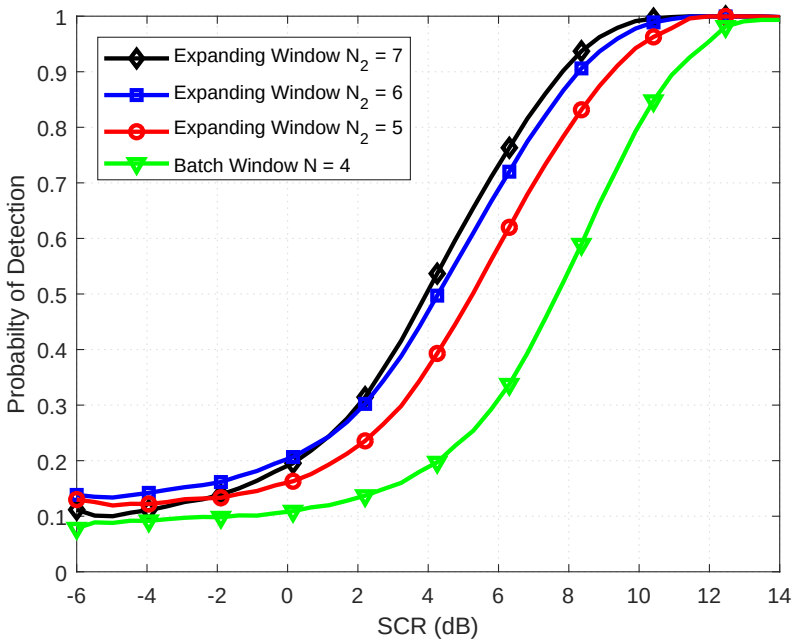

Figure 2.20: Probability of detection with expanding window processing for Case 3.

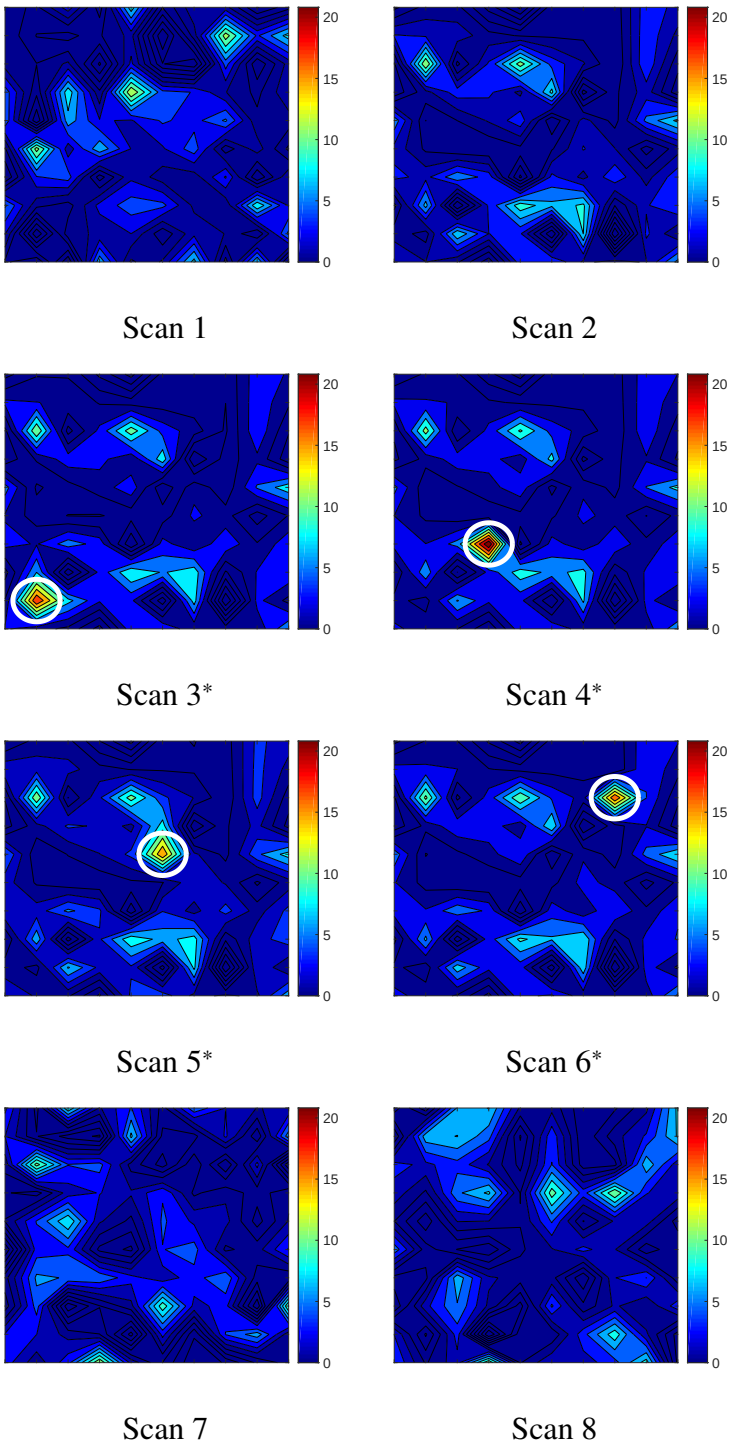

Figure 2.21: Received signal amplitude for eight scans in Weibull distributed clutter with SCR = 10 dB. An asterisk $*$ indicates that the target is present in the scan and a white circle indicates the target location.

Chapter 3

Order Statistics Dynamic Programming Track-Before-Detect in Non-Gaussian Clutter

3.1 Introduction

Early detection and tracking of moving targets is of great importance in modern radar systems. Target detection is a challenging task in radar signal processing and is typically the first step. This determines whether a target is present in a resolution cell by comparing the decision statistic with a threshold. The result is then processed by traditional tracking algorithms [15], [36]. Conventional detection and tracking algorithms [7] make a detection decision each frame and then use the results for tracking. However, these techniques provide poor performance when the target signal to clutter and noise ratio (SCNR) is low. In this case, the target signal may be discarded as only results above a given threshold are retained. Track-before-detect (TBD) techniques employ joint target detection and tracking and are

effective in low SCNR environments. A decision on the presence of a target is made using several consecutive frames of data [17], [9]. TBD uses a low or no threshold to ensure targets are captured for the detection and tracking process [18].

Recent studies on DP-TBD have determined that radar systems have significant heterogeneous background clutter [33]. In addition, the data obtained with a small grazing angle or high resolution radar from a heterogeneous terrain (e.g. urban and forested areas), is not Gaussian distributed. Experiments with HF surface wave radar [37] have shown that the clutter is highly heterogeneous. Thus, Gaussian and Rayleigh distributions are not suitable because of the heterogeneity of the surveillance region. Radar clutter is better modeled as compound-Gaussian. The Weibull, log-normal, K and $G0$ distributions are commonly used compound-Gaussian distributions in radar systems. The $G0$ distribution was first proposed in [38]. It can model extremely heterogeneous clutter in urban and forest areas which cannot be adequately described with other distributions. DP-TBD was investigated in [14] with the clutter received from high resolution radar and small grazing angles modeled as $G0$ distributed. The K distribution is a standard model employed for radar clutter [39] which was first proposed in [40]. In [36], DP-TBD was examined with heavy-tailed clutter modeled as K distributed.

The scoring function of the radar scan data is the main focus of DP-TBD research because it plays an essential role in detection and tracking. The amplitude of the radar data was employed in [8]. In [25], the log-likelihood ratio (LLR) of both the target-present and null-target hypotheses was used. DP-TBD using a LLR scoring function was shown in [14] to provide better detection and tracking performance than DP-TBD using an amplitude scoring function. Both of these functions consider only the magnitude of the radar data in each resolution cell. The phase information was considered in [26] to improve DP-TBD

detection performance. The logarithm of the complex data based likelihood ratio (LCLR) was used as the scoring function. Depending on the range and azimuth resolution, the target may appear as a point in some radar systems and there will be target energy spillover in other systems. This chapter assumes there is sufficient resolution so only point targets are considered.

This chapter considers the detection of Swerling type 0, 1 and 3 targets in non-Gaussian distributed clutter. The logarithm of the envelope likelihood ratio (LELR) is used as the scoring function in a DP-TBD system. The contributions of this chapter are as follows.

1. Order statistic DP-TBD (OS-DP-TBD) is proposed which selects the best candidate targets in each scan with non-Gaussian distributed clutter and complex Gaussian noise.

2. The detection and tracking of Swerling type 1 and 3 targets in K distributed clutter is evaluated using the proposed OS-DP-TBD technique.

3. The detection and tracking of Swerling type 0 and 1 targets in $G0$ distributed clutter is evaluated using the proposed OS-DP-TBD technique.

The rest of the chapter is organized as follows. The system model and notation are given in Section 3.2. Section 3.3 provides the problem formulation. The non-Gaussian clutter distributions are presented in Section 3.4, and the proposed OS-DP-TBD technique is introduced in Section 3.5. The performance of the proposed OS-DP-TBD technique is evaluated in Section 3.6 for Swerling type 0, 1 and 3 targets with complex Gaussian noise and non-Gaussian distributed clutter. Finally, some concluding remarks are given in Section 3.7.

3.2 System Model and Notation

In this section, the dynamic target model and measurement model are introduced.

3.2.1 Dynamic Target Model

We assume a two-dimensional surveillance radar in the range-azimuth plane as shown in Fig. 4.1. The surveillance region consists of $N_r \times N_b$ cells where $N_r = R/\Delta_r$ and $N_b = \omega/\Delta_b$ are the number of range and azimuth cells, respectively. R is the maximum range and ω is the azimuth extension of the surveillance region. The range resolution Δ_r is determined by the waveform bandwidth B, i.e. $\Delta_r = c/(2B)$ where c is the speed of light. The azimuth resolution Δ_b is given by the 3-dB beamwidth.

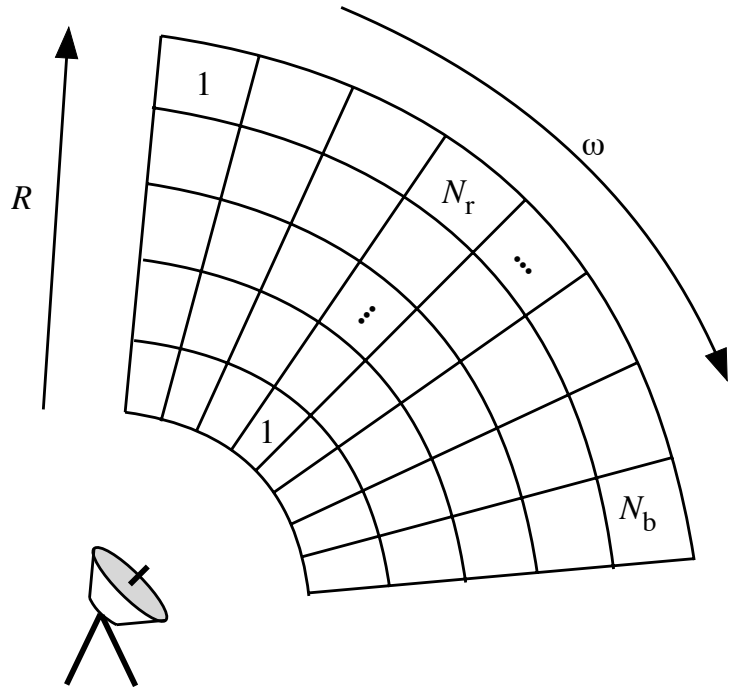

Figure 3.1: The radar surveillance region in the range and azimuth dimensions.

Let N be the number of consecutive frames processed with DP-TBD. The target is

assumed to move in the surveillance region with target state in the nth frame given by

$$\boldsymbol{x}_n = [x_{rn}, v_{rn}, x_{bn}, v_{bn}]', \qquad 1 \leq n \leq N \tag{3.1}$$

where $'$ denotes transpose, x_{rn} and x_{bn} are the range and azimuth target positions, respectively, and v_{rn} and v_{bn} are the range and azimuth target velocities, respectively. The target state evolution can be described by the Markov process

$$\boldsymbol{x}_{n+1} = F\boldsymbol{x}_n + \nu_n, \tag{3.2}$$

where ν_n is independent and identically distributed (i.i.d.) Gaussian noise and F is the transition matrix given by

$$F = I_2 \otimes \begin{bmatrix} 1 & T \\ 0 & 1 \end{bmatrix}, \tag{3.3}$$

where $\otimes$ denotes the Kronecker product, I_2 is the two-dimensional identity matrix, and T is the time between consecutive scans. This model is suitable for slow moving targets. Although a single target is considered in this chapter, the proposed technique can easily be extended to multiple targets.

3.2.2 Measurement Model

The observation region is divided into $N_r \times N_b$ resolution cells, and it is assumed that a target can only occupy and affect one cell at any given time. When a target is present in resolution cell (r, b), $1 \leq r \leq N_r$, $1 \leq b \leq N_b$, the radar measurement is given by

$$z_n^{r,b} = A_n \exp(j\phi_n) + C_n^{r,b} + \nu_n, \tag{3.4}$$

where A_n is the amplitude of the complex target measurement in the nth scan, ϕ_n is the target phase in the nth scan which is assumed to be uniformly distributed over $[0, 2\pi)$, $C_n^{r,b}$ denotes i.i.d. clutter which is assumed to be non-Gaussian distributed, and ν_n is additive noise which is assumed to be complex Gaussian distributed. If there is no target, the measurement in cell (r, b) in the nth frame is given by

$$z_n^{r,b} = C_n^{r,b} + \nu_n, \tag{3.5}$$

with amplitude

$$a_n^{r,b} = |z_n^{r,b}|.$$

The measurements for N frames can be expressed as

$$\boldsymbol{z}_n = \{z_n^{r,b}\},\ 1 \le r \le N_r,\ 1 \le b \le N_b,\ 1 \le n \le N, \tag{3.6}$$

which in vector form is $\mathbf{Z}_{1:N} = [\boldsymbol{z}_1, \boldsymbol{z}_2, \ldots, \boldsymbol{z}_N]$.

The Swerling models were introduced in [15] to describe the statistical properties of the radar cross-sections of targets. The scattering of the electromagnetic energy from a target depends on many factors such as target geometry, size, shape, viewing aspect and polarization. The models for Swerling type 0, 1 and 3 targets are given below.

Swerling Type 0 Target

The Swerling 0 model describes an idealized target without any fluctuations (constant radar cross-section) and constant amplitude given by

$$A_n = \sqrt{\sigma_t}, \tag{3.7}$$

where σ_t is the mean squared target amplitude.

Swerling Type 1 Target

In the Swerling 1 model, the radar cross-section is constant from pulse to pulse, but varies independently from scan to scan. The target amplitude A_n is Rayleigh distributed with probability density function (PDF)

$$P(A_n) = \frac{2A_n}{\sigma_t} \exp\left(-\frac{A_n^2}{\sigma_t}\right). \tag{3.8}$$

Swerling Type 3 Target

In the Swerling 3 model, the radar cross-section is constant during the radar antenna dwell time, but varies from scan to scan. The target amplitude A_n is Chi-square distributed with four degrees of freedom and PDF

$$P(A_n) = \frac{8\ A_n^3}{\sigma_t^2} \exp\left(-\frac{2\ A_n^2}{\sigma_t}\right). \tag{3.9}$$

3.3 Problem Formulation

At the nth scan, a list of candidate targets is obtained through the receiver processing chain consisting of matched filtering, moving target detection, constant false alarm rate (CFAR), detection, clustering and data extraction. In this chapter a low threshold is employed with the radar measurements (4.5) to provide a good tradeoff between performance and computational complexity. The sequence of candidate targets acquired at scan n is $m_n = 1, 2, \ldots, M_n$. This may include false targets due to the background clutter and noise.

The DP-TBD algorithm has two steps. First a decision is made concerning whether a

target is present or not. Then the trajectories which are most likely to correspond to actual targets are extracted. The consecutive scans $\boldsymbol{Z}_{1:N}$ can be expressed as $\boldsymbol{Z}_{1:N} = [z_1, z_2, \ldots, z_N]$. The integration process is given by [31]

$$I(\boldsymbol{x}_n|\boldsymbol{Z}_{1:n}) = \max_{x_{n-1}\in\Omega(x_n)} I(\boldsymbol{x}_{n-1}|\boldsymbol{Z}_{1:n-1}) + S(\boldsymbol{z}_n|\boldsymbol{x}_n), \tag{3.10}$$

where $I(\boldsymbol{x}_n|\boldsymbol{Z}_{1:n})$ is the merit function for state x_n, $S(z_n|x_n)$ is the scoring function [14, 26], and $\Omega(x_n)$ is the set of states at scan $(n-1)$ for which a transition to x_n is possible and is given by

$$\Omega(\boldsymbol{x}_n) = \arg \max_{\boldsymbol{x}_{n-1}\in\Omega(\boldsymbol{x}_{n-1})} I(\boldsymbol{x}_{n-1}). \tag{3.11}$$

The following commonly employed DP-TBD scoring functions are considered.

1. Amplitude scoring function [31], [8]

$$S(\boldsymbol{z}_n|\boldsymbol{x}_n) = a_n^{x_{rn},x_{bn}}. \tag{3.12}$$

2. Squared amplitude (SA) scoring function [22]

$$S(\boldsymbol{z}_n|\boldsymbol{x}_n) = (a_n^{x_{rn},x_{bn}})^2. \tag{3.13}$$

3. Logarithm of the envelope likelihood ratio (LELR) scoring function [16], [32]

$$S(\boldsymbol{z}_n|\boldsymbol{x}_n) = \ln\left(\frac{P(\boldsymbol{a}_n|\boldsymbol{x}_n)}{P(\boldsymbol{a}_n)}\right), \tag{3.14}$$

where $\boldsymbol{a}_n = \left[a_n^{1,1}, \ldots, a_n^{1,N_r}, \ldots, a_n^{N_r,N_b}\right]$ is the amplitude vector for the nth scan.

It was shown in [33] that DP-TBD with the LELR scoring function (4.20) provides better performance than (4.18) or (4.19). This is due to the use of both the clutter-only and clutter-plus-target distributions. Thus in this chapter, the LELR scoring function is considered.

3.4 Non-Gaussian Clutter Distributions

Clutter is a term used to describe anything that generates unwanted radar return backscatter. High resolution radars that operate at small grazing angles have heterogeneous surveillance regions and the clutter returns cannot be considered as stationary random processes. For this reason, Gaussian and Rayleigh distributions are not suitable for the clutter [41]. In addition, as the size of a radar resolution cell decreases, the clutter distribution becomes heavily-tailed compared to the Rayleigh distribution. Thus, high-resolution radar with non-Gaussian distributed background clutter is investigated here.

3.4.1 K Distributed Clutter

A wide range of recorded clutter returns have been analyzed and fit to the K distribution [40]. Compound K-distributed clutter consists of two components of the amplitude of the envelope of the clutter returns. The first is the local mean y with PDF $P(y)$ modelled as Chi distributed. The second is the speckle component which has a Rayleigh distribution $P(z|y)$ with mean y. The PDF of the K distribution is given by [36]

$$P(z) = \int_0^\infty P(z|y)P(y)\,dy, \tag{3.15}$$

with

$$P(z|y) = \frac{2z}{y} \exp\left(-\frac{z^2}{y}\right), \tag{3.16}$$

and

$$P(y) = \frac{y^{\alpha-1}}{\beta^{\alpha}\Gamma(\alpha)} \exp\left(-\frac{y}{\beta}\right). \tag{3.17}$$

Evaluating the integral in (3.15) gives

$$P(z;\alpha,\beta) = \frac{4z^{\alpha}}{\sqrt{\beta}^{\alpha+1}\Gamma(\alpha)} \boldsymbol{K}_{\alpha-1}\left(\frac{2z}{\sqrt{\beta}}\right), \tag{3.18}$$

and the corresponding cumulative distribution function (CDF) is

$$F(z;\alpha,\beta) = 1 - \frac{2z^{\alpha}}{\sqrt{\beta}^{\alpha}\Gamma(\alpha)} \boldsymbol{K}_{\alpha-1}\left(\frac{2z}{\sqrt{\beta}}\right), \tag{3.19}$$

where α is the shape parameter, β is the scale parameter, $\Gamma(\cdot)$ is the Gamma function, and $\boldsymbol{K}_{\nu}$ denotes the modified Bessel function of the second kind. The K-distribution can be considered as a Rayleigh distribution modulated by a Gamma distribution with finite moments given by [42]

$$m_n = \boldsymbol{E}[z^n] = \sqrt{\beta}^{n} \frac{\Gamma(1+\frac{n}{2})\Gamma(\alpha+\frac{n}{2})}{\Gamma(\alpha)}. \tag{3.20}$$

Figure 3.2 shows the effect of changing the shape parameter α and scale parameter β on the distribution. The shape parameter α is a measure of clutter peakedness, and a lower value of α corresponds to higher clutter peakedness. The red line in Fig. 3.2 is for $\alpha = 0.1$ and indicates a very heavy-tailed and peaked clutter distribution. Increasing the value of $\alpha \geq 0.5$ decreases the tail of the distribution. As $\alpha \to \infty$, the K-distribution approaches

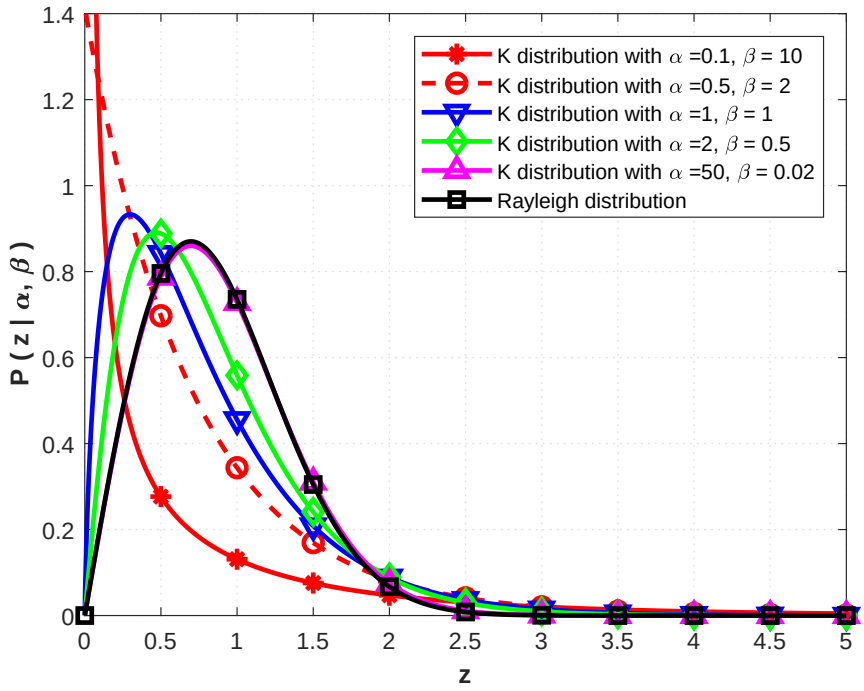

Figure 3.2: The PDF of the K distribution for values of the shape parameter α and scale parameter β.

the Rayleigh distribution.

The scoring function for Swerling type 1 and 3 targets in K-distributed clutter is considered in this subsection. The LELR in K-distributed clutter [36] is

$$L_E(\boldsymbol{z}_n|\boldsymbol{x}_n) = \ln\left(\frac{\sqrt{\beta}^{1-\alpha}\,{z_n}^{1-\alpha}\int_0^\infty f(y)\,dy}{2\boldsymbol{K}_{\alpha-1}\left(\frac{2z_n}{\sqrt{\beta}}\right)}\right), \tag{3.21}$$

and

$$L_E(\boldsymbol{z}_n|\boldsymbol{x}_n) = \ln\left(\frac{2\sqrt{\beta}^{1-\alpha}\,{z_n}^{1-\alpha}\int_0^\infty h(y)\,dy}{\boldsymbol{K}_{\alpha-1}\left(\frac{2z_n}{\sqrt{\beta}}\right)}\right), \tag{3.22}$$

for Swerling type 1 and 3 targets, respectively. The integrals $\int_0^\infty f(y)\,dy$ and $\int_0^\infty h(y)\,dy$

can be approximated using the trapezoidal rule [43]

$$\int_0^\infty w(y)\,dy = \sum_{i=0}^{N_s-1} \frac{w(y_i) + w(y_{i+1})}{2}\delta_i, \tag{3.23}$$

where N_s is the number of samples and $\delta_i = y_{i+1} - y_i$ is the sampling interval. This is used to evaluate the integrals in (3.21) and (3.22).

The trapezoidal rule typically uses a uniform grid to evaluate the integrals over discrete values of the integral variable y. However, both $f(y)$ and $h(y)$ have significant values only for small y and the remaining function values are small. Thus, using a fine uniform-grid is not efficient and will increase the computational complexity. One solution is to change the variable y using the substitution $y = \frac{1}{\eta^2}$. This change of variable has the effect of spreading the region where f and h have significant values and compressing the range where the functions have small values. The resulting functions are

$$f(\eta) = \frac{2\eta^{1-2\alpha}}{1+\eta^2\sigma_t} \exp\left(-\frac{z^2\eta^2}{1+\eta^2\sigma_t} - \frac{1}{\eta^2\beta}\right), \tag{3.24}$$

and

$$h(\eta) = \frac{2\eta^{1-2\alpha}(2+\sigma_t\eta^2+\sigma_t\eta^4z^2)}{(2+\eta^2\sigma_t)^3} \exp\left(-\frac{z^2\eta^2}{1+\eta^2\sigma_t} - \frac{1}{\eta^2\beta}\right). \tag{3.25}$$

To reduce the computational complexity two grids are used to cover the range of η. A fine uniform-grid is used for $\eta_i \in [0, 2\eta_p]$ where $\eta_p = \arg\max w(\eta)$, and a coarse non-uniform grid is used for $\eta_i \geq 2\eta_p + \sigma_i$ [42]

Substituting (3.24) and (3.25) in (3.21) and (3.22), respectively, the LELRs for Swerling

type 1 and 3 targets are given by

$$L_E(\boldsymbol{z}_n|\boldsymbol{x}_n) = \ln\left(\frac{\sqrt{\beta}^{1-\alpha}}{4}\right) + \ln\left(\frac{{z_n}^{1-\alpha}\sum_{i=1}^{N_s}\left(f(\eta_i)+f(\eta_{i+1})\right)\sigma_i}{\boldsymbol{K}_{\alpha-1}\left(\frac{2z_n}{\sqrt{\beta}}\right)}\right), \tag{3.26}$$

and

$$L_E(\boldsymbol{z}_n|\boldsymbol{x}_n) = \ln\left(\sqrt{\beta}^{1-\alpha}\right) + \ln\left(\frac{{z_n}^{1-\alpha}\sum_{i=1}^{N_s}\left(h(\eta_i)+h(\eta_{i+1})\right)\sigma_i}{\boldsymbol{K}_{\alpha-1}\left(\frac{2z_n}{\sqrt{\beta}}\right)}\right), \tag{3.27}$$

respectively, where σ_i is the sampling interval. For the fine uniform-grid

$$\sigma_i = \frac{2i\eta_p}{N_L - 1}, \qquad 0 \le i < N_L \tag{3.28}$$

where N_L is the number of discrete sample points in the lower range of η, and for the the coarse nonuniform-grid

$$\sigma_i = \Delta_0\, e^{i\gamma}, \qquad 0 \le i < N_U,\ \gamma > 1, \tag{3.29}$$

where

$$\Delta_0 = \left(\eta_U - \eta_p\right) \times \frac{1 - e^{2\gamma N_U}}{1 - e^{2\gamma}}, \tag{3.30}$$

N_U is the number of discrete sample points in the upper range of η, and η_U is the maximum value of η.

3.4.2 *G*0 Distributed Clutter

The *G*0 distribution was first proposed in [38] and is commonly used to model compound-Gaussian processes in radar systems. *G*0 distributed clutter can be interpreted as a Rayleigh

distribution whose mean squared value is inverse gamma-distributed [14]. If the mean squared value of the Rayleigh distribution is y, and given

$$P(z|y) = \frac{2z}{y} \exp\left(-\frac{z^2}{y}\right), \tag{3.31}$$

and

$$P(y) = \frac{\beta^\alpha y^{-\alpha-1}}{\Gamma(\alpha)} \exp\left(-\frac{\beta}{y}\right), \tag{3.32}$$

the PDF of the $G0$ distribution is [14]

$$\begin{aligned} P(z;\alpha,\beta) &= \int_0^\infty P(z|y)P(y)\,dy \\ &= \frac{2z\alpha\beta^\alpha}{\left(z^2+\beta\right)^{\alpha+1}}, \end{aligned} \tag{3.33}$$

where α and β are the the shape and scale parameters, respectively. Figure 3.3 shows the effect of changing the shape parameter α and scale parameter β on the distribution. The shape parameter α is a measure of clutter peakedness, and a smaller value of α results in more peakedness. The red line in Fig. 3.3 corresponds to $\alpha = 2$ and indicates a very heavy-tailed and peaked distribution. As $\alpha \to \infty$, the $G0$ distribution approaches the Rayleigh distribution. The LELRs for Swerling type 0 and 1 targets in $G0$ distributed clutter are [14]

$$L_E(\boldsymbol{z}_n|\boldsymbol{x}_n) = \left(\frac{(|z_n|^2+\beta)^{\alpha+1}}{\alpha\Gamma(\alpha)} \int_0^\infty g(y)\,dy\right), \tag{3.34}$$

and

$$L_E(\boldsymbol{z}_n|\boldsymbol{x}_n) = \left(\frac{(|z_n|^2+\beta)^{\alpha+1}}{\alpha\Gamma(\alpha)} \int_0^\infty s(y)\,dy\right), \tag{3.35}$$

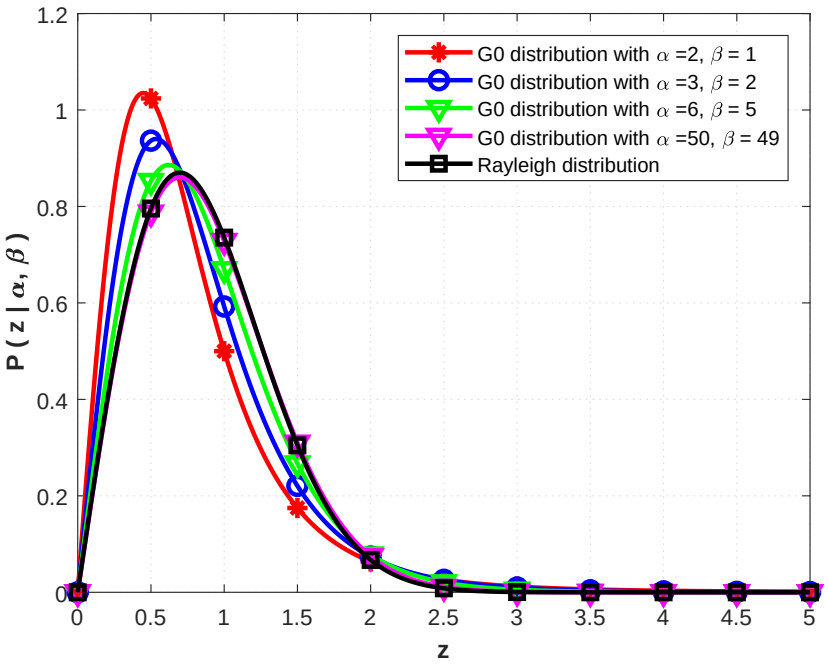

Figure 3.3: The PDF of the $G0$ distribution for values of the shape parameter α and scale parameter β.

respectively, where

$$g(y) = y^{-\alpha-2} \exp\left(\frac{|A_n|^2 + |z_n|^2 + \beta}{y} I_0\left(\frac{2|A_n|a_n}{y}\right)\right), \tag{3.36}$$

and

$$s(y) = \frac{y^{-\alpha-1}}{y + \sigma_t} \exp\left(-\frac{\beta}{y} - \frac{{a_n}^2}{y + \sigma_t}\right). \tag{3.37}$$

From Section 3.4.1, the trapezoidal rule [43] to approximate $L_E(\boldsymbol{z}_n|\boldsymbol{x}_n)$ which gives

$$L_E(\boldsymbol{z}_n|\boldsymbol{x}_n) = \frac{(|z_n|^2 + \beta)^{\alpha+1}}{\alpha\Gamma(\alpha)} \sum_{i=0}^{N_s-1} \frac{w(y_i) + w(y_{i+1})}{2} \delta_i, \tag{3.38}$$

where N_s is the number of samples and $\delta_i = y_{i+1} - y_i$ is the sampling interval. Further, $w(y_i) = g(y_i)$ and $w(y_i) = s(y_i)$ for Swerling type 0 and 1 targets, respectively. Evaluating

the Bessel function for Swerling type 0 targets and the large number of samples required for Swerling type 1 targets makes this approximation computationally complex. In [14], the following LELR approximations were given.

1. Swerling 0 model: The sum of the weighted incomplete gamma functions for a Swerling type 0 target in $G0$ distributed clutter is used to approximate the LELR and is given by

$$\begin{aligned} L_E(\boldsymbol{z}_n|\boldsymbol{x}_n) &= \left[\left(\frac{\Upsilon_L((\alpha+1), uq_1)}{{q_1}^{(\alpha+1)}}\right)\right. \\ &\quad + \left(\frac{|A_n|^2 + |z_n|^2 + \Upsilon_L((\alpha+3), uq_1)}{{q_1}^{(\alpha+3)}}\right) \\ &\quad \left. + \left(\frac{\Upsilon_U((\alpha+0.5), uq_2)}{2\sqrt{\pi|A_n|\boldsymbol{z}_n}{q_2}^{(\alpha+0.5)}}\right)\right] \\ &\quad \times \left(\frac{\left(\alpha + |z_n|^2\right)^{\alpha+1}}{\alpha\Gamma(\alpha)}\right), \end{aligned} \tag{3.39}$$

where

$$q_1 = |A_n|^2 + |z_n|^2 + \beta, \tag{3.40}$$

$$q_2 = (|z_n| - |A_n|)^2 + \beta, \tag{3.41}$$

$$u = \frac{1.827}{2|z_n||A_n|}, \tag{3.42}$$

and $\Upsilon_L(.)$ and $\Upsilon_U(.)$ are the lower and upper incomplete gamma functions, respectively.

2. Swerling 1 model: The LELR in (3.35) is evaluated using the trapezoidal rule with

uniform and nonuniform grids as discussed in Section 3.4.1. This gives

$$L_E(\boldsymbol{z}_n|\boldsymbol{x}_n) = \frac{\left(|z_n|^2 + \beta\right)^{\alpha+1}}{\alpha\Gamma(\alpha)} \left(\frac{\sum_{i=1}^{N_s} \left(s(\eta_i) + s(\eta_i + 1)\right) \sigma_i}{2} \right). \tag{3.43}$$

3.5 Order Statistics Dynamic Programming TBD (OS-DP-TBD)

Order statistics (OS) is used to determine the best candidate targets in a radar scan. This controls the number of targets to be processed based on the merit function values. Back-tracking is then used to estimate the trajectories of these targets. Pseudo code for the order statistics dynamic programming track-before-detect (OS-DP-TBD) algorithm is given in Algorithm 3.1.

The algorithm requires the following input parameters: number of integration frames N, dimensions of the range and azimuth cells N_r and N_b, respectively, and the scanned frames to be processed F_n. D is a design parameter that is a compromise between detection performance and computational complexity. In this chapter we chose the value of $D = N_r \times N_b/50$. As discussed in Section 3.2, N_r and N_b depend upon range and azimuth resolution of the radar system, respectively. d_r and d_b are the number of cells that the target can move to in the next scan in the range and azimuth directions, respectively, according to the motion model.

Line 2 applies the *point_threshold* function to the nth frame to extract the number of

Algorithm 3.1 The OS-DP-TBD Algorithm with K and $G0$ Clutter Distributions

Input: N, N_r, N_b, F, D, d_r, d_b

1: **for** $n = 1$ to N **do**
2: $[\boldsymbol{X}_n, M_n]$ = point_threshold(F, n);
3: **end for**
4: **for** $n = 1$ to N **do**
5: **if** $n = 1$ **then**
6: **for** $m = 1, 2, \ldots, M_n$ **do**
7: $I(\boldsymbol{x}_{n,m}) = S(\boldsymbol{z}_n|\boldsymbol{x}_{n,m})$;
8: $\Omega(\boldsymbol{x}_{n,m}) = Null$;
9: **end for**
10: **else**
11: **for** $m = 1, 2, \ldots, M_n$ **do**
12: $I(\boldsymbol{x}_{n,m}) = \max_{x_{n-1} \in \Omega(x_{n,m})} I(\boldsymbol{x}_{n-1,m}) + S(\boldsymbol{z}_n|\boldsymbol{x}_{n,m})$;
13: $\Omega(\boldsymbol{x}_{n,m}) = \arg \max_{\boldsymbol{x}_{n-1} \in \Omega(\boldsymbol{x}_{n-1})} I(\boldsymbol{x}_{n-1,m})$;
14: **end for**
15: **end if**
16: **end for**
17: Ordered_targets_list = SORT $(I(\boldsymbol{x}_{N,M_N}))$;
18: Best_targets = SELECT (Ordered_targets_list, D);
19: Search_zone = CONE(d_r, d_b);
20: Trajectory = BACKTRACK (Best_targets, Search_zone);

potential targets M_n and their associated states

$$\boldsymbol{X}_n = [\boldsymbol{x}_{n,1},\ \boldsymbol{x}_{n,2},\ \cdots,\ \boldsymbol{x}_{n,M_n}],$$

where $\boldsymbol{x}_{n,m}$ is the state vector for candidate target m, $1 \leq m \leq M_n$. Applying low pre-processing threshold to the received measurements $\boldsymbol{z}_n$ at each scan plays an important role in decreasing the computational complexity of the proposed algorithm. The adaptive pre-processing threshold in this chapter is set to be $0.1 \times mean(\boldsymbol{z}_n)$.

Lines 4 to 16 evaluate the merit function $I(\boldsymbol{x}_{n,m})$ and $\Omega(\boldsymbol{x}_{n,m})$ for each scan. $\Omega(\boldsymbol{x}_{n,m})$ in lines 8 and 13 is the set of target states in the $(n-1)$th scan from which a transition to $\boldsymbol{x}_n$ is possible to identify potential target trajectories.

The scoring function $S(\boldsymbol{z}_n|\boldsymbol{x}_{n,m})$ in lines 7 and 12 is evaluated using (4.21), (4.23) and (4.25) for Swerling type 0, 1 and 3 targets, respectively.

Lines 4 to 9 initialize the merit function $I(\boldsymbol{x}_{1,m})$ and $\Omega(\boldsymbol{x}_{1,m})$ for states $\boldsymbol{x}_{1,m}$.

Lines 11 to 14 integrate the merit function values $I(\boldsymbol{x}_{n,m})$ and $\Omega(\boldsymbol{x}_{n,m})$ for all candidate target states $\boldsymbol{x}_{n,m}$ in the nth scan obtained using the scoring function, $2 \leq n \leq N$.

Line 17 applies the OS-DP-TBD algorithm to the candidate targets in the last scan N to sort the merit function values $I(\boldsymbol{x}_{N,M_N})$ in the last scan.

Line 18 selects the best D targets that have the highest merit scores.

Line 19 uses the parameters d_r and d_b to define the search zone in the previous scan relative to the position of the selected target in the current scan.

Line 20 constructs the target trajectories using backtracking. The target trajectories are built with a search area around each candidate target location at each scan based on the target motion model. Moving targets with a constant velocity are considered in this chapter.

3.6 Performance Results

In this section, the performance of the proposed technique is examined. First, the performance of OS-DP-TBD is presented for Swerling type 1 and 3 targets in K distributed clutter, and then OS-DP-TBD is evaluated for Swerling type 0 and 1 targets in $G0$ distributed clutter. These results are compared with the DP-TBD techniques given in [36] and [14] to show the performance improvement with the proposed algorithm. The probability of detection P_D is defined as the probability of determining the target trajectory within 2 cells of the actual target cell throughout the entire trajectory. The simulation parameters are $N_r = 50$, $N_b = 50$, and $N_s = 100$, $N_U = 60$, $N_L = 40$. The number of integration frames is $N = 6$

and the number of simulation trials is 100, 000.

3.6.1 OS-DP-TBD Performance in K Distributed Clutter

The detection performance of OS-DP-TBD using the LELR score function for Swerling type 1 and 3 targets in K distributed clutter is given in Figs. 3.4 and 3.5, respectively, for $N = 6$. These figures show the effect of the shape parameter α and scale parameter $\beta = 1/\alpha$ on the detection performance of the proposed technique for Swerling type 1 and 3 targets, respectively. Comparing these results with those for the DP-TBD technique given in [36] shows that the proposed approach provides better detection performance. Table 3.1 gives the performance gain of the proposed OS-DP-TBD technique in K distributed clutter over the technique in [36] for Swerling type 1 and 3 targets with $N = 6$, $P_D = 0.5$ and different values of α. Note that the gain is positive in all cases. Further, the gain is larger for larger values of α.

Table 3.1: Performance gain (dB) of OS-DP-TBD for Swerling type 1 and 3 targets in K distributed Clutter with $N = 6$ and $P_D = 0.5$.

	Shape Parameter α			
Swerling Type	0.1	0.5	1	2
1	0.5	1.4	1.5	2.0
3	0.5	1.6	1.4	1.8

The detection performance of OS-DP-TBD using the LELR score function for Swerling type 1 and 3 targets in K distributed clutter and complex Gaussian noise is given in Figs. 3.6 and 3.7, respectively, for $N = 6$ and SNR = 10 dB. To investigate the effect of complex Gaussian noise on the performance of the proposed technique, we define the performance

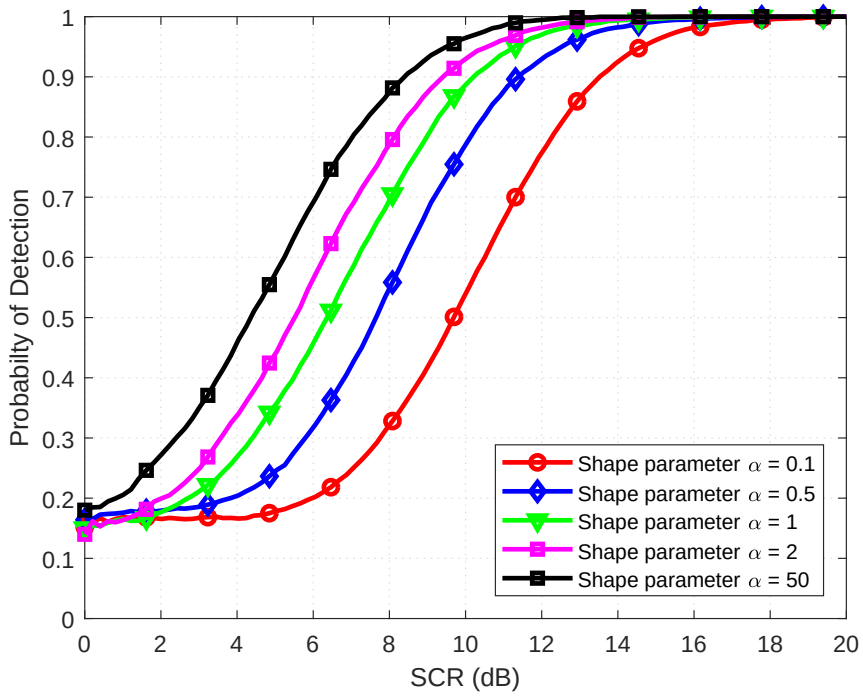

Figure 3.4: Probability of detection of a Swerling 1 target with K distributed clutter for different values of the shape parameter α and scale parameter $\beta = 1/\alpha$, and $N = 6$.

loss at $P_D = 0.5$ as the difference in SCR when Gaussian noise is present and absent. Table 3.2 gives the performance loss with the proposed OS-DP-TBD technique with K distributed clutter and complex Gaussian noise for a Swerling type 1 target, $N = 6$ and $P_D = 0.5$ for different shape parameter values α and scale parameter $\beta = 1/\alpha$. This shows that the performance loss is less than 1 dB for the values of α considered and the loss decreases with increasing α.

Table 3.3 gives the performance loss with the proposed OS-DP-TBD technique with K distributed clutter and complex Gaussian noise for Swerling type 3 targets, $N = 6$, $P_D = 0.5$, and different values of the shape parameter α and scale parameter $\beta = 1/\alpha$. In this case, the greatest performance loss occurs when $\alpha = 0.5$. Further, the loss is greater than for Swerling 1 targets. However, Tables 3.2 and 3.3 indicate that the performance loss is not

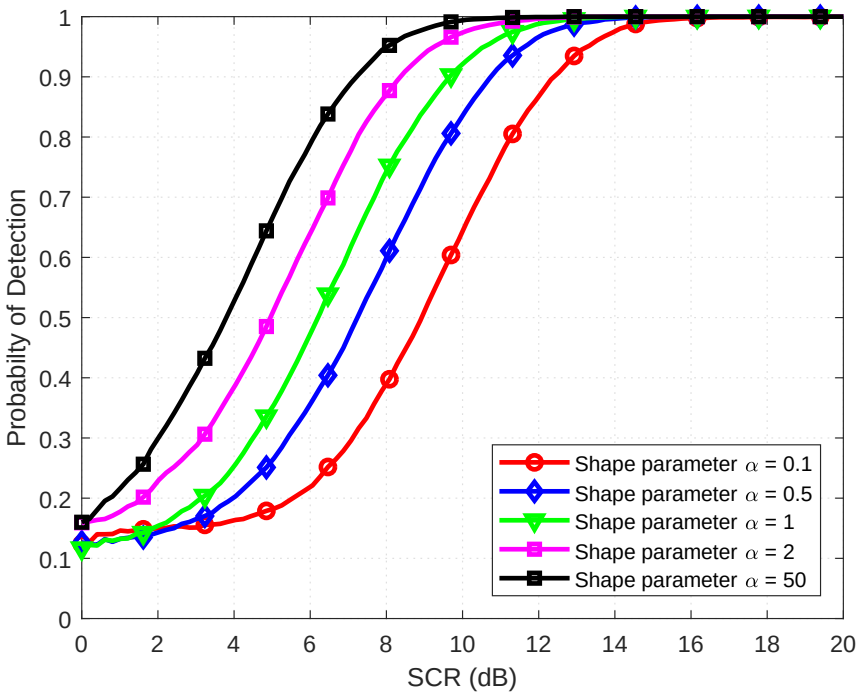

Figure 3.5: Probability of detection of a Swerling 3 target with K distributed clutter and different values of the shape parameter α and scale parameter $\beta = 1/\alpha$, and $N = 6$.

Table 3.2: OS-DP-TBD performance loss for a Swerling 1 target with K distributed clutter, $N = 6$, $P_D = 0.5$ and SNR = 10 dB.

Shape Parameter α	K Clutter and Noise	K Clutter Only	Loss (dB)
0.1	10.3	9.6	0.7
0.5	8.5	7.6	0.9
1.0	6.9	6.4	0.5
2.0	5.9	5.4	0.5

great for either Swerling type.

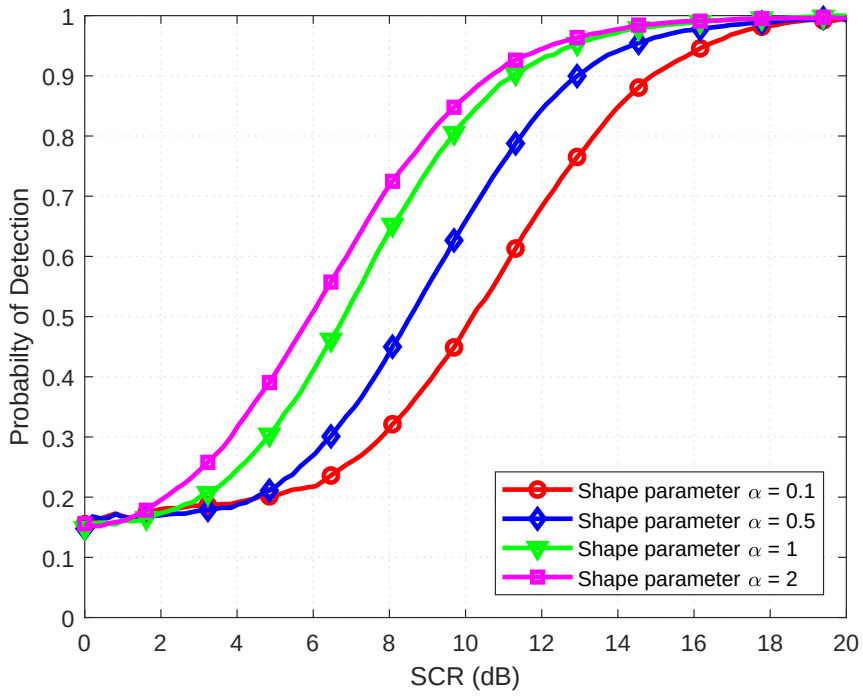

Figure 3.6: Probability of detection of a Swerling 1 target with K distributed clutter for different values of the shape parameter α and scale parameter $\beta = 1/\alpha$, $N = 6$ and complex Gaussian noise with SNR = 10 dB.

Table 3.3: OS-DP-TBD performance loss for a Swerling 3 target with K distributed clutter, $N = 6$, $P_D = 0.5$ and SNR = 10 dB.

Shape Parameter α	K Clutter and Noise	K Clutter Only	Performance Loss (dB)
0.1	9.5	8.8	0.7
0.5	8.5	7.3	1.2
1.0	6.9	6.3	0.6
2.0	5.6	5.0	0.6

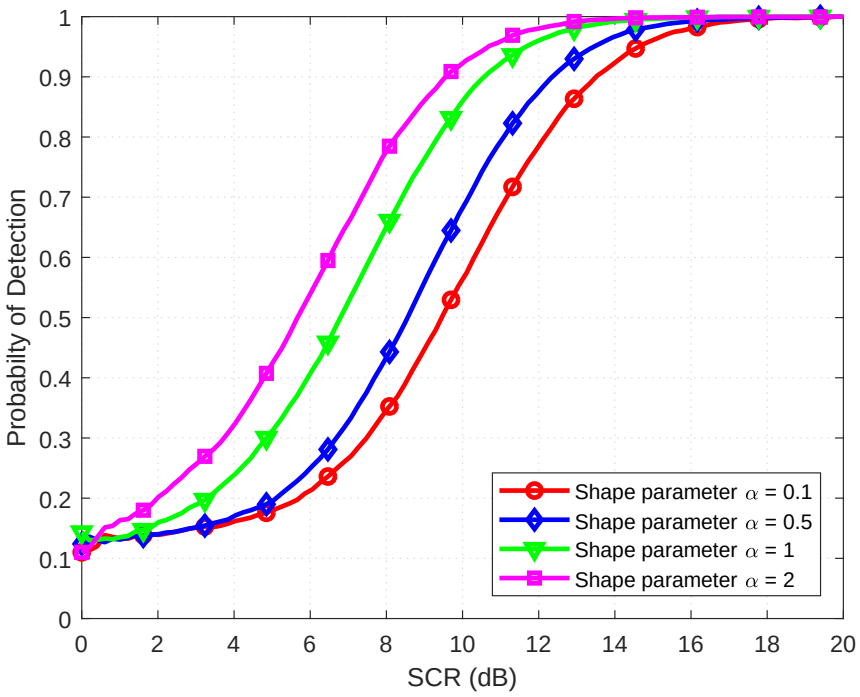

Figure 3.7: Probability of detection of a Swerling 3 target with K distributed clutter for different values of the shape parameter α and scale parameter $\beta = 1/\alpha$, $N = 6$ and complex Gaussian noise with SNR = 10 dB.

3.6.2 OS-DP-TBD Performance in $G0$ Distributed Clutter

The detection performance of OS-DP-TBD using the LELR scoring function for Swerling type 0 and 1 targets in $G0$ distributed clutter is given in Figs. 3.8 and 3.9, respectively, for $N = 6$. These figures show the effect of changing the shape parameter α and scale parameter $\beta = \alpha - 1$ on the detection performance of the proposed technique for Swerling type 0 and 1 targets, respectively.

Comparing these results with those for the DP-TBD technique given in [14] shows that the proposed approach provides better detection performance. Table 3.4 gives the performance gain of the proposed OS-DP-TBD technique in $G0$ distributed clutter over the technique in [14] for Swerling type 0 and 1 targets with $N = 6$, $P_D = 0.5$ and different values

of α. Again, the gain is positive in all cases. Further, The gain increases with increasing α.

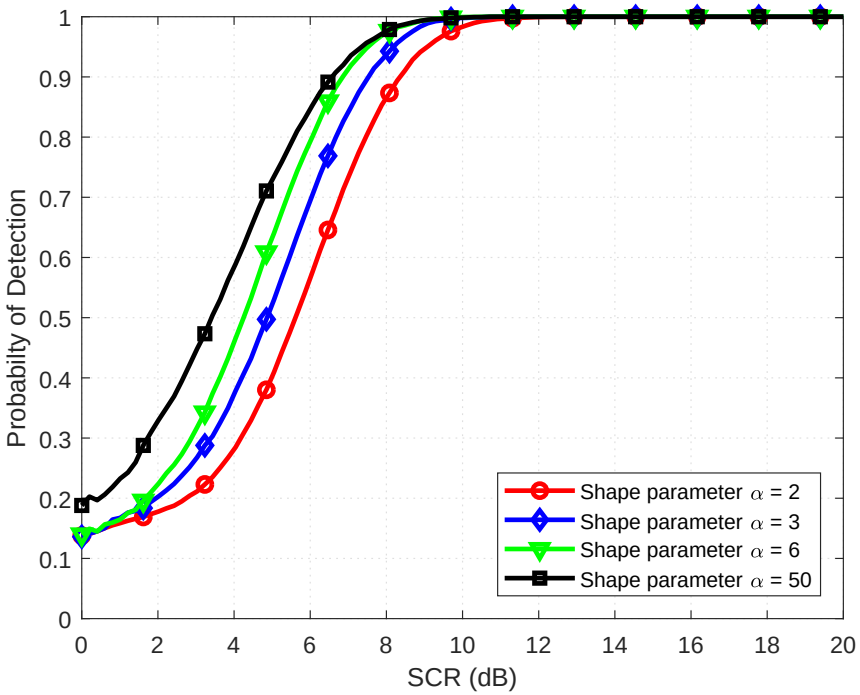

Figure 3.8: Probability of detection of a Swerling 0 target with $G0$ distributed clutter for different values of the shape parameter α and scale parameter $\beta = \alpha - 1$, and $N = 6$.

Table 3.4: Performance gain (dB) of the OS-DP-TBD technique for Swerling type 0 and 1 targets in $G0$ distributed clutter with $N = 6$ and $P_D = 0.5$.

	Shape Parameter		
Swerling Type	$\alpha = 2$	$\alpha = 3$	$\alpha = 6$
0	0.4	1.2	1.8
1	0.6	2.0	2.1

The detection performance of OS-DP-TBD using the LELR score function for Swerling type 0 and 1 targets in $G0$ distributed clutter and complex Gaussian noise is given in Figs. 3.10 and 3.11, respectively, for $N = 6$ and SNR $= 10$ dB. Table 3.5 gives the

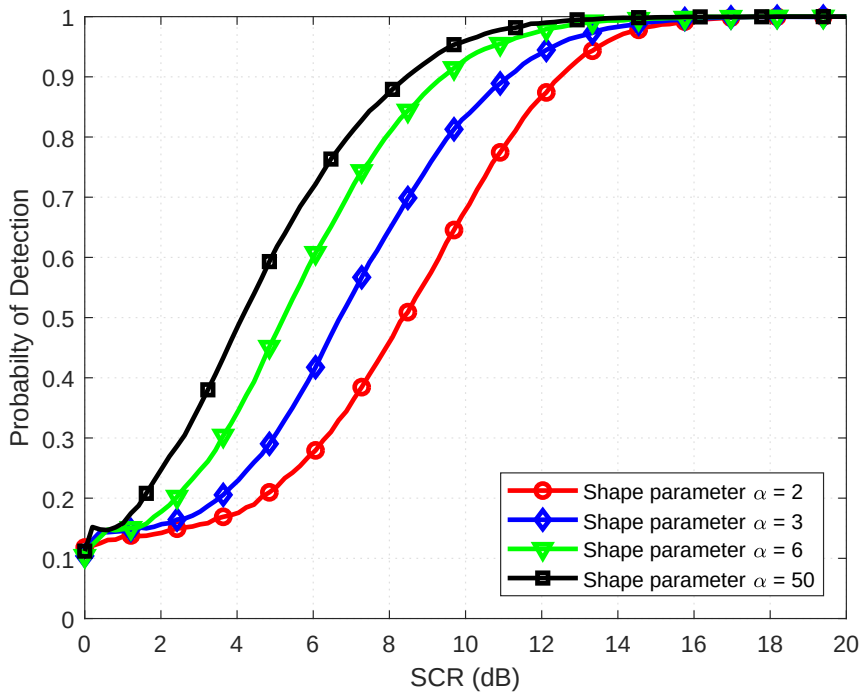

Figure 3.9: Probability of detection of a Swerling 1 target with $G0$ distributed clutter for different values of the shape parameter α and scale parameter $\beta = \alpha - 1$, and $N = 6$.

performance loss of the proposed OS-DP-TBD technique with $G0$ distributed clutter and complex Gaussian noise for a Swerling type 0 target, $N = 6$ and $P_D = 0.5$, for different values of α and $\beta = \alpha - 1$. These results show that there is a loss when noise is present, as expected. Further, the loss decreases with increasing α.

Table 3.6 gives the performance loss of the proposed OS-DP-TBD technique with $G0$ distributed clutter and complex Gaussian noise for Swerling type 1 targets, $N = 6$, $P_D = 0.5$, and different values of α and $\beta = \alpha - 1$. Again, this shows that the loss decreases with increasing α. Tables 3.5 and 3.6 indicate that the performance loss for either Swerling type is not great.

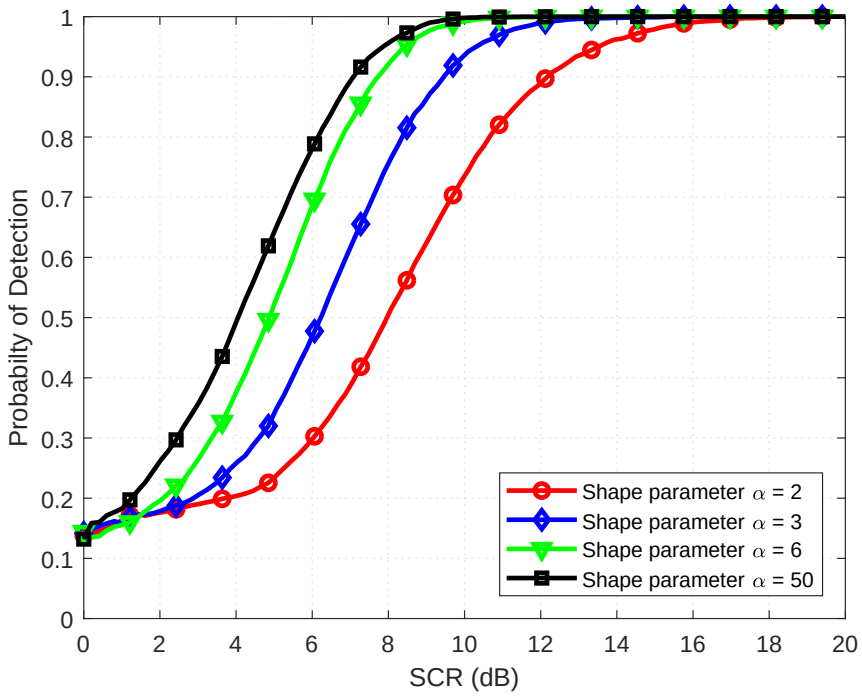

Figure 3.10: Probability of detection of a Swerling 0 targets with $G0$ distributed clutter for different values of shape parameter α, scale parameter $\beta = \alpha - 1$, $N = 6$, and complex Gaussian noise with SNR = 10 dB.

Table 3.5: OS-DP-TBD performance loss for a Swerling 0 target with $G0$ distributed clutter, $N = 6$, $P_D = 0.5$ and SNR = 10 dB.

Shape Parameter α	$G0$ Clutter and Noise	$G0$ Clutter Only	Performance Loss (dB)
2	8	5.6	2.4
3	6.3	4.9	1.4
6	4.9	4.3	0.6
50	4.1	3.5	0.6

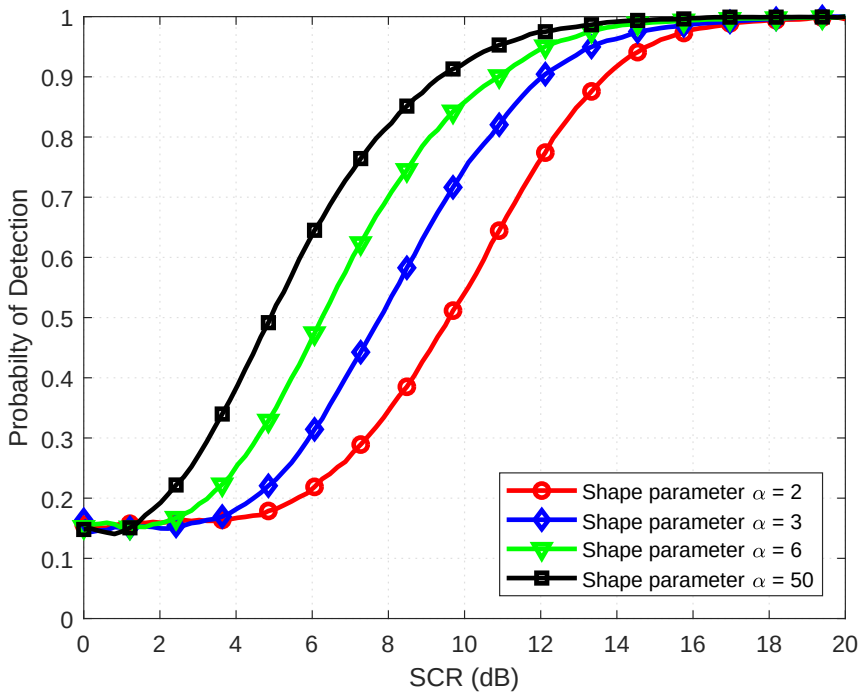

Figure 3.11: Probability of detection of a Swerling 1 target with $G0$ distributed clutter for different values of the shape parameter α and scale parameter $\beta = \alpha - 1$, $N = 6$ and complex Gaussian noise SNR = 10 dB.

Table 3.6: OS-DP-TBD performance loss for a Swerling 1 target with $G0$ distributed clutter, $N = 6$, $P_D = 0.5$ and SNR = 10 dB.

Shape Parameter α	$G0$ Clutter and Noise	$G0$ Clutter Only	Performance Loss (dB)
2	9.5	8.4	1.1
3	7.9	6.7	1.2
6	6.3	5.3	1.0
50	4.9	4.1	0.8

3.7 Conclusion

This chapter considered the detection of fluctuating targets in non-Gaussian distributed clutter. An OS-DP-TBD algorithm was proposed and evaluated for Swerling type 0, 1 and

3 targets in non-Gaussian clutter. Results were presented which show that the proposed OS-DP-TBD technique performs better than the DP-TBD technique in [36] with gains of 0.5 to 2 dB in K distributed clutter. The proposed technique also performs better than DP-TBD technique in [14] with gains of 0.4 to 2.1 dB in $G0$ distributed clutter. Further, the effect of complex Gaussian noise was considered. It was shown that the performance loss due to noise with the proposed technique is not great.

Chapter 4

Order Statistics Dynamic Programming Track-Before-Detect for Extended Targets in Weibull Distributed Clutter

4.1 Introduction

Most target tracking algorithms consider a single moving target as a point and estimate its center of mass based on the incoming sensor data such as range and azimuth. However, recently developed high resolution radar systems are able to resolve individual features of the targets [44]. In addition, advances in pulse compression techniques for radar receivers allows the generation of high resolution radar data where targets typically occupy more than one resolution cell [1]. Thus, the target does not appear as a point target [45]. Depending on the range and azimuth resolution, the target may appear as a point in some systems while there may be target energy spillover in other systems. This chapter considers the case where the resolution is not sufficient so an extended target model is considered. An

extended target model is also useful when the size of the target is small [46]. Detecting and tracking extended targets were considered in [45, 47, 48]. A realistic extended target model for TBD was presented in [45], To improve target tracking, a point spread function was employed. In [47], range distributed target detection in compound-Gaussian clutter was considered. Particle filter TBD with a marked Poisson point process (MPPP) model was proposed in [48] to estimate the extended target signals and the corresponding centroid direction Of arrival (DOA).

The decision as to whether a target is present in a resolution cell is central to modern radar systems. It is a key task in radar signal processing and is typically the first step. A target is determined to be present in a resolution cell by comparing the decision statistic with a threshold. The results are then processed using traditional tracking algorithms [15]. However, when the signal to noise ratio (SNR) is low ,the target signal is often discarded since the detector only retains measurements above an intensity threshold, resulting in poor detection performance [7]. Track-before-detect (TBD) techniques employ joint target detection and tracking and are effective in low SNR environments. A decision on the presence of a target is made using several consecutive frames of data [17], [9]. TBD uses no threshold or a very low threshold in order to capture low SNR radar measurements and then detection and tracking is conducted [18].

Recent research has determined that radar systems have significant heterogeneous background clutter [33]. In addition, the data obtained with a small grazing angle or high resolution radar from a heterogeneous terrain such as urban and forested areas is not Gaussian distributed. Experiments conducted with an HF surface wave radar [37] have shown that the clutter is highly heterogeneous. The Weibull, log-normal, K [36] and $G0$ distributions [14] are commonly used compound-Gaussian distributions for such clutter. The

Weibull distribution was first validated with land clutter returns observed by high resolution radars. The skewness of this distribution was shown to increase as the radar depression angle decreases [28]. Recently, this distribution was used to characterize weather clutter and sea clutter. These results motivate the use of the Weibull clutter model here.

Order statistics (OS) is widely employed in wireless communication systems to mitigate the effects of fading [29]. It has been shown to be effective for different types of fading distributions with unknown parameters. This chapter considers OS to detect Swerling type 0, 1 and 3 targets in heterogeneous background clutter which is Weibull distributed. The logarithm of the envelope likelihood ratio (LELR) is used as the scoring function with DP-TBD. The contributions of this chapter are as follows.

1. Order statistic DP-TBD (OS-DP-TBD) is proposed which selects the best candidate targets in each scan. The proposed algorithm provides significantly improved detection performance for extended targets with different energy spillover levels compared to basic DP-TBD in [26].

2. The proposed OS-DP-TBD technique is evaluated in Weibull distributed background clutter for Swerling type 0, 1 and 3 targets with different target energy spillover levels.

The rest of the chapter is organized as follows. The system model and notation are given in Section 4.2. Section 4.3 provides the problem formulation and the OS-DP-TBD technique is introduced in Section 4.4. The performance of OS-DP-TBD for different target energy spillover levels with Weibull distributed clutter is evaluated in Section 4.5 for Swerling type 0, 1 and 3 targets. Finally, some concluding remarks are given in Section 4.6.

4.2 System Model and Notation

In this section, the dynamic target model and measurement model are introduced.

4.2.1 Dynamic Target Model

We assume a two-dimensional surveillance radar in the range-azimuth plane. The surveillance region has $N_r \times N_b$ cells where $N_r = R/\Delta_r$ and $N_b = \omega/\Delta_b$ are the number of range and azimuth cells, respectively. R is the maximum range and ω is the azimuth extension of the surveillance region. The range resolution Δ_r is determined by the waveform bandwidth B where $\Delta_r = c/(2B)$ and c is the speed of light. The azimuth resolution Δ_b is given by the 3-dB beamwidth.

Let N be the number of consecutive frames processed with DP-TBD. The target is assumed to move in the surveillance region with target state in the nth frame given by

$$\boldsymbol{x}_n = [x_{n,r}, v_{n,r}, x_{n,b}, v_{n,b}]', \qquad 1 \leq n \leq N, \tag{4.1}$$

where $'$ denotes transpose, $x_{n,r}$ and $x_{n,b}$ are the range and azimuth target positions, respectively, and $v_{n,r}$ and $v_{n,b}$ are the range and azimuth target velocities, respectively. The target state evolution can be described by the Markov process

$$\boldsymbol{x}_{n+1} = F\boldsymbol{x}_n + \nu_n, \tag{4.2}$$

where ν_n is an independent and identically distributed (i.i.d.) Gaussian noise process. F is

the transition matrix given by

$$F = I_2 \otimes \begin{bmatrix} 1 & T \\ 0 & 1 \end{bmatrix}, \tag{4.3}$$

where $\otimes$ is the Kronecker product, I_2 is the two-dimensional identity matrix, and T is the time between consecutive scans.

The noise process v_n is typically Gaussian with covariance matrix Q given by

$$Q = \begin{bmatrix} Q_s & 0 \\ 0 & Q_s \end{bmatrix}, \qquad Q_s = q_s \begin{bmatrix} T^3/3 & T^2/2 \\ T^2/2 & T \end{bmatrix}, \tag{4.4}$$

where q_s is the power spectral density of the acceleration noise in the spatial dimensions. This model is suitable for slow moving targets [49]. Although a single target is considered in this chapter, the proposed technique can easily be extended to multiple targets.

4.2.2 Measurement Model

The observation region is divided into $N_r \times N_b$ resolution cells. When a target is present, let $h^{r,b}(x_n)$ denote the point spread function which accounts for the spillover of target energy to the (r, b)th resolution cell. The point spread function parameters are chosen based on the characteristics of the radar system. As shown in in Fig. 4.1, the adjacent resolution cells may contain target energy spillover which makes the measurements in these resolution cells target-like.

Note that the target energy can spillover not only to adjacent range cells but also to adjacent azimuth cells [16].

When a target is present in resolution cell (r, b), $1 \leq r \leq N_r$, $1 \leq b \leq N_b$, the radar

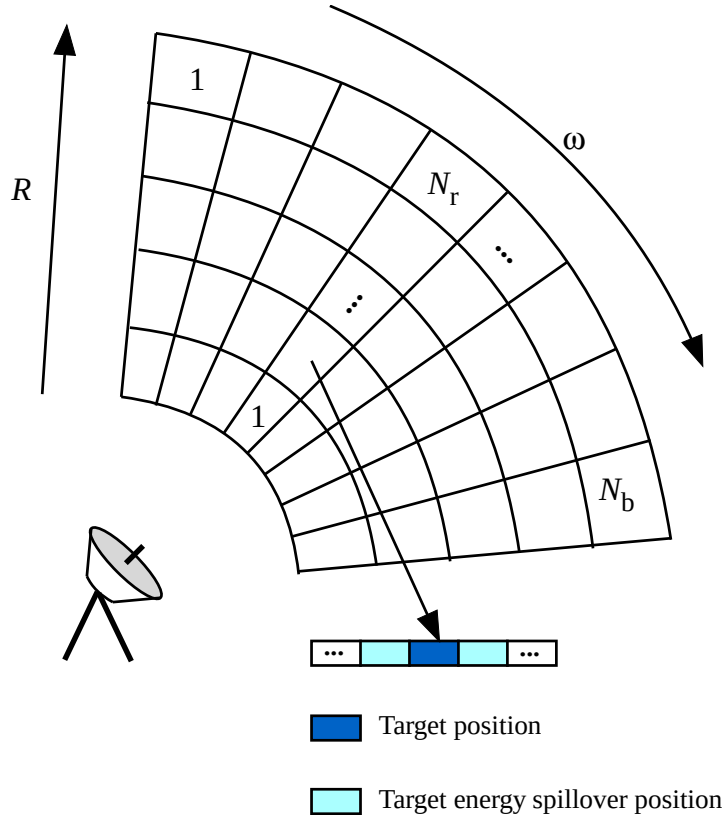

Figure 4.1: The radar surveillance region in the range and azimuth dimensions.

measurement is given by

$$z_n^{r,b} = A_n \exp(j\phi_n)\, h^{r,b}(x_n) + C_n^{r,b}, \tag{4.5}$$

where A_n is the amplitude of the complex measurement of the target in the nth scan, ϕ_n is the corresponding target phase which is assumed to be uniformly distributed over $[0, 2\pi)$, and $C_n^{r,b}$ denotes i.i.d. clutter which is assumed to be Weibull distributed. If there is no target, the measurement in cell (r, b) in the nth frame is given by

$$z_n^{r,b} = C_n^{r,b}, \tag{4.6}$$

with amplitude

$$a_n^{r,b} = |z_n^{r,b}|,$$

where $1 \leq r \leq N_r$, $1 \leq b \leq N_b$, $1 \leq n \leq N$. The measurements for frame n can be expressed as

$$\boldsymbol{z}_n = [z_n^{1,1}, \ldots, z_n^{1,N_b}, \ldots, z_n^{N_r,N_b}]'. \tag{4.7}$$

The measurements for the N frames can be expressed as an $N_r N_b \times N$ matrix

$$\mathbf{Z}_{1:N} = [\boldsymbol{z}_1, \boldsymbol{z}_2, \ldots, \boldsymbol{z}_N], \tag{4.8}$$

where $\mathbf{Z}_{1:N}$ denotes columns 1 to N.

The Swerling models were introduced in [15] to describe the statistical properties of the radar cross-sections of targets. The scattering of the electromagnetic energy from a target depends on many factors such as target geometry, size, shape, viewing aspect, and polarization. The models for Swerling type 0, 1 and 3 targets are given below.

Swerling Type 0 Target

The Swerling type 0 model describes an idealized target without any fluctuations (constant radar cross-section), and constant amplitude A_n given by

$$A_n = \sqrt{\sigma_t}, \tag{4.9}$$

where σ_t is the mean squared target amplitude.

Swerling Type 1 Target

For the Swerling type 1 model, the radar cross-section is constant from pulse to pulse, but varies independently from scan to scan. The target amplitude A_n is Rayleigh distributed with probability density function (PDF)

$$P(A_n) = \frac{2A_n}{\sigma_t} \exp\left(-\frac{A_n^2}{\sigma_t}\right). \tag{4.10}$$

Swerling Type 3 Target

For the Swerling type 3 model, the radar cross-section is constant during the radar antenna dwell time, but varies from scan to scan. The target amplitude A_n is chi-square distributed with four degrees of freedom and has PDF

$$P(A_n) = \frac{8\ A_n^3}{\sigma_t^2} \exp\left(-\frac{2\ A_n^2}{\sigma_t}\right). \tag{4.11}$$

Clutter is a term used to describe any object that generates unwanted radar return backscatter. In many cases, the clutter signal level is much higher than the receiver noise level. The ability of a radar to detect targets embedded in clutter depends on the signal-to-clutter ratio (SCR) [2]. Clutter includes earth surface echoes (terrain and sea), weather echoes (rain and clouds), and man-made clutter such as chaff clouds which consist of strips of reflective material. Clutter echoes differ from both target echoes and noise, and can appear as either a target or noise [3]. In this chapter, the SCR is defined as

$$\text{SCR} = 10 \log_{10}\left(\frac{\sigma_t}{\sigma_c}\right), \tag{4.12}$$

where σ_c denotes the mean of the clutter power.

The Weibull distribution has been used to model clutter at low grazing angles (less than five degrees) for frequencies between 1 GHZ and 10 GHZ [2]. Further, shadowing at low grazing angles can hide large scatterers so that the clutter distribution has long tails. The PDF of the Weibull distribution is

$$f(x|A,B) = \frac{B}{A}(x/A)^{(B-1)}e^{-(x/A)^B}, \tag{4.13}$$

with mean and variance

$$\mu = A\Gamma\left(1+\frac{1}{B}\right), \tag{4.14}$$

$$Var = A^2\left(\Gamma\left(1+\frac{2}{B}\right) - \left(\Gamma\left(1+\frac{1}{B}\right)\right)^2\right), \tag{4.15}$$

respectively [2], where $\Gamma(\cdot)$ denotes the Gamma function, and A and B are the Weibull scale and shape parameters, respectively. Figure 4.2 shows the effect of changing B on the PDF with scale parameter $A = 1$. For $B = 2$, the Weibull distribution becomes a Rayleigh distribution, and for small values of B the tail is long. For $B \leq 1$, the Weibull distribution becomes an exponential distribution.

4.3 Problem Formulation

At the nth scan, a list of candidate targets is obtained from the receiver processing chain consisting of matched filtering, moving target detection, CFAR (constant false alarm rate), detection, clustering and data extraction. In this chapter a low pre-processing threshold is employed with the radar measurements (4.5) to provide a good tradeoff between performance and computational complexity. The sequence of candidate targets acquired at scan n is $m_n = 1, 2, \ldots, M_n$. This may include false targets due to noise or background clutter. An

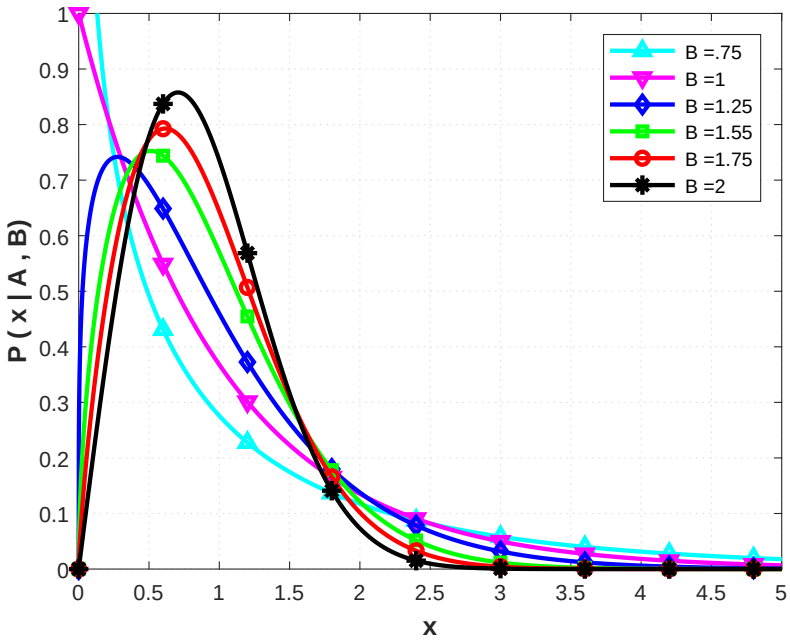

Figure 4.2: The PDF of the Weibull distribution for values of the shape parameter B.

extended target model with different target energy spillover is considered in this chapter.

The DP-TBD algorithm has two steps. First a decision is made concerning whether a target is present or not. Then the trajectories which are most likely to correspond to actual targets are extracted. For the N consecutive scans $\boldsymbol{Z}_{1:N}$, the integration process is given by [31]

$$I(\boldsymbol{x}_n|\boldsymbol{Z}_{1:n}) = \max_{x_{n-1}\in\Omega(x_n)} I(\boldsymbol{x}_{n-1}|\boldsymbol{Z}_{1:n-1}) + S(\boldsymbol{z}_n|\boldsymbol{x}_n), \tag{4.16}$$

where $I(\boldsymbol{x}_n|\boldsymbol{Z}_{1:n})$ is the merit function for state x_n, $S(z_n|x_n)$ is the scoring function [14], [26], and $\Omega(x_n)$ is the set of states at scan $n-1$ for which a transition to x_n is possible and is given by

$$\Omega(\boldsymbol{x}_n) = \arg \max_{\boldsymbol{x}_{n-1}\in\Omega(\boldsymbol{x}_{n-1})} I(\boldsymbol{x}_{n-1}). \tag{4.17}$$

The following commonly employed DP-TBD scoring functions are considered.

1. Amplitude scoring function [31], [8]

$$S(\boldsymbol{z}_n|\boldsymbol{x}_n) = a_n^{x_{rn},x_{bn}}. \tag{4.18}$$

2. Squared amplitude (SA) scoring function [22]

$$S(\boldsymbol{z}_n|\boldsymbol{x}_n) = (a_n^{x_{rn},x_{bn}})^2. \tag{4.19}$$

3. Logarithm of envelope likelihood ratio (LELR) scoring function [16], [32]

$$S(\boldsymbol{z}_n|\boldsymbol{x}_n) = \ln\left(\frac{P(\boldsymbol{a}_n|\boldsymbol{x}_n)}{P(\boldsymbol{a}_n)}\right), \tag{4.20}$$

where $\boldsymbol{a}_n = [a_n^{1,1}, \ldots, a_n^{1,N_r}, \ldots, a_n^{N_r,N_b}]$ is the amplitude vector for the nth scan.

It was shown in [33] that DP-TBD with the LELR scoring function (4.20) provides better performance than with (4.18) or (4.19). This is due to the use of both clutter-only and clutter-plus-target distributions. The LELR for the three Swerling types are given below [26].

1. Swerling 0 model

$$L_E(\boldsymbol{a}_n|\boldsymbol{x}_n) = -\frac{2A_n^2\boldsymbol{h}'\boldsymbol{h}}{\sigma_c} + \sum_{r=1}^{N_r}\sum_{b=1}^{N_b} \ln\left(I_0\left(\frac{2A_n a_n^{r,b}}{\sigma_c}\right)\right), \tag{4.21}$$

where $I_0(.)$ is the modified first order Bessel function and $\boldsymbol{h}$ denotes the N_rN_b dimensional vector formed by

$$h^{r,b}(x_n);\ r = 1, \ldots, N_r,\ b = 1, \ldots, N_b,$$

so that

$$\boldsymbol{h} = [h^{1,1}(x_n), \ldots, h^{1,N_b}(x_n), \ldots, h^{N_r,N_b}(x_n)]'. \tag{4.22}$$

2. Swerling 1 model

$$\begin{aligned} L_E(\boldsymbol{a}_n|\boldsymbol{x}_n) &= -\frac{1}{\sigma_c}\sum_{r=1}^{N_r}\sum_{b=1}^{N_b}\frac{\psi^{r,b}}{\sigma_c+\psi^{r,b}}\left(a_n^{r,b}\right)^2 \\ &+ \sum_{r=1}^{N_r}\sum_{b=1}^{N_b}\ln\left(\frac{\sigma_c}{\sigma_c+\psi^{r,b}}\right). \end{aligned} \tag{4.23}$$

where

$$\psi^{r,b} = \left(h^{r,b}(x_n)\right)^2\sigma_t. \tag{4.24}$$

3. Swerling 3 model

$$\begin{aligned} L_E(\boldsymbol{a}_n|\boldsymbol{x}_n) &= \sum_{r=1}^{N_r}\sum_{b=1}^{N_b}\ln\left(\frac{4\sigma_c^2\psi^{r,b}}{(2\sigma_c+\psi^{r,b})^2}\right) \\ &+ \sum_{r=1}^{N_r}\sum_{b=1}^{N_b}\ln\left(1+\frac{\psi^{r,b}(a_n^{r,b})^2}{\sigma_c(2\sigma_c+\psi^{r,b})}\right) \\ &+ \frac{1}{\sigma_c}\sum_{r=1}^{N_r}\sum_{b=1}^{N_b}\frac{\psi^{r,b}}{2\sigma_c+\psi^{r,b}}\left(a_n^{r,b}\right)^2. \end{aligned} \tag{4.25}$$

4.4 Order Statistics Dynamic Programming TBD (OS-DP-TBD)

Order statistics (OS) is used to determine the best candidate targets in a radar scan. This controls the number of targets to be processed based on the merit function values. Back-tracking is then used to estimate the trajectories of these targets. Pseudo-code for the order

statistics dynamic programming track-before-detect (OS-DP-TBD) algorithm is given in Algorithm 4.1.

Algorithm 4.1 The OS-DP-TBD Algorithm for Extended Target with Different Energy Spillover

Input: N, N_r, N_b, L, F, D, d_r, d_b

for $n = 1$ to N **do**
  $[\boldsymbol{X}_n, M_n]$ = point_threshold(F, n);
end for
for $n = 1$ to N **do**
  if $n = 1$ **then**
    for $m = 1, 2, \ldots, M_n$ **do**
      $I(\boldsymbol{x}_{n,m}) = S(\boldsymbol{z}_n|\boldsymbol{x}_{n,m})$;
      $\Omega(\boldsymbol{x}_{n,m}) = Null$;
    end for
  else
    for $m = 1, 2, \ldots, M_n$ **do**
      $I(\boldsymbol{x}_{n,m}) = \max_{x_{n-1} \in \Omega(x_{n,m})} I(\boldsymbol{x}_{n-1,m}) + S(\boldsymbol{z}_n|\boldsymbol{x}_{n,m})$;
      $\Omega(\boldsymbol{x}_{n,m}) = \arg \max_{\boldsymbol{x}_{n-1} \in \Omega(\boldsymbol{x}_{n-1})} I(\boldsymbol{x}_{n-1,m})$;
    end for
  end if
end for
Ordered_targets_list = SORT $(I(\boldsymbol{x}_{N,M_N}))$;
Best_targets = SELECT (Ordered_targets_list, D);
Search_zone = CONE(d_r, d_b);
Trajectory = BACKTRACK (Best_targets, Search_zone);

The algorithm requires the following input parameters: number of integration frames N, dimensions of the range and azimuth cells N_r and N_b, respectively, the scanned frames to be processed F_n, target energy spillover L where the number of range resolution cells that contain target energy is $2L + 1$, and the number of ordered candidate targets to be processed D. D is a design parameter that is a compromise between detection performance and computational complexity which here is et to $D = N_r \times N_b/50$. As discussed in Section 4.2, N_r and N_b depend upon range and azimuth resolution of the radar system, respectively. d_r and d_b are the number of cells that the target can move to in the next scan in the range

and azimuth directions, respectively, according to the motion model.

Line 2 applies the *point_threshold* function to the nth frame to extract the number of potential targets M_n and their associated states

$$\boldsymbol{X}_n = [\boldsymbol{x}_{n,1},\ \boldsymbol{x}_{n,2},\ \ldots,\ \boldsymbol{x}_{n,M_n}],$$

where $\boldsymbol{x}_{n,m}$ is the state vector for candidate target m, $1 \leq m \leq M_n$. Using a low pre-processing threshold (rather than none) on the received measurements $\boldsymbol{z}_n$ at each scan will reduce the computational complexity of the algorithm. An adaptive pre-processing threshold is used here which is $0.1 \times \text{mean}(\boldsymbol{z}_n)$.

Lines 4 to 16 evaluate the merit function $I(\boldsymbol{x}_{n,m})$ and $\Omega(\boldsymbol{x}_{n,m})$ for each scan. $\Omega(\boldsymbol{x}_{n,m})$ in lines 8 and 13 is the set of target states in the $(n-1)$th scan from which a transition to $\boldsymbol{x}_n$ is possible to identify potential target trajectories.

The scoring function $S(\boldsymbol{z}_n|\boldsymbol{x}_{n,m})$ in lines 7 and 12 is evaluated using (4.21), (4.23) and (4.25) for Swerling type 0, 1 and 3 targets, respectively.

Lines 4 to 9 initialize the merit function $I(\boldsymbol{x}_{1,m})$ and $\Omega(\boldsymbol{x}_{1,m})$ for states $\boldsymbol{x}_{1,m}$.

Lines 11 to 14 integrate the merit function values $I(\boldsymbol{x}_{n,m})$ and $\Omega(\boldsymbol{x}_{n,m})$ for all candidate target states $\boldsymbol{x}_{n,m}$ in the nth scan obtained using the scoring function, $2 \leq n \leq N$.

Line 17 sorts the merit function values $I(\boldsymbol{x}_{N,M_N})$ of the candidate targets in the last scan (N).

Line 18 selects the best D targets that have the highest merit scores.

Line 19 uses the parameters d_r and d_b to define the search zone in the previous scan relative to the position of the selected target in the current scan.

Line 20 constructs the target trajectories using backtracking. The target trajectories are

built with a search area around each candidate target location at each scan based on the target motion model. Moving targets with a constant velocity are considered in this chapter.

4.5 Performance Results

The performance of the proposed techniques is examined in this section. First, the performance of OS-DP-TBD is presented for Swerling type 0, 1 and 3 targets with different target energy spillover L. These results are compared with those with DP-TBD [26] to demonstrate the improvement with the proposed algorithm. We assume that the target moves in the far zone of the radar system, in which case the target energy spills over only to the adjacent range resolution cells and not to the adjacent azimuth resolution cells. Then $h^{r,b}(x_n)$ is given by

$$h^{r,b}(x_n) = \exp\left(-\frac{(r - x_{rn})^2}{8}\right). \tag{4.26}$$

We define the probability of detection P_D as the probability of determining the target trajectory within 2 cells of the actual target cell throughout the entire trajectory. The probability of false alarm P_{fa} is defined as the probability of detecting a false track in the absence of a target. The signal-to-noise ratio (SNR) is defined as

$$\text{SNR} = 10\log_{10}\left(\frac{\sigma_t}{\sigma_n}\right), \tag{4.27}$$

where σ_n is the complex Gaussian noise power. The P_D results for the proposed algorithm are obtained based on the desired P_{fa} which here is 10^{-4}.

The position root-mean-squared error (RMSE) is defined as

$$\text{RMSE} = \frac{1}{MN}\sum_{m=1}^{M}\sum_{n=1}^{N}\sqrt{(\hat{x}_{r,n}^{m} - x_{r,n}^{m})^2 + (\hat{x}_{b,n}^{m} - x_{b,n}^{m})^2}, \tag{4.28}$$

where $(\hat{x}_{r,n}^{m}, \hat{x}_{b,n}^{m})$ and $(x_{r,n}^{m}, x_{b,n}^{m})$ are the estimated and true target positions at the nth scan during the mth simulation, respectively. The simulation parameters are $N_r = 50$, $N_b = 50$, and $N = 5$ and 10 integration frames. Unless otherwise specified, the scale and shape parameters for the Weibull distribution are $A = 1.0$ and $B = 1.5$, respectively. The number of simulation trials is $100,000$ for each probability of detection result.

4.5.1 OS-DP-TBD Performance with Complex Gaussian Noise

The detection performance of OS-DP-TBD using the LELR scoring function with $N = 5$, target energy spillover $L = 1$, and complex Gaussian noise for Swerling type 0, 1 and 3 targets is presented in Figs. 4.3, 4.4 and 4.5, respectively.

Basic-DP-TBD in these figures denotes LELR-DP-TBD in [26]. Figures 4.6, 4.7 and 4.8 give the corresponding performance with $L = 2$. These results show that OS-DP-TBD performs better than basic DP-TBD. This is because of the noncoherent intraframe integration with the order statistics algorithm. Tables 4.1 and 4.2 give the performance gain of OS-DP-TBD over basic DP-TBD for Swerling type 0, 1 and 3 targets, $N = 5$, and $P_D = 0.5$ with target energy spillover $L = 1$ and $L = 2$, respectively. This shows that the improvement with the proposed technique is between 0.9 and 1.7 dB. Further, the processing gain of the proposed algorithm increases with the number of integration frames, but the workload also increases.

Table 4.3 gives the performance loss of the proposed OS-DP-TBD algorithm for Swerling

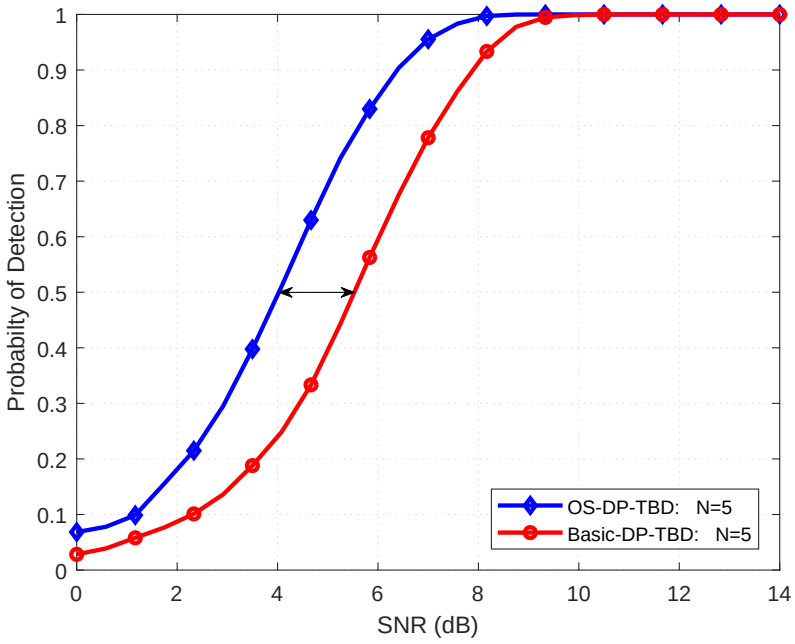

Figure 4.3: Probability of detection of a Swerling 0 target using OS-DP-TBD and Basic DP-TBD for target energy spillover $L = 1$ with complex Gaussian distributed noise and $N = 5$.

type 0, 1 and 3 targets, $N = 5$, and $P_D = 0.5$ with complex Gaussian noise with different target energy spillover L. This shows the performance loss is 0.4 to 0.6 dB greater with $L = 2$.

Table 4.1: Performance Gain of OS-DP-TBD Compared with Basic DP-TBD for $L = 1$, $N = 5$ and $P_D = 0.5$.

Swerling Type	**Performance Gain (dB)**
0	1.7
1	1.1
3	1.2

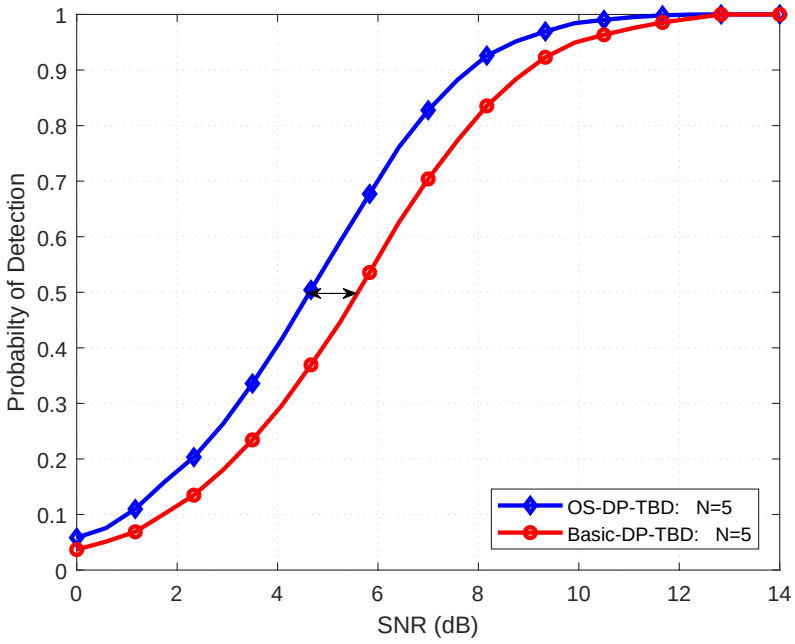

Figure 4.4: Probability of detection of a Swerling 1 target using OS-DP-TBD and Basic DP-TBD for target energy spillover $L = 1$ with complex Gaussian distributed noise and $N = 5$.

Table 4.2: Performance Gain of OS-DP-TBD Compared with Basic DP-TBD for $L = 2$, $N = 5$ and $P_D = 0.5$.

Swerling Type	**Performance Gain (dB)**
0	1.3
1	0.9
3	1.4

4.5.2 OS-DP-TBD Performance with Weibull Distributed Clutter

The detection performance of the proposed OS-DP-TBD algorithm for Weibull distributed background clutter with different shape parameters B, scale parameter $A = 1$, $N = 5$, and $L = 1$ and 2 is given in Figs. 4.9, 4.10 and 4.11 for Swerling type 0, 1, and 3 targets, respectively. These results show the effect of the background clutter on the detection performance. In particular, a smaller shape parameter B results in worse performance. In

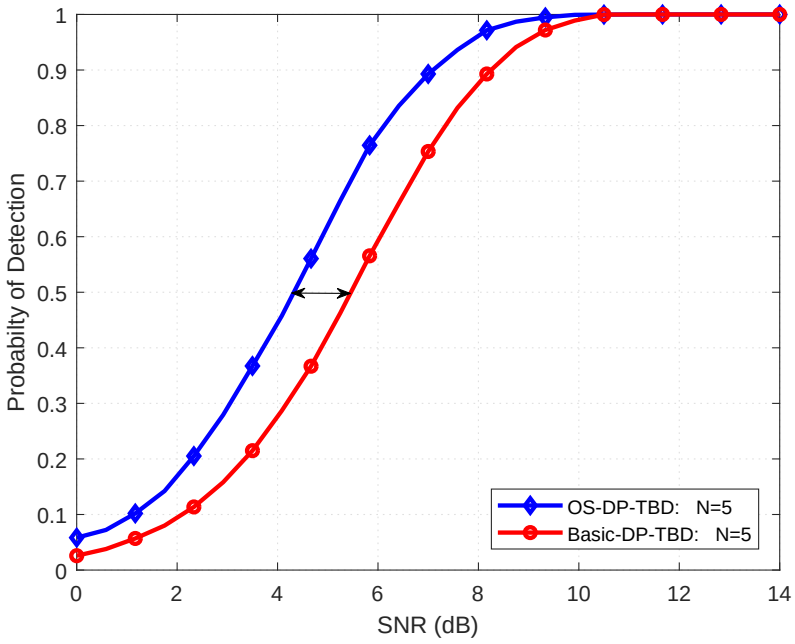

Figure 4.5: Probability of detection of a Swerling 3 target using OS-DP-TBD and Basic DP-TBD for target energy spillover $L = 1$ with complex Gaussian distributed noise and $N = 5$.

Table 4.3: Performance Loss of the Proposed OS-DP-TBD Algorithm with Complex Gaussian Noise, $L = 1$ and $L = 2$, $N = 5$ and $P_D = 0.5$.

Swerling Type	**Energy Spillover** $L = 1$	**Energy Spillover** $L = 2$	**Performance Loss (dB)**
0	4.1	4.6	0.5
1	4.6	5.2	0.6
3	4.3	4.7	0.4

addition, as L increases, the performance of the proposed OS-DP-TBD algorithm suffers because with a fixed target energy, the noncoherent intraframe integration performance is degraded. For $P_D = 0.5$ and a fixed shape parameter B, the performance loss with $L = 2$ compared to $L = 1$ is 0.5 to 1.5 dB for Swerling target types 0, 1, and 3.

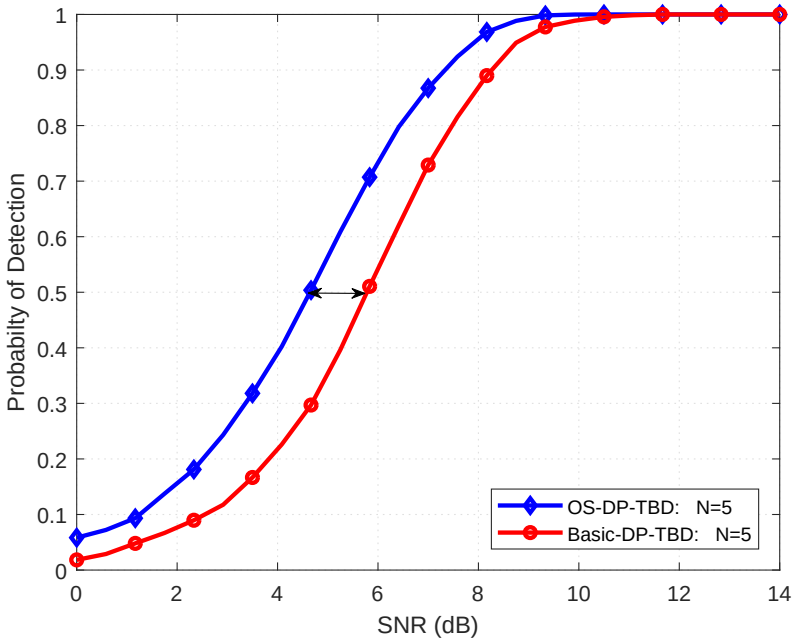

Figure 4.6: Probability of detection of a Swerling 0 target using OS-DP-TBD and Basic DP-TBD for target energy spillover $L = 2$ with complex Gaussian distributed noise and $N = 5$.

Table 4.4 gives the performance loss of the proposed OS-DP-TBD algorithm for Swerling type 0, 1 and 3 targets, $N = 5$, and $P_D = 0.5$ with Weibull distributed clutter, shape parameter $B = 1.5$ with different target energy spillover L. This shows that the performance loss is 1 to 1.6 dB greater with $L = 2$.

Table 4.4: Performance Loss of the Proposed OS-DP-TBD Algorithm with Weibull Distributed Clutter for $L = 1$ and $L = 2$, $N = 5$, $B = 1.5$ and $P_D = 0.5$.

Swerling Type	**Energy Spillover** $L = 1$	**Energy Spillover** $L = 2$	**Performance Loss (dB)**
0	5.4	6.6	1.2
1	7.2	8.7	1.5
3	6.2	7.5	1.3

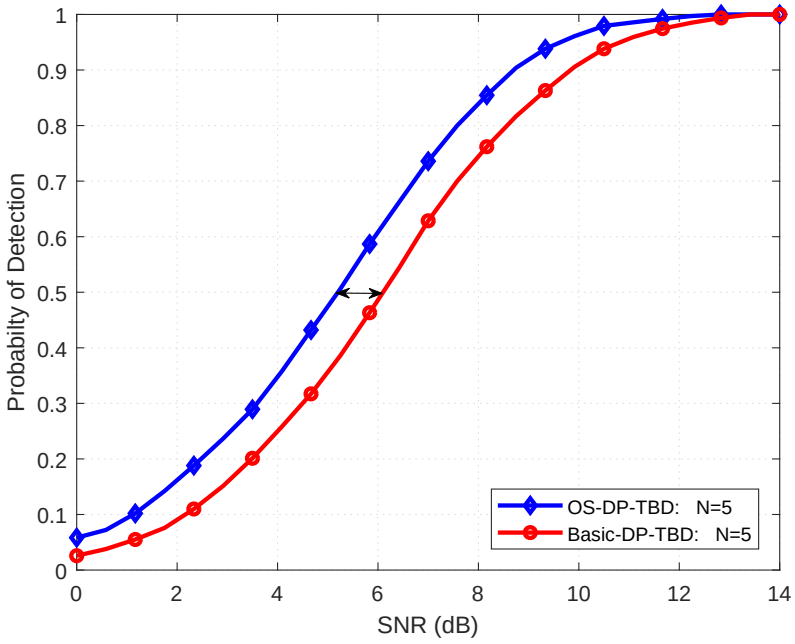

Figure 4.7: Probability of detection of a Swerling 1 target using OS-DP-TBD and Basic DP-TBD for target energy spillover $L = 2$ with complex Gaussian distributed noise and $N = 5$.

Figures 4.12, 4.13 and 4.14 present the detection performance of the proposed OS-DP-TBD algorithm with Weibull distributed clutter, $B = 1.5$, $A = 1$, $N = 5$ and 10, and $L = 1$ and 2 for Swerling type 0, 1, and 3 targets, respectively. These results indicate that increasing the number of integration frames improves the detection performance, but at a cost of increasing the computational complexity.

The RMSE for the proposed OS-DP-TBD algorithm with Weibull distributed background clutter and $L = 1$ and 2 is given in Figs.4.15, 4.16 and 4.17 for Swerling targets types 0, 1, and 3, respectively. This shows that the RMSE decreases with increasing SCR and is greatest with Swerling type 1 targets. Furthermore, a larger L results in worse tracking accuracy for all three Swerling target types.

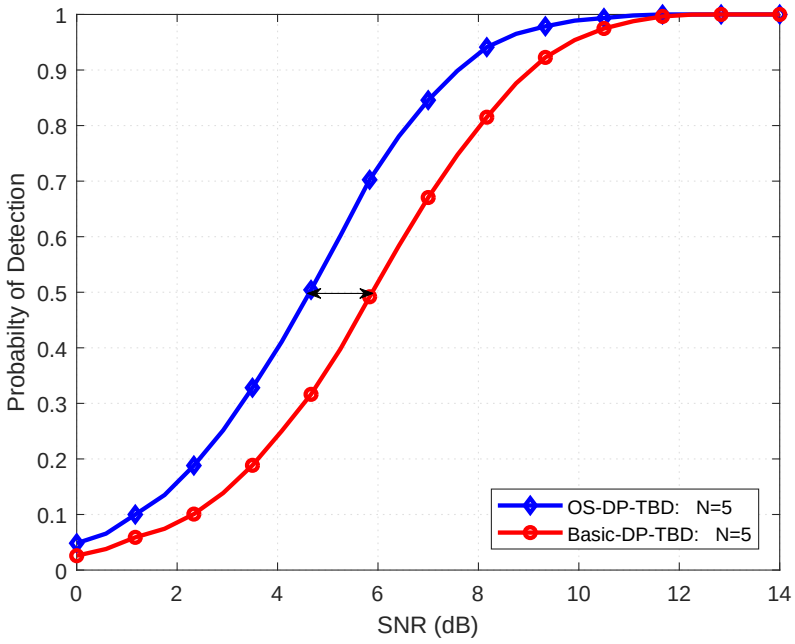

Figure 4.8: Probability of detection of a Swerling 3 target using OS-DP-TBD and Basic DP-TBD for target energy spillover $L = 2$ with complex Gaussian distributed noise and $N = 5$.

4.6 Conclusion

The detection of fluctuating targets in complex Gaussian noise and Weibull distributed clutter was considered. An OS-DP-TBD algorithm was proposed which employs order statistics to determine the best targets. The performance was evaluated for Swerling type 0, 1 and 3 targets and an extended target with target energy spillover in the range resolution cells was considered. Results were presented which show that the proposed OS-DP-TBD algorithm performs better than basic DP-TBD with a gain of approximately 1 to 2 dB. Furthermore, the effect of Weibull distributed clutter was examined. The detection performance of the proposed OS-DP-TBD algorithm decreased with increased target energy spillover for all Swerling target types. Although the detection of a single target was considered in this chapter, the proposed OS-DP-TBD algorithm can be employed to detect

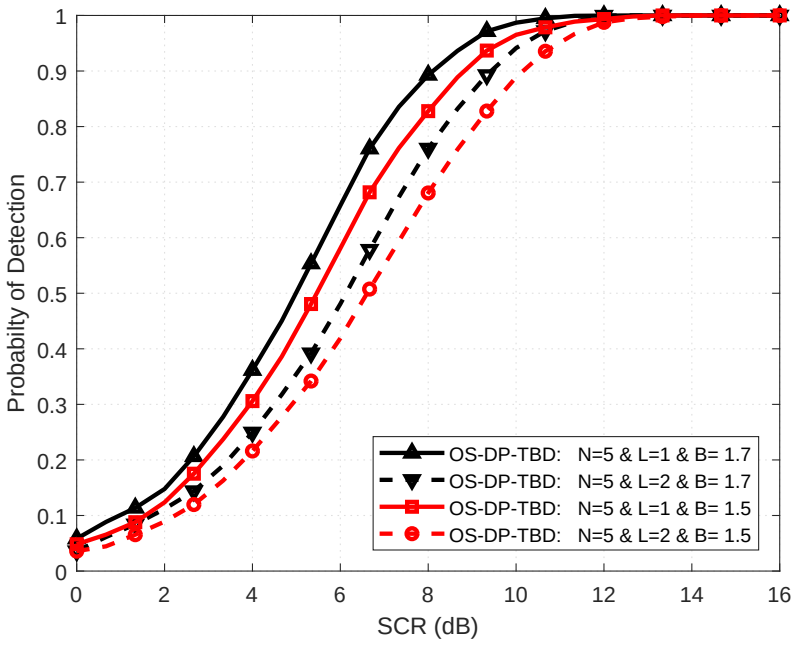

Figure 4.9: OS-DP-TBD probability of detection of a Swerling 0 target for $L = 1$ and 2 with Weibull distributed clutter for different shape parameters B, $A = 1$, and $N = 5$.

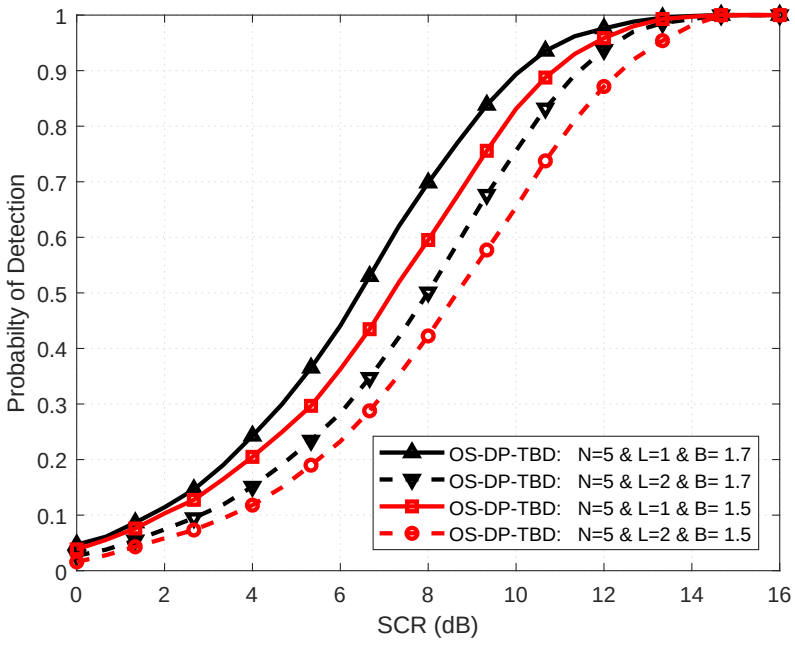

Figure 4.10: OS-DP-TBD probability of detection of a Swerling 1 target for $L = 1$ and 2 with Weibull distributed clutter for different shape parameters B, $A = 1$, and $N = 5$.

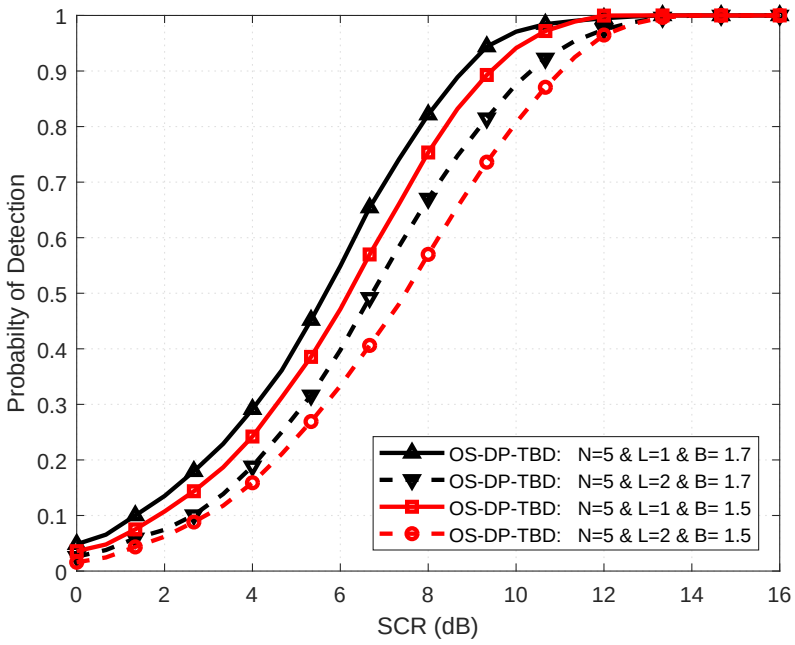

Figure 4.11: OS-DP-TBD probability of detection of a Swerling 3 target for $L = 1$ and 2 with Weibull distributed clutter for different shape parameters B, $A = 1$, and $N = 5$.

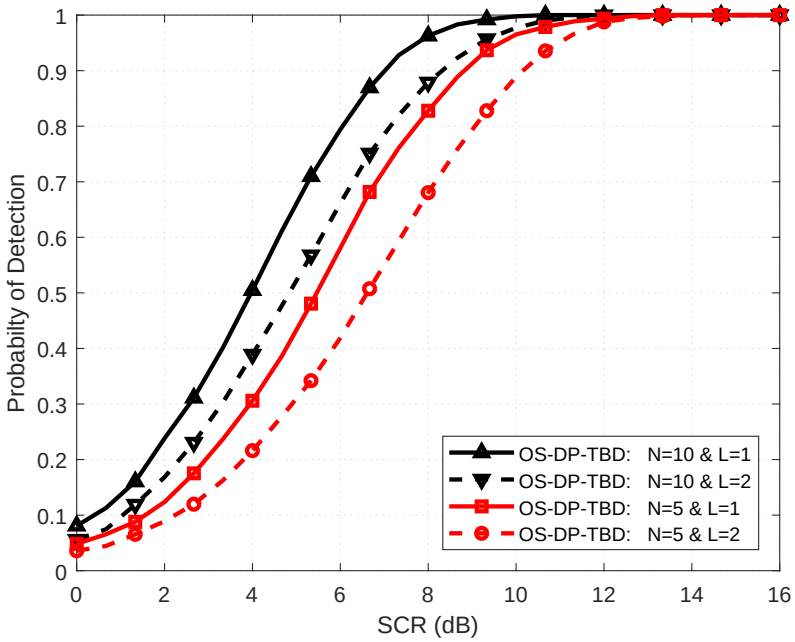

Figure 4.12: OS-DP-TBD probability of detection of a Swerling 0 target for $L = 1$ and 2 with Weibull distributed clutter for $B = 1.5$, $A = 1$, and $N = 5$ and 10.

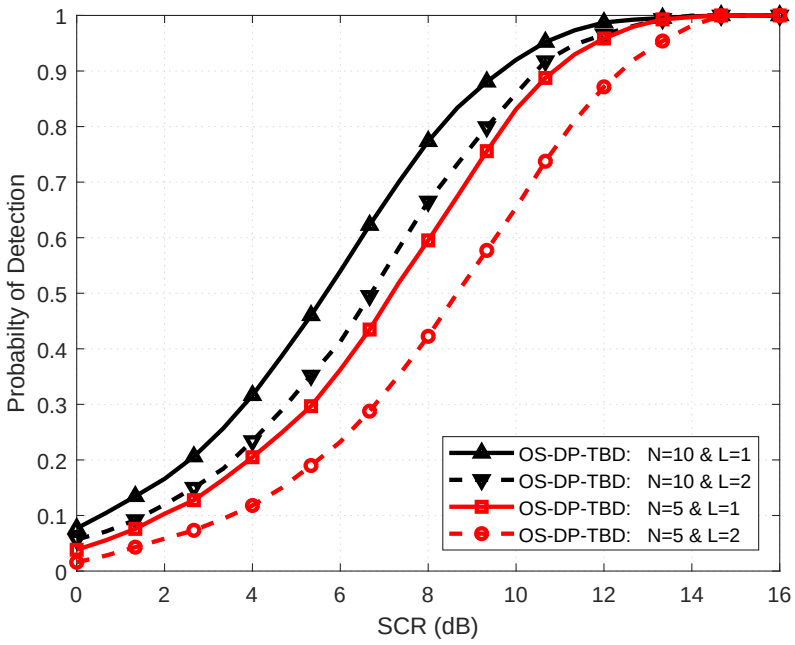

Figure 4.13: OS-DP-TBD probability of detection of a Swerling 1 target for $L = 1$ and 2 with Weibull distributed clutter for $B = 1.5$, $A = 1$, and $N = 5$ and 10.

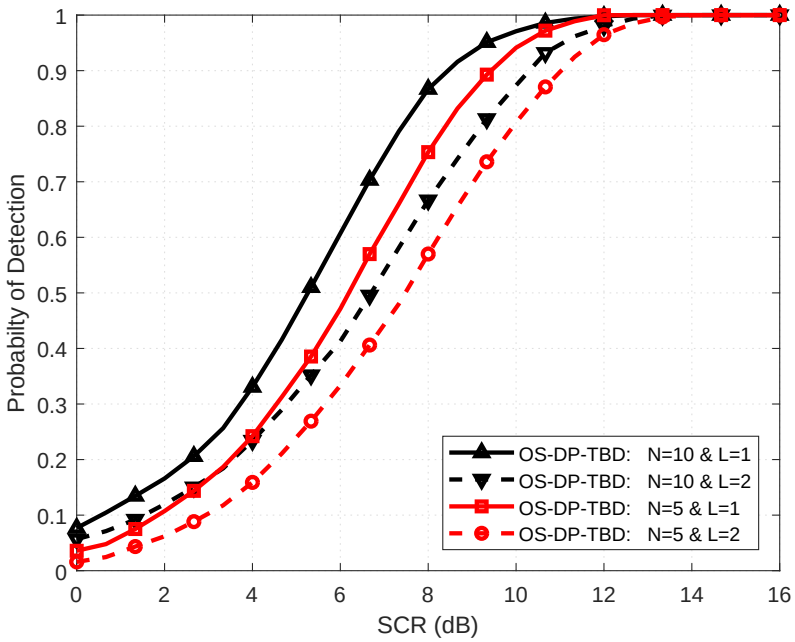

Figure 4.14: OS-DP-TBD probability of detection of a Swerling 3 target for $L = 1$ and 2 with Weibull distributed clutter for $B = 1.5$, $A = 1$, and $N = 5$ and 10.

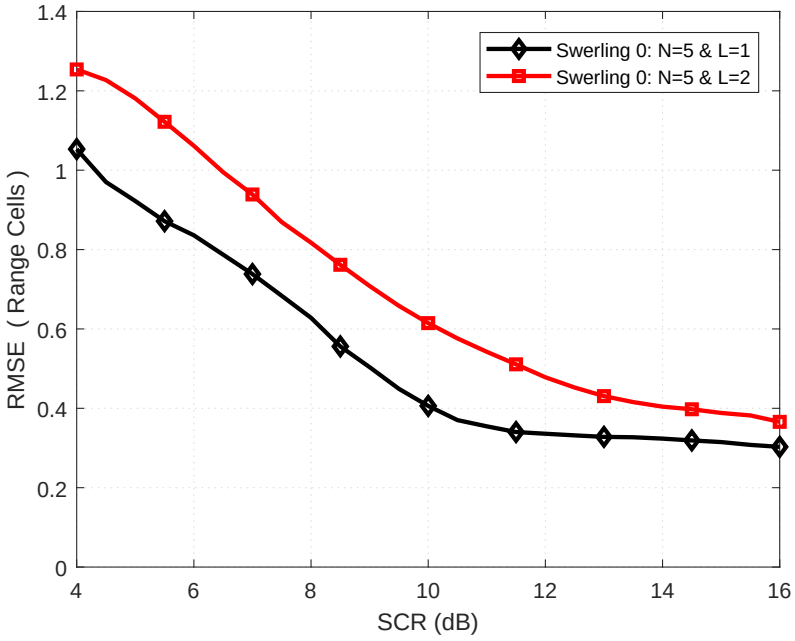

Figure 4.15: RMSE of a Swerling 0 target for $L = 1$ and 2 with Weibull distributed clutter with $B = 1.5$, $A = 1$, and $N = 5$.

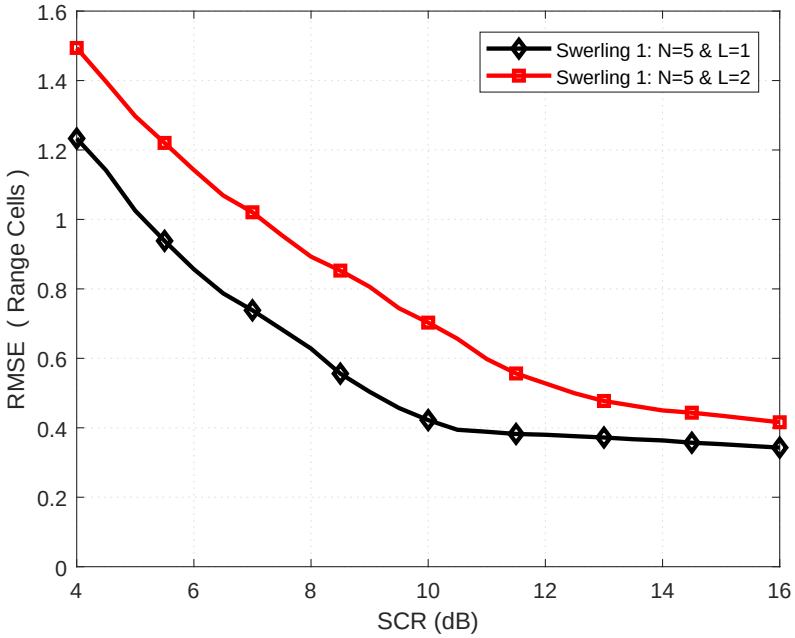

Figure 4.16: RMSE of a Swerling 1 target for $L = 1$ and 2 with Weibull distributed clutter with $B = 1.5$, $A = 1$, and $N = 5$.

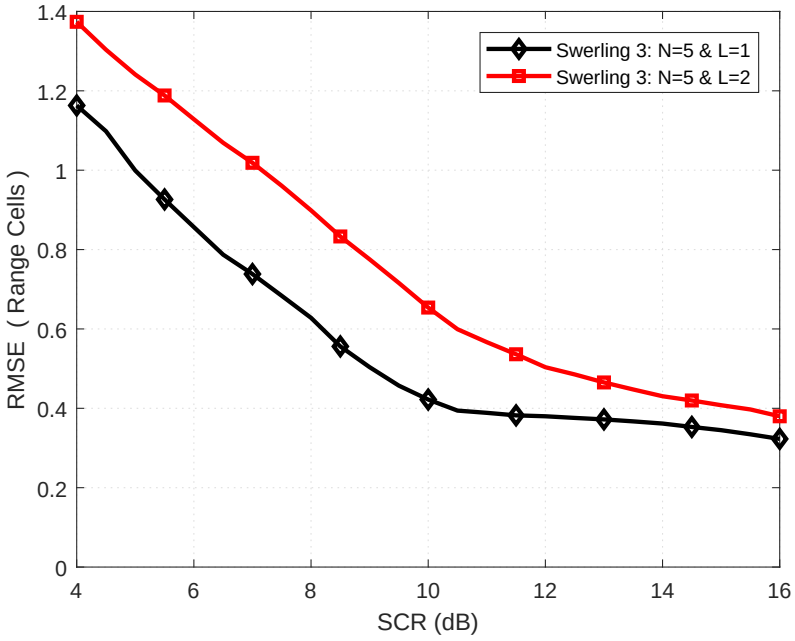

Figure 4.17: RMSE of a Swerling 3 target for $L = 1$ and 2 with Weibull distributed clutter with $B = 1.5$, $A = 1$, and $N = 5$.

multiple targets.

Chapter 5

Conclusion and Future Work

5.1 Conclusion

The main goal of this work is to improve the target detection and tracking of weak fluctuating targets. In this dissertation, two novel techniques have been proposed.

In Chapter 2, the detection of fluctuating targets in Weibull distributed clutter was considered. A new OS-DP-TBD algorithm was proposed and evaluated for Swerling type 0, 1 and 3 targets. In addition, a new expanding window technique EW-TBD for multiframe integration was proposed. It was shown that EW-TBD outperforms conventional batch window processing in terms of both detection performance and computational complexity. Simulation results were presented which show that the proposed OS-DP-TBD algorithm performs better than basic DP-TBD with a gain of 1 to 2 dB. Furthermore, the effect of Weibull distributed clutter was examined. It was shown that the performance with EW-TBD is better than batch window processing with reasonable computational complexity and no latency.

In Chapter 3, the detection of fluctuating targets in non-Gaussian distributed clutter was

evaluated. The proposed OS-DP-TBD algorithm was evaluated for Swerling type 0, 1 and 3 targets in non-Gaussian clutter. Results were presented which show that the proposed OS-DP-TBD technique performs better than the DP-TBD technique in [36] with gains of 0.5 to 2 dB in K distributed clutter. The proposed technique also performs better than the DP-TBD technique in [14] with gains of 0.4 to 2.1 dB in $G0$ distributed clutter. Further, the effect of complex Gaussian noise was considered. It was shown that the performance loss due to noise with the proposed technique is small.

In Chapter 4, the detection of fluctuating extended targets in complex Gaussian noise and Weibull distribution clutter was considered. The proposed OS-DP-TBD algorithm was evaluated for Swerling type 0, 1 and 3 targets and different target energy spillover levels in the range resolution were considered. Simulation results were presented which show that the proposed OS-DP-TBD performs better than basic DP-TBD with a gain of 1 to 2 dB. The detection performance of the proposed algorithm decreased with higher target energy spillover L for all types of Swerling targets.

5.2 Future Work

In the course of this research, several ideas arose that could lead to interesting results. The following topics can be considered in the future.

1. Investigate the effect of using the logarithm of the complex data based likelihood ratio (LCLR) as the scoring function for different types of Swerling targets.

2. Eliminate the zero merit function values of the candidate targets of the proposed algorithm to reduce the computational complexity.

3. Evaluate the proposed techniques for the multiple targets scenario.

4. Develop a detection function based on the first and second order differences of the candidate tracks to eliminate uncorrelated trajectories to improve the detection performance of maneuvering targets.

References

[1] M. I. Skolnik, *Introduction to Radar Systems*. McGraw Hill, Chicago, IL, 2001.

[2] B. R. Mahafza and Z. Elsherbeni, *Matlab Simulation for Radar System Design*. Chapman & Hall/CRC, Boca Raton, FL, 2004.

[3] M. A. Richards, *Fundamentals of Radar Signal Processing*. McGraw-Hill, Chicago, IL, 2005.

[4] S. Blackman and R. Popoli, *Design and Analysis of Modern Tracking Systems*. Artech House, New York, NY, 1999.

[5] N. Levanon and E. Mozeson, *Radar Signals*. John Wiley & Sons, New York, NY, 2004.

[6] Y. Bar-Shalom, P. K. Willett, and X. Tian, *Tracking and Data Fusion*. YBS Publishing, Storrs, CT, USA, 2011.

[7] Y. Bar-Shalom and W. D. Blair, *Multitarget/Multisensor Tracking Applications and Advances, Volume III*. Artech House, New York, NY, 2000.

[8] S. M. Tonissen and R. J. Evans, "Peformance of dynamic programming techniques for track-before-detect," *IEEE Transactions on Aerospace and Electronic Systems*, vol. 32, no. 4, pp. 1440–1451, 1996.

[9] S. J. Davey, M. G. Rutten, and B. Cheung, "A comparison of detection performance for several track-before-detect algorithms," *EURASIP Journal on Advances in Signal Processing*, vol. 2008, pp. 41–47, 2008.

[10] M. J. Walsh, M. L. Graham, R. L. Streit, T. E. Luginbuhl, and L. A. Mathews, "Tracking on intensity-modulated sensor data streams," in *IEEE Aerospace Conference*, 2001, pp. 4–1901.

[11] L. R. Moyer, J. Spak, and P. Lamanna, "A multi-dimensional Hough transform-based track-before-detect technique for detecting weak targets in strong clutter backgrounds," *IEEE Transactions on Aerospace and Electronic Systems*, vol. 47, no. 4, pp. 3062–3068, 2011.

[12] T. Kirubarajan and Y. Bar-Shalom, "Low observable target motion analysis using amplitude information," *IEEE Transactions on Aerospace and Electronic Systems*, vol. 32, no. 4, pp. 1367–1384, 1996.

[13] Y. Boers and J. N. Driessen, "Multitarget particle filter track before detect application," *IEE Proceedings-Radar, Sonar and Navigation*, vol. 151, no. 6, pp. 351–357, 2004.

[14] W. Yi, H. Jiang, T. Kirubarajan, L. Kong, and X. Yang, "Track-before-detect strategies for radar detection in G0-distributed clutter," *IEEE Transactions on Aerospace and Electronic Systems*, vol. 53, no. 5, pp. 2516–2533, 2017.

[15] S. M. Kay, *Fundamentals of Statistical Signal Processing. Detection Theory, Volume II*. Prentice-Hall, Englewood Cliffs, NJ, 1998.

[16] S. Buzzi, M. Lops, and L. Venturino, "Track-before-detect procedures for early detection of moving target from airborne radars," *IEEE Transactions on Aerospace and Electronic Systems*, vol. 41, no. 3, pp. 937–954, 2005.

[17] A. Aprile, E. Grossi, M. Lops, and L. Venturino, "Track-before-detect for sea clutter rejection: Tests with real data," *IEEE Transactions on Aerospace and Electronic Systems*, vol. 52, no. 3, pp. 1035–1045, 2016.

[18] D. Zheng, S. Wang, and Q. Meng, "Dynamic programming track-before-detect algorithm for radar target detection based on polynomial time series prediction," *IET Radar, Sonar and Navigation*, vol. 10, no. 8, pp. 1327–1336, 2016.

[19] Y. Barniv, "Dynamic programming solution for detecting dim moving targets," *IEEE Transactions on Aerospace and Electronic Systems*, vol. 21, no. 1, pp. 144–156, 1985.

[20] W. R. Wallace, "The use of track-before-detect in pulse-Doppler radar," in *IET Radar Conference*, 2002, pp. 315–319.

[21] S. Buzzi, M. Lops, L. Venturino, and M. Ferri, "Track-before-detect procedures in a multi-target environment," *IEEE Transactions on Aerospace and Electronic Systems*, vol. 44, no. 3, pp. 1135–1150, 2008.

[22] E. Grossi, M. Lops, and L. Venturino, "A novel dynamic programming algorithm for track-before-detect in radar systems," *IEEE Transactions on Signal Processing*, vol. 61, no. 10, pp. 2608–2619, 2013.

[23] L. Mo, S. L. Wu, and E. Mao, "Radar detection for dim moving target using DP algorithm," *Chinese Journal of Electronics*, vol. 13, no. 3, pp. 486–490, 2004.

[24] D. Zheng, S. Wang, and X. Qin, "A dynamic programming track-before-detect algorithm based on local linearization for non-Gaussian clutter background," *Chinese J. Elect.*, vol. 25, no. 3, pp. 583–590, 2016.

[25] J. Arnold, S. Shaw, and H. Pasternack, "Efficient target tracking using dynamic programming," *IEEE Transactions on Aerospace and Electronic Systems*, vol. 29, no. 1, pp. 44–56, 1993.

[26] H. Jiang, W. Yi, T. Kirubarajan, L. Kong, and X. Yang, "Multiframe radar detection of fluctuating targets using phase information," *IEEE Transactions on Aerospace and Electronic Systems*, vol. 53, no. 2, pp. 736–749, 2017.

[27] R. B. Abernethy, *The New Weibull Handbook: Reliability and Statistical Analysis for Predicting Life, Safety, Supportability, Risk, Cost and Warranty Claims*, 2004.

[28] M. Sekine and Y. Mao, *Weibull Radar Clutter*. IET, London, UK, 1990.

[29] H.-C. Yang and M.-S. Alouini, *Order Statistics in Wireless Communications: Diversity, Adaptation, and Scheduling in MIMO and OFDM Systems*. Cambridge University Press, UK, 2011.

[30] J. Wang, W. Yi, T. Kirubarajan, and L. Kong, "An efficient recursive multiframe track-before-detect algorithm," *IEEE Transactions on Aerospace and Electronic Systems*, vol. 54, no. 1, pp. 190–204, 2018.

[31] L. A. Johnston and V. Krishnamurthy, "Performance analysis of a dynamic programming track before detect algorithm," *IEEE Transactions on Aerospace and Electronic Systems*, vol. 38, no. 1, pp. 228–242, 2002.

[32] D. Orlando, L. Venturino, M. Lops, and G. Ricci, "Track-before-detect strategies for STAP radars," *IEEE Transactions on Signal Processing*, vol. 58, no. 2, pp. 933–938, 2010.

[33] H. Jiang, W. Yi, L. Kong, G. Cui, and X. Yang, "Track-before-detect for fluctuating targets in heterogeneous clutter," in *IEEE Radar Conference*, 2014, pp. 496–501.

[34] J. Wang, W. Yi, and L. Kong, "Improved DP-TBD methods based on multiple hypothesis testing for target early detection," in *IEEE International Conference on Information Fusion*, 2016, pp. 1406–1413.

[35] D. Callaghan, J. Burger, and A. K. Mishra, "A machine learning approach to radar sea clutter suppression," in *IEEE Radar Conference*, 2017, pp. 1222–1227.

[36] H. Jiang, W. Yi, G. Cui, L. Kong, and X. Yang, "Knowledge-based track-before-detect strategies for fluctuating targets in K-distributed clutter," *IEEE Sensors Journal*, vol. 16, no. 19, pp. 7124–7132, 2016.

[37] L. Bruno, P. Braca, J. Horstmann, and M. Vespe, "Experimental evaluation of the range–Doppler coupling on HF surface wave radars," *IEEE Geoscience and Remote Sensing Lett.*, vol. 10, no. 4, pp. 850–854, 2013.

[38] A. C. Frery, H.-J. Muller, C. d. C. F. Yanasse, and S. J. S. Sant'Anna, "A model for extremely heterogeneous clutter," *IEEE Transactions on Geoscience and Remote Sensing*, vol. 35, no. 3, pp. 648–659, 1997.

[39] P. Z. Peebles, *Radar Principles*, New York: John Wiley & Sons, New York, NY, 2007.

[40] E. Jakeman and P. N. Pusey, "A model for non-Rayleigh sea echo," *IEEE Transactions on Antennas and Propagation*, vol. 24, no. 6, pp. 806–814, 1976.

[41] S. Watts, "Radar detection prediction in sea clutter using the compound K-distribution model," in *IEE Proceedings F-Communications, Radar and Signal Processing*, vol. 132, no. 7, 1985, pp. 613–620.

[42] E. Brekke, O. Hallingstad, and J. Glattetre, "Tracking small targets in heavy-tailed clutter using amplitude information," *IEEE Journal of Oceanic Engineering*, vol. 35, no. 2, pp. 314–329, 2010.

[43] D. Kincaid, D. R. Kincaid, and E. W. Cheney, *Numerical Analysis: Mathematics of Scientific Computing*. American Mathematical Soc., 2009, vol. 2.

[44] D. Angelova and L. Mihaylova, "Extended object tracking using Monte Carlo methods," *IEEE Transactions on Signal Processing*, vol. 56, no. 2, pp. 825–832, 2008.

[45] B. Errasti-Alcala, W. Fuscaldo, P. Braca, and G. Vivone, "Realistic ship model for extended target tracking algorithms," in *IEEE International Geoscience and Remote Sensing Symposium*, 2015, pp. 3135–3138.

[46] Y. Boers, H. Driessen, J. Torstensson, M. Trieb, R. Karlsson, and F. Gustafsson, "Track-before-detect algorithm for tracking extended targets," *IEE Proceedings-Radar, Sonar and Navigation*, vol. 153, no. 4, pp. 345–351, 2006.

[47] H. Jiang, W. Yi, G. Cui, L. Kong, and X. Yang, "Track-before-detect strategies for range distributed target detection in compound-Gaussian clutter," *Signal Processing*, vol. 120, pp. 462–467, 2016.

[48] A.-A. Saucan, T. Chonavel, C. Sintes, and J.-M. Le Caillec, "Track before detect DOA tracking of extended targets with marked Poisson point processes," in *International Conference on Information Fusion*, 2015, pp. 754–760.

[49] S. J. Davey, M. G. Rutten, and B. Cheung, "Using phase to improve track-before-detect," *IEEE Transactions on Aerospace and Electronic Systems*, vol. 48, no. 1, pp. 832–849, 2012.